New Views on
the Cosmological Big Bang

by

Elizabeth Gould

A thesis
presented to the University of Waterloo
in fulfillment of the
thesis requirement for the degree of
Doctor of Philosophy
in
Physics

Waterloo, Ontario, Canada, 2017

Examining Committee Membership

The following served on the Examining Committee for this thesis. The decision of the Examining Committee is by majority vote.

External Examiner	Professor Eugene Lim
Supervisor	Professor Niayesh Afshordi
Internal Member	Professor Avery Broderick
Internal-external Member	Professor Florian Girelli
Other Member	Professor Lee Smolin

This thesis consists of material all of which I authored or co-authored: see Statement of Contributions included in the thesis. This is a true copy of the thesis, including any required final revisions, as accepted by my examiners.

I understand that my thesis may be made electronically available to the public.

Statement of Contributions

This dissertation is partially the product of collaborative research and co-authored publications as follows:

- **Chapter 2** Niayesh Afshordi, Elizabeth Gould, and Kostas Skenderis, "Constraining holographic cosmology using Planck data", Phys. Rev. D 95, 123505 (2017). Copyright 2017 by the American Physical Society.

  Some text from this paper has been moved to Chapter 1 of this dissertation, specifically for the summary before the first section and Section 1.4.3.

  A summary of these results paired with the theoretical side was published in: Niayesh Afshordi, Claudio Corianò, Luigi Delle Rose, Elizabeth Gould, and Kostas Skenderis, "From Planck data to Planck era: Observational tests of Holographic Cosmology" Phys. Rev. Lett. 118, 041301 (2017).

- **Chapter 3** Elizabeth Gould and Niayesh Afshordi, "Does History Repeat Itself? Periodic Time Cosmology", currently unpublished with preliminary data

- **Chapter 4** Natacha Altamirano, Elizabeth Gould, Niayesh Afshordi, and Robert B. Mann, "Cosmological Perturbations in the 5D Holographic Big Bang Model", arXiv:1703.00954

- **Chapter 5** Elizabeth Gould and Niayesh Afshordi, "A Non-Local Reality: Is there a Phase Uncertainty in Quantum Mechanics?", Foundations of Physics 45, 1620 (2015).

Abstract

This dissertation is a collection of four different proposals to describe the early universe. Each will draw from insights of different areas of physics to suggest a description which differs from the standard inflationary paradigm.

First we start with holographic cosmology in which cosmological predictions of the very early Universe are expressed in terms of the observables of a three dimensional quantum field theory (QFT). This framework includes conventional slow-roll inflation, which is described in terms of a strongly coupled QFT, but it also allows for qualitatively new models for the very early Universe, where the dual QFT may be weakly coupled. The new models describe a universe which is non-geometric at early times. While standard slow-roll inflation leads to a (near-)power-law primordial power spectrum, perturbative superrenormalizable QFT's yield a new holographic spectral shape. Here, we compare the two predictions against cosmological observations. We use CosmoMC to determine the best fit parameters, and MultiNest for Bayesian Evidence, comparing the likelihoods. We find that the dual QFT should be non-perturbative at the very low multipoles ($l \lesssim 30$), while for higher multipoles ($l \gtrsim 30$) the new holographic model, based on perturbative QFT, fits the data just as well as the standard power-law spectrum assumed in ΛCDM cosmology. This finding opens the door to applications of non-perturbative QFT techniques, such as lattice simulations, to observational cosmology on gigaparsec scales and beyond.

We then turn to the suggestion that the universe repeats in cycles, with an infinite series of similar cycles in the past and the future. Here, we instead propose that the cosmic history repeats itself exactly, constructing a universe on a periodic temporal history, which we call *periodic time cosmology*. In particular, the primordial power spectrum, convolved with the transfer function throughout the cosmic history, would form the next cycle's primordial power spectrum. By matching the big bang to the infinite future using a conformal rescaling (*a la* Penrose), we uniquely determine the primordial power spectrum, in terms of the transfer function up to two free parameters. While nearly scale invariant with a red tilt, using Planck and Baryonic Acoustic Oscillation observations, we find the minimal model is disfavoured compared to a power-law power spectrum at 5.1σ. However, extensions of ΛCDM cosmic history change the large scale transfer function and can provide better relative fits to the data. For example, the best fit seven parameter model for our Periodic Time Cosmology, with $w = -1.024$ for dark energy equation of state, is only disfavoured relative to a power-law power spectrum at 1.8σ level. Therefore, consistency between cosmic history and initial conditions provides a viable description of cosmological observations in the context of Periodic Time Cosmology.

Next, we discuss the 5D holographic big bang model, a novel model for the emergence of the early universe out of a 5D collapsing star (an apparent white hole), in the context of Dvali-Gabadadze-Porrati (DGP) cosmology. The model does not have a big bang singularity, and yet can address cosmological puzzles that are traditionally solved within inflationary cosmology. We compute the exact power spectrum of cosmological curvature perturbations due to the effect of a thin atmosphere accreting into our 3-brane. The spectrum is scale-invariant on small scales and red on intermediate scales, but becomes blue on scales larger than the height of the atmosphere. While this behaviour is broadly consistent with the non-parametric measurements of the primordial scalar power spectrum, it is marginally disfavoured relative to a simple power law (at 2.7σ level). Furthermore, we find that the best fit nucleation temperature of our 3-brane is at least 3 orders of magnitude larger than the 5D Planck mass, suggesting an origin in a 5D quantum gravity phase.

Finally, we turn to the status of locality in quantum mechanics. Motivations for violations of the notion of relativistic locality include the Bell's inequalities for hidden variable theories, the cosmological horizon problem, and Lorentz-violating approaches to quantum geometrodynamics, such as Horava-Lifshitz gravity. We explore a proposal for a "real ensemble" non-local description of quantum mechanics, in which "particles" can copy each others' observable values AND phases, independent of their spatial separation. We first specify the exact theory, ensuring that it is consistent and has (ordinary) quantum mechanics as a fixed point, where all particles with the same values for a given observable have the same phases. We then study the stability of this fixed point numerically, and analytically, for simple models. We provide evidence that most systems (in our study) are locally stable to small deviations from quantum mechanics, and furthermore, the phase variance per value of the observable, as well as systematic deviations from quantum mechanics, decay as $\sim (\text{Energy} \times \text{Time})^{-2n}$, where $n \geq 1$. Interestingly, this convergence is controlled by the *absolute* value of energy (and not energy difference), suggesting a possible connection to gravitational physics. Finally, we discuss different issues related to this theory, as well as potential novel applications for the spectrum of primordial cosmological perturbations and the cosmological constant problem.

Acknowledgements

First, I would like to thank my advisor Niayesh Afshordi. Though our styles often clashed, he was always willing to support whatever I needed to his ability, and encouraged me to work on and helped me work on research of interest to me. When it came time to write up my research or my research statement for post-docs, he put time when editing into making sure it sounded just right.

I want to express my gratitude to Erik Schnetter and Jonah Miller for their help with various aspects of numerical calculations and especially for installing the Planck Likelihood Code on the Perimeter Institute computer system and helping to get CosmoMC to run on these computers, even when the code seemed to refuse to work. On the side of CosmoMC, despite no direct contact, Antony Lewis provided technical support over the CosmoCoffee forum and manages to keep the code up to date.

It gives me pleasure to acknowledge Kostas Skenderis with whom I had regular contact online while working on the holographic cosmology project, and who had managed to find me some funding for after my PhD. I would also like to acknowledge my other collaborators Natacha Altamirano and Robert B. Mann.

I want to express my gratitude to Lee Smolin for talking to me about the real ensemble model and encouraging me on my more unusual projects and Rafael Sorkin for numerous conversations about physics and politics.

I would like to thank Raphael Flauger for collaboration at early stages of the holographic cosmology project, and Lucien Hardy, and Steve Weinstein for their comments on the real ensemble draft.

I wish to thank Neil Turok and Latham Boyle for helping me put together the introduction of this thesis – for being willing to edit the draft, for suggesting references to help put it together, and for understanding what I wanted with the introduction and encouraging me to do what I felt I needed.

On the quantum foundations side, I would like to thank Robert Spekkens and Lucien Hardy, who have both talked to me over the years on various topics and helped me in reading articles and staying connected with the field.

I am grateful to have Tibra Ali as a friend, as he was often there to talk to me when I struggled and give me advice when I needed it. Christopher Granade had also been a great friend while he was in Waterloo, including engaging many conversations about various topics and helping me to have contact with the Institute of Quantum Computing.

I am forever indebted to everyone who has talked to me when I was struggling and needed someone to talk to, including those with UW Health Services and MATES, and my mother, with whom I had frequent contact.

And I truly appreciate all the people with whom I have talked over the years about physics, including many whose names I may have forgotten.

Table of Contents

List of Tables

List of Figures

xvii

Chapter 1

Introduction

Cosmology seeks to describe the universe as a whole, including its origin, evolution and final fate.

Our current model of cosmology originated with the development and confirmation of Einstein's theory of general relativity, combined with the discovery, originally by Hubble, that our universe is expanding. From there, the model had been further refined with observations of the cosmic microwave background, the light coming to us from the earliest times, of increasing accuracy as well as the application of particle physics and other theoretical tools to our analysis of our expectations.

When we make these observations and calculations, we see that our universe must have evolved from a nearly isotropic, homogeneous, and flat background with small anisotropies that are nearly scale invariant.

We can using this construct a fit to the six-parameter ΛCDM model. This model is an empirical parameterization for cosmology, combining four parameters of the transfer function with two of the primordial power spectrum. For the transfer function, the parameters correspond to the matter contents of the universe, the current rate of expansion of the universe, and the optical depth (which is related to the time of reionization). This part is well-understood in the context of the ΛCDM framework. The other two parameters, Δ_0^2 and n_s, are those of the scalar primordial power spectrum $\mathcal{P}(k)$, which is taken to have a power-law form:

$$\mathcal{P}\left(k\right) = \Delta_0^2 \left(\frac{k}{k_*}\right)^{n_s - 1}, \tag{1.1}$$

where k_*, the pivot scale, is an (arbitrary) reference scale.

This part has several issues. We calculate that there is not enough time for all regions of the universe we see to have come in contact with each other for interaction of the various regions to produce the needed correlations. We do not know what produced the homogeneity and isotropy. Neither do we know what produced the primordial power spectrum.

Typically the primordial power spectrum is explained using slow-roll inflation in which the early universe undergoes a phase of rapid accelerated expansion. This is used to explain the homogeneity and isotropy of the universe by having the expansion increase the size of the regions which were in causal contact after the big bang to our entire visible universe as well as making it look flat by being large enough that the curvature is not visible. In addition, starting from the quantum adiabatic vacuum, inflationary models typically predict a primordial power spectrum well approximated by the power-law form (1.1). While inflation is often considered to be the best scenario to explain cosmological observations, it suffers from shortcomings such as lack of predictivity and falsifiability, sparking a search for alternative possibilities.

In this dissertation, I describe four such alternative possibilities on which I have worked. First, however, the remainder of this chapter describes our current knowledge. I go through the developments of modern cosmology in modern history, in order to explain where current theory comes from, and hopefully make a case for questioning this standard paradigm. During this process, I explain the tools used in modern cosmology as well as how inflation became the consensus model.

In putting together this chapter, I relied on several secondary sources in addition to memory and conversations. For the basic outline, I used two popular science books [1, 2] to help structure the historical story. For the equations and other details, I used class notes by Latham Boyle [3], Wikipedia, and three cosmology books [4, 5, 6].

1.1 Early 20th Century: Is the Universe Changing With Time?

Our history will begin at the start of the 20th century. This is when modern cosmology begins, when we first learned that the universe extends beyond our galaxy, and when we first see the tools constructed which describe the universe as we know it today. Specifically, two main discoveries emerged which helped define modern cosmology and the limits of our knowledge with it. The first is Einstein's theory of general relativity [7]. This provided a theory of gravity for very large scales, from which we could calculate the interaction

between matter and space-time, allowing for the possibility of an evolution of the universe. The second is Hubble's discovery of the expansion of the universe [8]. Specifically, Hubble calculated the relation between the velocity of galaxies and their distance from us. Quantum theory was also first discovered and developed during this time period, but it did not become relevant to cosmology until later.

1.1.1 Einstein and GR

In 1905, Einstein developed the theory of special relativity [9]. He described it as a theory of electromagnetism and developed it from asking what happens if he were to chase a beam of light. By allowing time to rotate into space, the speed of light can remain constant for all observers. This "rotation" is applied when one moves from one inertial (non-accelerating) reference frame to another, so that in every such reference frame, the speed of light appears to have the same fixed value.

However, time is not the same as space, so an ordinary rotation would not provide such an effect. The mathematics required, however, had already been developed previously in attempts to explain the constant speed of light. These rotations go by the name Lorentz transformations, which for the case of a change in velocity in the x direction are,

$$
t' = \gamma \left(t - \frac{vx}{c^2} \right)
$$
$$
x' = \gamma \left(x - vt \right)
$$
$$
y' = y
$$
$$
z' = z
$$

where

$$
\gamma = \frac{1}{\sqrt{1 - \frac{v^2}{c^2}}}. \tag{1.2}
$$

In this formulation, the invariant distance between events (localized space-time points) is given by

$$
ds^2 = -c^2 dt^2 + dx^2 + dy^2 + dz^2, \tag{1.3}
$$

replacing the original invariant distance between objects from the Pythagorean theorem,

$$
ds^2 = dx^2 + dy^2 + dz^2.
$$

From this, Einstein found that not only space and time transform into each other, but also matter and energy [10]. For an object at rest, the famous equation expressing

3

this equivalence is, $E = mc^2$, which when extended to the case for an object in motion, becomes,

$$E^2 = m^2c^4 + p^2c^2. \tag{1.4}$$

In this theory, massless particles always move at the speed of light, but they do have momentum.

However, these relations work only for initial reference frames and objects which are not accelerating at the time at which they are analyzed. While there is a lot which can be calculated with this given conservation laws, it does not provide a complete picture of reality.

By 1915, in order to fix this issue, Einstein developed the theory of general relativity (GR) [7], which describes gravity. This originally came from thought experiments involving the equivalence principle, which states that gravitational and inertial mass are identical. Einstein interpreted this as meaning that gravitation and acceleration are identical, leading to a geometric description of space-time. The resulting theory describes a universe where gravity bends space-time, replacing the fixed background of Newton with a dynamical one.

Given a metric $g_{\mu\nu}$ and its inverse defined by,

$$g^{\alpha\beta}g_{\beta\gamma} = \delta^\alpha_\gamma, \tag{1.5}$$

and an energy-momentum or stress tensor calculated from the Lagrangian of matter $\mathcal{L}_m$,

$$T_{\mu\nu} = g_{\mu\nu}\mathcal{L}_m - 2\frac{\partial \mathcal{L}_m}{\partial g^{\mu\nu}}, \tag{1.6}$$

Einstein's field equations for this relation are,

$$G_{\mu\nu} + \Lambda g^{\mu\nu} = 8\pi G_N T_{\mu\nu}, \tag{1.7}$$

where

$$G_{\mu\nu} = R_{\mu\nu} - \frac{1}{2}g_{\mu\nu}R. \tag{1.8}$$

The Ricci tensor $R_{\mu\nu}$ and scalar R come from the Riemann tensor $R^\alpha_{\beta\gamma\delta}$ by equations

$$R_{\mu\nu} = R^\gamma_{\mu\gamma\nu}, \quad R = g^{\alpha\beta}R_{\alpha\beta}. \tag{1.9}$$

The Riemann tensor and the metric are related to each other through the curvature, which for the case of a torsion-free metric compatible connection $\Gamma^\alpha_{\beta,\gamma}$,

$$\Gamma^\alpha_{\beta\gamma} = \frac{1}{2}g^{\alpha\delta}\left(g_{\gamma\delta,\beta} + g_{\beta\delta,\gamma} - g_{\beta\gamma,\delta}\right). \tag{1.10}$$

With this, we calculate the Riemann tensor as,

$$R^{\alpha}_{\beta\gamma\delta} = \Gamma^{\alpha}_{\delta\beta,\gamma} - \Gamma^{\alpha}_{\gamma\beta,\delta} + \Gamma^{\alpha}_{\gamma\mu}\Gamma^{\mu}_{\delta\beta} - \Gamma^{\alpha}_{\delta\mu}\Gamma^{\mu}_{\gamma\beta}. \tag{1.11}$$

The resulting theory was found to explain previously unexplained effects and to predict new effects which were later found to be accurate. It also predicted a changing universe. In order to maintain a static universe, Einstein set Λ to a non-zero value. However the result would be an unstable equilibrium. When the universe was seen to be expanding, Einstein called this his "biggest blunder."

1.1.2 Hubble

It has been noted that the universe can not be of infinite age and of infinite size. The reason for this it that the night sky would not be dark – everywhere one would look, there would be a star. If the night sky is dark, this means that there is a finite amount of light which reaches us.

By 1923, it was known there were many galaxies. The universe also appeared to be isotropic and homogeneous on large scales. This is the cosmological principle.

It was during this time that Hubble originally discovered the expansion of the universe. He did so by measuring the distances to visible galaxies and compared this to their velocity away from us. His plot from 1929 is shown in Figure 1.1 [8]. For a constant rate of expansion and no preferred position or direction, there should be a linear relation between distance and velocity which is the same in any direction. The slope of this line is called the Hubble constant. Hubble's calculated Hubble constant was 500 (km/s)/Mpc which is almost an order of magnitude above its known modern value.

To calculate the velocities and distances, he used certain known relations. For velocity, it was well known that when a wave moves towards or away from an observer, its frequency shifts. This is known as the Doppler shift. For light this can be calculated in special relativity by

$$\nu_{observed} = \gamma \left(1 - \frac{v}{c} \right) \nu_{source} \tag{1.12}$$

with ν being the frequency and γ given by Equation 1.2. We can rewrite the Doppler shift as

$$z = \frac{\lambda_{observed} - \lambda_{source}}{\lambda_{source}} = \frac{\sqrt{1 + \frac{v}{c}}}{\sqrt{1 - \frac{v}{c}}} - 1, \tag{1.13}$$
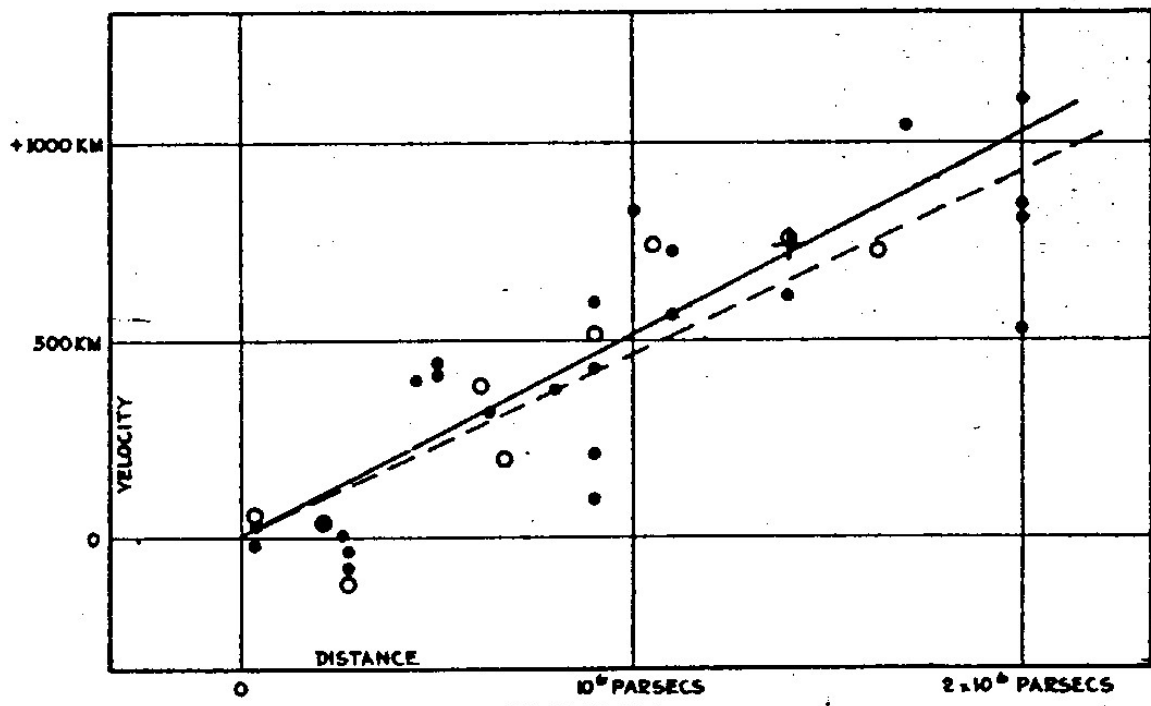
Figure 1.1: Hubble's original plot of velocity of a galaxy away from us vs its distance from us. This image originally appeared in [8].

where λ is the wavelength of the wave. If the Doppler shift is known, typically from the measured frequency of spectral lines produced by atomic transitions, it can be used to calculate an object's relative velocity towards or away from us, blue-shifted if moving towards us and red-shifted away from us.

Distance can be measured from standard candles, stellar objects with a known brightness. For Hubble, he used Cepheid variable stars, which vary in brightness but have a known, fixed relation between their maximum brightness and the frequency of their variation in brightness.

1.1.3 The Friedmann Equations

While Equation 1.3 from special relativity gives the distance measure for a flat maximally symmetric space-time, general relativity allows for more forms of this separation. The invariant separation in general relativity is given by

$$ds^2 = g_{\mu\nu}dx^\mu dx^\nu. \tag{1.14}$$

For special relativity in Cartesian coordinates (Minkowski space), we have [1]

$$g_{\mu\nu} = \eta_{\mu\nu} \equiv \begin{bmatrix} -1 & 0 & 0 & 0 \\ 0 & 1 & 0 & 0 \\ 0 & 0 & 1 & 0 \\ 0 & 0 & 0 & 1 \end{bmatrix}. \tag{1.15}$$

However, for general relativity there are more possibilities. For the case of maximally symmetric metric, there are two other possibilities, that with positive curvature (similar to a sphere) and that with negative curvature. The general form of the metric is

$$g_{\mu\nu} = \eta_{\mu\nu} + K\frac{x_\mu x_\nu}{\rho^2 - Kx^2}, \tag{1.16}$$

where ρ is the radius of curvature, and K is $-1, 0, +1$, determining the type of curvature – hyperbolic, flat, or spherical. For $3 + 1$ dimensions, as is presented here, the names for the types of spacetime are Anti de Sitter, Minkowski, and de Sitter.

For this case, however, these metrics solve the Einstein equations for the case when $T_{\mu\nu} = 0$. If we have matter and energy in the universe, this is not the solution.

---

[1] As the speed of light c is effectively a ratio of conversion between spatial and temporal coordinates, the standard notation is to set $c = 1$ which I will do here and for the rest of the document.

If we allow for an asymmetry in time, the natural extension is the FRW metric. This describes an isotropic and homogeneous space-time like our universe, but allows for the universe to change in time. The model was developed first by Friedmann in 1922 [11], then by Lemaître in the late 1920s [12, 13], and developed by Robertson [14, 15, 16] and Walker [17, 18] in the 1930s. The metric is given by

$$g_{\mu\nu} = \begin{bmatrix} -1 & 0 & 0 & 0 \\ 0 & a^2(t) & 0 & 0 \\ 0 & 0 & a^2(t) & 0 \\ 0 & 0 & 0 & a^2(t) \end{bmatrix} \tag{1.17}$$

for the flat case in Cartesian coordinates, or,

$$ds^2 = -dt^2 + a^2(t) \left[\frac{dr^2}{1 - Kr^2} + r^2 d\Omega \right] \tag{1.18}$$

in spherical coordinates for any of the three cases. This can also be represented using conformal time τ where $dt = a d\tau$. In this case,

$$ds^2 = a^2(\tau) \left[-d\tau^2 \frac{dr^2}{1 - Kr^2} + r^2 d\Omega \right]. \tag{1.19}$$

For the case of FRW, $T_{\mu\nu}$ is

$$T_{\mu\nu} = \begin{bmatrix} -\rho & 0 & 0 & 0 \\ 0 & p & 0 & 0 \\ 0 & 0 & p & 0 \\ 0 & 0 & 0 & p \end{bmatrix}. \tag{1.20}$$

This means that we now have matter in our theory, and the Einstein equations can be solved for the behavior of the entire system. Here, ρ is the density of matter, and p is its pressure. We will define the Hubble constant $H = \frac{\dot{a}}{a}$ and an equation of state of the matter or energy contained in the system $w = \frac{p}{\rho}$. The Einstein equations reduce to the Friedmann equation

$$H^2 = \frac{8\pi G_N \rho + \Lambda}{3} - \frac{K}{a^2} \tag{1.21}$$

and the continuity equation

$$\dot{\rho} = -3H(\rho + p). \tag{1.22}$$

8

From this, the shape of the universe, and its evolution, can be determined by comparing the density of matter in the universe to a critical density

$$\rho_{crit}(t) = \frac{3H^2(t)}{8\pi G_N}. \tag{1.23}$$

In general, $\dot{a} \neq 0$. For a flat case, since $\dot{a} > 0$, we know the universe is expanding, and if we reverse this process, we predict everything started from a point, a hot big bang. In the infinite future, $a \to \infty$.

The energy density of our universe is comprised of several components. First, there is matter (or non-relativistic particles), $\rho_m = \rho_b + \rho_c$, which has an equation of state $w = 0$. There is also radiation (or relativistic particles), $\rho_r = \rho_\gamma + \rho_\nu$, with an equation of state of $w = \frac{1}{3}$. We can also express two other terms in Equation 1.21 as if they were an energy density. For dark energy, ρ_Λ has an effective $w = -1$ if it is a cosmological constant. Alternative models may alter this. The curvature term can also be expressed as ρ_k, such that

$$\rho_m + \rho_r + \rho_\Lambda + \rho_k = \rho_{crit}. \tag{1.24}$$

Since ρ_k varies with time as a^{-2}, we see that its effective equation of state is $w = -\frac{1}{3}$.

Using Equation 1.22, we can calculate the dependence of each type of energy density on the scale factor $a(t)$. From this, we get $\rho_m(t) = \frac{\rho_{m0}}{a^3(t)}$ and $\rho_r(t) = \frac{\rho_{r0}}{a^4(t)}$. The other two energy densities had already been calculated in reverse: $\rho_\Lambda(t) = \rho_{\Lambda 0}$ and $\rho_k = \frac{\rho_k}{a^2(t)}$. From this, we can rewrite Equation 1.21 as

$$H^2(t) = \frac{8\pi G_N}{3} \left[\frac{\rho_r}{a^4} + \frac{\rho_m}{a^3} + \frac{\rho_k}{a^2} + \rho_\Lambda \right] \tag{1.25}$$

This can be integrated by separation of variables to calculate the age of the universe. The modern estimate is about 13.8 billion years [19].

1.2 Mid 20th Century: The Discovery of the CMB

While the Friedmann equations and the FRW metric were developed in the 1920s and 30s, it wasn't until later when the implications of the possibility of calculating the beginning of the universe were fully realized.

1.2.1 Theoretical Prediction

In 1946, George Gamow first calculated the implications of a universe which stared in a hot big bang [20]. This conception was based on Lemaître's comments about how, if continued into the past, an expanding universe would imply that everything must have started from a single point. Gamow performed the first calculations for Big Bang Nucleosynthesis (BBN), where the primordial abundances of atoms were formed in the cooling of the universe. Working with him, Ralph Alpher and Robert Herman estimated the temperature of the Cosmic Microwave Background (CMB) [21, 22].

The conception was reproduced by other groups independently of this in the 1960s, just before the first experimental confirmations emerged.

1.2.2 Experimental Confirmation

Experimental confirmation of this model occurred in 1964, when Penzias and Wilson at Bell Labs were trying to figure out the source of and remove the noise from their radio antenna [23]. What they found was a signal, corresponding to about 3 K originating from space with no preferred direction. The conclusion is that it came from outside of our galaxy. The measurement was identified by a physicist Burke to fit the predictions of the hot big bang model of Dicke, Peeble, and Wilkinson [24]. Others confirmed this measurement with ground based telescopes at different frequencies and eventually with a balloon based experiment designed to get above the atmosphere and measure frequencies absorbed by the atmosphere [25].

1.2.3 A Brief History of the Universe

The universe was not always full of stars and galaxies. Based on the thermodynamics of various processes, we can work out the history of the universe. NASA has produced pictorial schematics of this, as seen in Figure 1.2.

Since our model becomes more and more speculative as we go to earlier and earlier times, I will start this history after the suspected time of inflation. After this time is speculated that the origin of the matter / antimatter asymmetry originated. This is around the time when the electroweak force and strong force are expected to be unified, a symmetry suspected of breaking around 10^{16} GeV.

As we move to times we can begin to calculate with modern theories, the electromagnetic force and weak force are expected to be unified into an electroweak force above 200
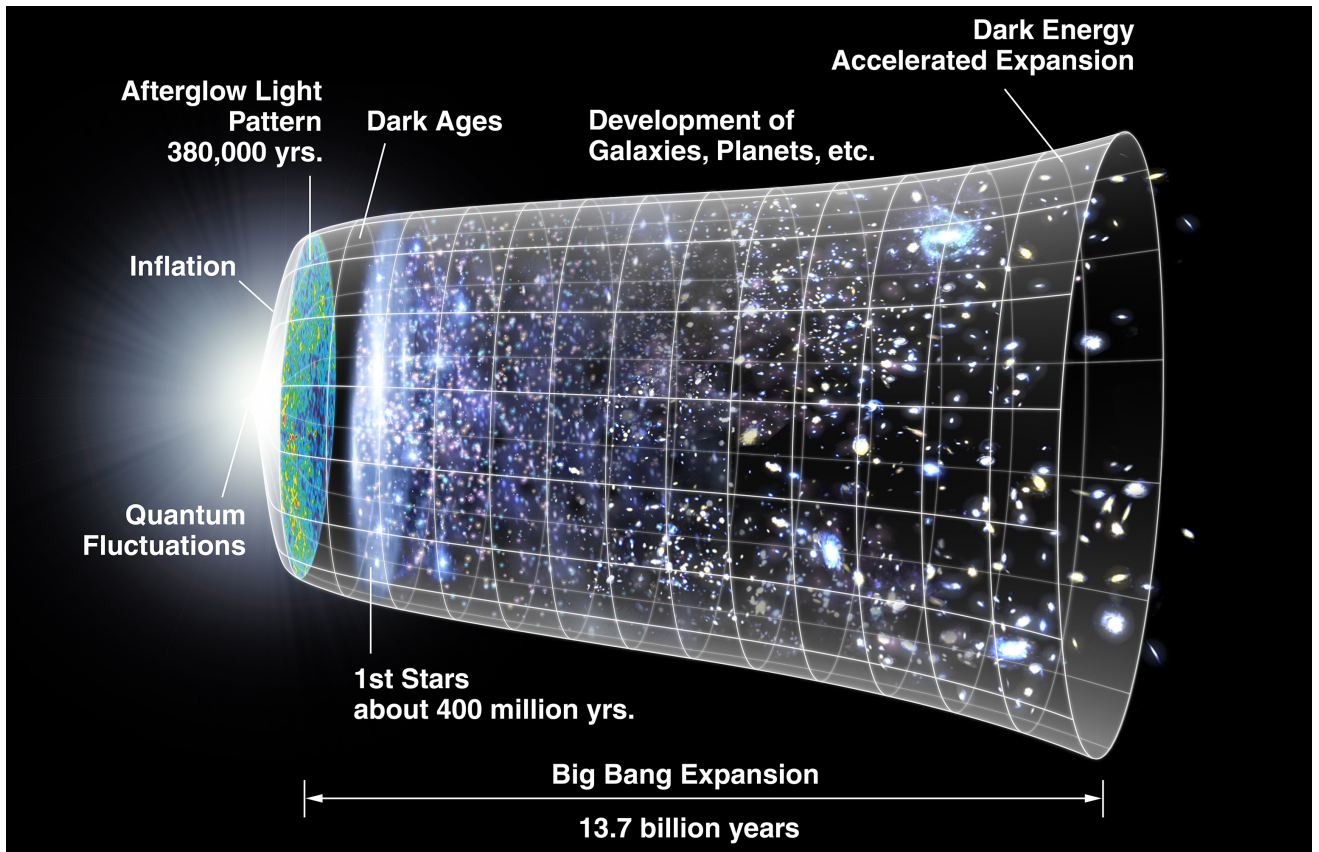
Figure 1.2: The history of the universe according to our current understanding. This image was created by NASA.

GeV. The breaking of this symmetry occurred around 10^{-12} s after the big bang. After this symmetry breaking, the universe consisted of a quark-gluon plasma. Quarks and gluons later became confined in baryons and mesons around 10^{-6} s after the big bang.

Neutrinos freeze out – decouple from other matter and radiation – around 0.2 s after the big bang. Reactions based on the weak force are no longer a factor in maintaining equilibrium, so the neutron / proton ratio freezes except for a slow decay of neutrons until they are stabilized in nuclei after BBN.

Electron / positron reactions completely annihilate the remaining positrons after the temperature drops below the mass of an electron and new pairs can no longer form readily around 1 s after the big bang. The annihilation heats up the photons, contributing to the higher cosmic microwave background temperature compared to the predicted cosmic neutrino background temperature.

BBN occurs about 3 min after the big bang. At this point, the temperature is low enough for nuclear reactions to be favorable, causing all the remaining neutrons to combine with protons to form nuclei. The resulting fractions are about 75% H and 25% He with some heavier elements. The remaining heavier elements will be formed much later in stars.

The matter/radiation equality, when $\rho_m = \rho_r$ is at around 75,000 years after the big bang.

Electrons are captured by nuclei at around 380,000 years after the big bang. This is called recombination, and at this time photons decoupled from charged particles and the universe became transparent. This is what we see when we observe the cosmic microwave background.

Structure formation begins after recombination, when gravity finally causes the inhomogeneities to form stars.

As the stars emitted radiation, the universe became reionized at some point in its history, although we do not know exactly when. This is a free parameter in our model, although it is known that $z_{reionization} > 6$ [26].

The final significant event known in our universe as a whole is the time of matter / dark energy equality. This is defined as when $\rho_m = \rho_\Lambda$ and is at around 10 billion years after the big bang [27].

1.3 Late 20th Century: Anisotropies or Measuring the CMB

By the end of the 20th century, we had entered the era of precision cosmology with the launch of the first satellite dedicated to cosmology. The big bang model had been confirmed as the only surviving explanation of all existing data. However, the model appeared to require precise initial conditions to explain certain features of our observations. Out of all of the models of the time to explain this, only inflation survived the comparison to data to become the modern standard. However, this model was found to have numerous conceptual issues.

1.3.1 The Era of Precision Cosmology

What is known as the era of precision cosmology got its start with the launch of the COBE satellite by NASA. Satellite based maps of the CMB enabled a bypassing of the atmospheric absorption of relevant frequencies of radiation, thus enabling the very precise measurements of CMB temperature required to measure the CMB anisotropies. The first results of COBE in 1989 confirmed the homogeneity and isotropy of the CMB to extreme precision, measuring a temperature of 2.735 K. In 1992, the first low resolution map of the anisotropies was released [28]. COBE was followed by WMAP in 2001 [29] and Planck in 2009 [30], providing a very precise map of the CMB. Supplemented by various ground based and balloon based measurements, this provides an extremely precise measurement a model must be able to reproduce.

1.3.2 Theoretical Issues

While the standard big bang model, when analysed using thermodynamics and our current understanding of nature worked well in explaining the structure of the universe (after dark matter and dark energy were added), there was a limit to how far back the calculations could take us. And it became clear that what happened before then was relevant for what we observe today. Several mysteries remained.

While the evolution of the universe seems to produce a uniform temperature, there is a fundamental issue – if evolved to past, not enough time to for all of the visible sky to become correlated. This is called the horizon problem. In addition, if universe is not exactly flat, it appears now to be close enough for the deviations to not be detectable.

Since the expansion of the universe is slowing down, the curvature should be getting more noticeable over time. So the curvature was even smaller at earlier times, requiring exact precision in the various energy densities. This is called the flatness problem.

In the 1970s, one more issue was noted. Theoretical calculations implied that the universe should be filled with magnetic monopoles [31, 32].

Later, as anisotropies began to be observed in the CMB, what was responsible for forming them and their precise shape also became important.

The Horizon Problem

A brief summary of the issue is that light required more time than there exists in universe to allow for the causal contact between disjoint regions of the universe required for them to have the same temperature. While the universe would have been smaller in the past, the distances between points decrease slower than the age of the universe decreases. This is because matter is slowing the expansion of the universe.

For a slightly more technical explanation, we can define a particle horizon to be the furthest light could have travelled from to still be able to reach us now given the finite age of the universe. We can calculate the maximum comoving distance

$$\chi_{max} = \tau_0 - \tau_{BB} = \int_{t_{BB}}^{t_0} \frac{dt}{a\left(t\right)} = \int_0^{a_0} \frac{1}{\dot{a}} \frac{da}{a}. \tag{1.26}$$

From this, we can see that for a value of $\ddot{a} < 0$, this will have a finite size. To find out how it varies, we can differentiate Equation 1.25 with respect to time. If we define for each type of effective energy density

$$\Omega_a \equiv \frac{8\pi G_N}{3H^2} \rho_a \tag{1.27}$$

to be its fraction of the critical density, we get,

$$\ddot{a} = a\Omega_\Lambda - \frac{1}{2a^2}\Omega_m - \frac{1}{a^3}\Omega_r. \tag{1.28}$$

We can see that a dark energy term will accelerate the expansion, while matter and radiation will slow it down. As Ω_Λ was much smaller in the past, $\dot{a}$ was shrinking, and the Hubble horizon $\frac{1}{aH}$ was thus growing. This means that as time goes on, larger comoving scales come into contact, so there are regions which are becoming visible now, but shouldn't have been in contact in order to thermalize in the past.

14

The Flatness Problem

From Equation 1.25, we see that there are four effective energy densities which must all add up to the critical density: ρ_m, ρ_r, ρ_Λ, and ρ_k. Each of these vary at a different rate with respect to the scale factor a. As a increases, ρ_r, dominant for small a values will loose its dominance to ρ_m, then ρ_k, and finally ρ_Λ. However, we do not see any curvature at all, and we are reasonably close to the matter / dark energy equality time. In order for the curvature to be undetectable now, it must have much smaller (by a factor of 10^{-30}) at early times in comparison to the other terms.

Anisotropies

A mechanism to produce anisotropies in order to provide an original deviation from homogeneity required to produce the structure seen in the universe does not exist without theory of the very early universe. However, we not only see structure in the universe, but also we can calculate the structure of the early anisotropies which produced it by analyzing the CMB.

The anisotropies in the CMB are small, on the order of 10^{-5} times the average temperature. When analyzed, the standard deviation of their two-point correlations fits a model with a primordial scalar power spectrum which is close to scale invariant scale invariance, with a slight red tilt. The spectrum is well fit by a power law with no running of the tilt as in Equation 1.1.

A Potential Solution

As discussed, with a decelerating universe, the Hubble horizon is growing, bringing into view more of the universe. However, if the universe instead accelerates, this process would be reversed, decreasing the field of view and making the universe appear flatter. This realization leads to the proposal of inflation, that the early universe went through a phase of rapid expansion and acceleration of that expansion. Combining inflation with quantum field theory, one can then produce a semi-classical approximation for the expected shape of the anisotropies emerging from this period of time.

1.3.3   A Summary of Inflation

Inflation is a conception developed in the 1980s [33, 34] to solve these issues by having the initial universe expand so rapidly that universe becomes approximately flat and the

comoving scales seen today are smaller than what were in causal contact in the early universe. In order to cause the expansion, the theorists needed to introduce some type of inflaton – typically a scalar field responsible for the inflation which decays away after inflating the early universe [35]. By applying quantum field theory in a curved spacetime background, one can produce calculations for the expected anisotropies by explaining them as coming from quantum fluctuations. They would be predicted here to be small, close to scale invariant, but with a red tilt, just as observed.

Anisotropies from Slow-Roll Inflation

In order to produce anisotropies, inflation takes advantage of quantum fluctuations of the inflaton field. During the inflationary phase, the system is close to the Planck scale, causing it to oscillate rapidly. As the system expands, comoving scales will leave the Hubble horizon and will freeze out, or stop changing. Calculations can show that if this were to go on forever, this would produce a scale invariant power spectrum. But the finite time of this phase of expansion combined with the details of the calculations will cause a power loss on smaller scales relative to the larger scales, creating a red shift in the power spectrum.

Inflation produces both scalar and tensor modes, of which only the scalar modes have been detected. The details of the spectrum depend on the model, although most of them match reasonably well even the very precise modern measurements.

The Basic Mathematics

The for the case of single-field slow-roll inflation, start with an action with only the metric and the inflaton being relevant. This action is

$$S = \int d^4x \sqrt{-g} \left[\frac{R}{16\pi G_N} - \frac{1}{2} g^{\mu\nu} \partial_\mu \phi \partial_\nu \psi - V(\phi) \right]. \tag{1.29}$$

We also define the slow-roll parameters

$$\epsilon = \frac{1}{2} \frac{m_{pl}^2}{8\pi} \left[\frac{V'(\phi)}{V(\phi)} \right]^2$$

and

$$\eta = \frac{m_{pl}^2}{8\pi} \frac{V''(\phi)}{V(\phi)}.$$

16

When these parameters are both $\ll 1$, the field is in a state of slow-roll, falling down the potential with negligible acceleration.

From the potential we can calculate the pressure and density of the field within the FRW spacetime. Our density is

$$\rho = \frac{1}{2}\dot{\phi}^2 + V(\phi) \tag{1.30}$$

and our pressure is

$$p = \frac{1}{2}\dot{\phi}^2 - V(\phi). \tag{1.31}$$

We can put this into Equation 1.22 to get

$$\ddot{\phi} + 3H\dot{\phi} + V'(\phi) = 0. \tag{1.32}$$

In the slow-roll regime, we can calculate $\dot{\phi}^2 \ll V(\phi)$, giving us a cosmological constant-like field and exponential expansion. The term slow-roll comes from the part of the approximation where the acceleration $\ddot{\phi}$ is negligible. Later, the system will leave the slow-roll exponential expansion as $V(\phi)$ decreases in comparison to the approximately constant $\dot{\phi}^2$.

The calculation of the leading order perturbations is more involved. By using quantum field theory, the uncertainties of the scalar $(\zeta(\tau, \vec{k}))$ and tensor $(h_{ij}(\tau, \vec{k}))$ perturbations can be calculated. The end result is a prediction of the power spectrum of perturbations after they leave the Hubble horizon. The power spectra are defined as

$$P_\zeta = \frac{d\langle 0| \hat{\zeta}^2(\tau, \vec{x}) |0\rangle}{d\ln k}, \tag{1.33}$$

and the results are

$$P_\zeta = \left[\frac{k}{2\pi z}\right]^2 \approx \frac{1}{2\epsilon}\left[\frac{H}{2\pi m_{pl}}\right]^2 \tag{1.34}$$

and

$$P_h(k) = \left[\frac{k}{2\pi m_{pl} a}\right]^2 = 8\left[\frac{H}{2\pi m_{pl}}\right]^2. \tag{1.35}$$

1.3.4   The Issues with Inflation

However, many issues remain. In order to have inflation, there must be some field driving the expansion, but no known fields would produce this effect. So to solve this issue, a new field, the inflaton, must be proposed. In order for this inflaton to not be observed, it must

decay away at the end of the inflationary phase. So the inflaton is specifically constructed to provide its intended effect and is not observed elsewhere, meaning the field and process has the effect of something put in by hand to cover up our lack of knowledge [35].

This has the added effect of allowing the construction of many inflation models with only the CMB to guide which ones are viable. This causes a loss in predictivity of the theory as it is adapted to new results since theorists can modify their theory to accommodate any contradictory result.

The next major critique is about what aspects of quantum mechanics are retained and what are ignored. Continuing with the standard semi-classical approximation required to calculate anisotropies, one can come to the conclusion that some small regions may fall out of the inflationary stage later, or even never. Due to the nature of inflation, these extremely unlikely regions will expand exponentially faster than the standard region, causing them to take up a much larger portion of the phase space volume. This has the effect of inverting probabilities in a sense, as seemingly unlikely possibilities become much more likely. Our theory now no longer predicts anything as it predicts everything should exist somewhere. This issue is called internal inflation, and those who take it seriously as a solution effectively construct a multiverse and use the anthropic principle to explain our universe [36, 37].

Others may question if it even makes sense to quantize the perturbations without quantizing the background metric. The reason this was done is due to the lack of a quantum theory of gravity, but the understanding inflation tries to impart may require a theory of quantum gravity to have any meaningful interpretations. An approximation may give predictions, but they will have limited precision and will not give true understanding [38].

And the notions such as the start of time and the origin of the universe have not been solved, only pushed back further.

1.3.5 Further Note

There is no reason to expect that inflation is the only explanation for our observations. The power law expansion of the anisotropies is a phenomenological expansion which happens to be able to be fit by inflationary models. Many of the observations which we currently use inflation to explain had been expected before inflation was developed (e.g. [39, 40]). Later models have been developed which can explain the observations without relying on inflation [41]. And the reason inflation works well may have to do with the fact that the math is the same or similar to the actual solution without the reason for it having

any relation to reality. Considering the mathematics of special relativity were worked out before Einstein proposed the theory, it would not even be unheard of in physics.

1.4 Experimental Tools

To compare inflation or alternative to model, we need to be able to match our models to the observational data. This means we need to know what our models predict in terms of what we would be able to measure. On the observational side, this means we need to know what to measure, how to remove as much noise as possible, and how to put the data in a form for which our models give us a prediction. On the model building side, this means we need to have a small number of parameters for which we fit and everything beyond that is calculated by numerically solving the equations governing the evolution of the system. In order to do this matching, we use specialized software developed to calculate the predictions of the models and analyze how well they fit to the data.

1.4.1 Model Parametrization

Each model has a number of parameters which determines the various components in the theory. Then each theory can be evolved through time using statistics and the laws of nature provided by the model. After the effects of the evolution are worked out, certain predictions will result of what the results of observations should be. The results will depend on the parameters, so we need to find the best fit parameters to match our theory.

Our standard model is ΛCDM. Any alternative or extension tends to draw from similar parameters and a similar structure of evolution of cosmology. Some parameters can be directly measured, while others can only be determined by a model fitting procedure. Parameters will fit into several types which can be grouped into astrophysical parameters, determining anything between the earliest times we can calculate and now, and primordial parameters, which measure what we detect from the early universe.

The astrophysical parameters are:

- H_0, the Hubble constant at the present. Once we have the present value for the Hubble constant, its history can be calculated. Often times, we will use 100θ, where θ is the angular scale of the sound horizon, instead of the Hubble constant in our parametrization, as this has a Gaussian probability distribution in our parameter space exploration.

- The present energy densities: ρ_b of baryons and ρ_c of cold dark matter are typically fit for, while ρ_ν is typically fixed. ρ_γ for photons is effectively zero at present, and ρ_Λ for dark energy is calculated from the constraint that the sum of all the densities must add up to the critical density, for the system to be spatially flat. If we were to extend this model, we can add in the contribution from curvature, ρ_k, to maintain the constraint even in the case with spatial curvature. These numbers can be rewritten in terms of their ratio to the critical density, Ω_x, and are often multiplied by a Hubble constant parameter $h = \frac{H_0}{100 km/s/Mpc}$ squared to get the Gaussian parameters $\Omega_b h^2$, $\Omega_c h^2$ and $\Omega_k h^2$.

- τ_{od}, the optical depth to reionization.

- The primordial helium fraction Y_{He} is typically calculated by our present best big bang neucleosynthesis model, but can also be varied as a parameter to determine how good this is.

- The exact details of neutrinos are unknown, so the parameters should be fit for. However, they do not have much effect on the shape of the CMB, so they are typically fixed instead. The two typical numbers expected to make some effect on the observed CMB are N_ν, the effective number of neutrinos, and Σm_ν, the sum of the masses of the neutrinos. N_ν is calculated from particle physics to be 3.046. Σm_ν is typically set to 0.06 eV, its minimum value according to present knowledge.

- The exact form of dark energy is unknown, but it is typically regarded as a cosmological constant, with no new parameters added to the model. Standard extensions of this model add in an unknown equation of state parameter w, which is -1 for the case of a cosmological constant. The model can be extended with another phenomenological parameter w_a, which introduces a linear dependence on a of the equation of state.

Primordial parameters are grouped based on what primordial power spectrum they describe. The parametrize the primordial power spectra. The typical parametrization for this spectrum is as a power law, given by Equation 1.1. Here, there are two unknown parameters, Δ_0^2, the overall amplitude and n_s, the tilt in power spectrum. The model can be further expanded to add a running term to the expansion parametrized by n_{run}:

$$\mathcal{P}(k) = \Delta_0^2 \left(\frac{k}{k_*}\right)^{(n_s-1)+\frac{n_{run}}{2}\ln\left(\frac{k}{k_*}\right)}. \tag{1.36}$$

The primordial perturbations are grouped into three types of power spectra: scalars, vectors, and tensors. Only scalars have been detected so far, and so only scalars will be covered here. Inflation typically predicts a form similar to the power law for both scalars and tensors[2], although the power law expansion itself is phenomenological and could be fit by other models, like bounce models.

1.4.2 Observation and Data

The CMB Maps

There are multiple sources of data with which to analyze the models. Of these, the largest and most publicized are the satellite-based full sky temperature and polarization maps. There are three such satellites: COBE launched in 1989 [28] and WMAP launched in 2001 [29] by NASA and Planck launched in 2009 [30] by the ESA. After analysis and processing by the scientific teams working on each of the satellites, the processed data is released publically, along with instructions for how to install the datasets for use with other analyses.

The basic function of the satellites are to map the effective temperature and polarization of photons at various frequencies across the entire sky. From this, the foreground needs to be removed to get the CMB maps[3] [30]. Having multiple frequencies, external observations of the foreground, good models for the foreground, and good masking techniques are all important to reduce the errors of this process while retaining as much useful data as possible. The satellite itself also has various imprecisions which can produce both systematic errors and noise. This process will add to our analysis nuisance parameters, additional parameters which need to be fit for in our analysis of the data.

The basic temperature and polarization maps are not what we need, however. In order for these to be useful, they need to be in the form of something calculable by our theory. Since our model is statistical, we do not have a prediction for what the temperature will be at certain points in the sky. We can, however, calculate the probabilities for various 2-point correlation functions at a given physical scale or size.

From the data, we have a two dimensional angular map of the sky. Such a map can be decomposed into spherical harmonics or multipoles, $Y_l^m(\theta, \phi)$, a spherical version of a

---

[2]For tensors, Δ_0^2 is replaced by r which gives the ratio between Δ_0^2 for tensors and Δ_0^2 for scalars, while n_s becomes n_t and n_{run} $n_{t,run}$.

[3]The foreground is used for other analyses, but for the purpose of the CMB, it is noise.

Fourier expansion. By performing the relevant integral,

$$a_{lm} = \int d\Omega \mathcal{M}\left(\theta, \phi\right) Y_{lm}^*\left(\theta, \phi\right), \tag{1.37}$$

with $\mathcal{M}$ being the map, the map can be converted from one based on angular positions $\theta = [0, \pi)$ and $\phi = [0, 2\pi)$ to one based on integers l and m, where $l = [0, \infty)$ measures the scale and $m = [-l, l]$ counts the particular mode with that scale. The monopole $l = 0$ gives the average temperature, and does not measure an anisotropy. The dipole $l = 1$ measures our particular velocity with respect to the rest frame of the CMB. So our analysis of the CMB anisotropies begins with $l = 2$ as the largest scale we can measure. The smallest scale is around $l = 2500$ for the Planck satellite data.

The second number we have is m which determines the direction and shape of each spherical harmonic. However, our theory does not predict the exact shape, only statistics. Given that the universe is isotropic, each such spherical harmonic with the same value of l gives us another sample from the same ensemble. This is important since we have only one universe, so we do not have anything else to increase the number of realizations and compare statistics.

The next thing we want to do is to reduce this data into the statistics of the anisotropies. For the case of a single anisotropy, the average a_{lm}, $\langle a_{lm} \rangle$, is by definition zero. But the variance $\langle a_{lm} a_{lm}^* \rangle \equiv C_l$ is not. This can be calculated from the theory and here from the observational data. Figure 1.3 shows a sample plot of these C_ls for the temperature data calculated from Planck and matched to ΛCDM.

Much of the error from Figure 1.3 comes from the cosmic variance:

$$\frac{\Delta C_l}{C_l} = \sqrt{\frac{2}{2l+1}}. \tag{1.38}$$

This is due to the limited number of samples of a given C_l we can observe, that number being $2l + 1$, the number of m values at a given value of l. The rest of the error comes from the instruments and the data cleaning. For higher values of l, the ls can be binned and averaged in order to increase the number of samples and reduce all the errors. For the Planck data, this is done starting at $l = 30$ for every 30 ls. Below $l = 30$, as much of the data as possible for comparison is kept and compared to theory.

We can measure three signals from the CMB, temperature (T) and two polarizations. The polarization channels can be split into a curl-free component called E and a gradiant-free component called B. An analysis of the mathematics involve tell us that we expect to calculate variances for TT, TE, EE, and BB, but not TB or EB. In addition, ET will be

22
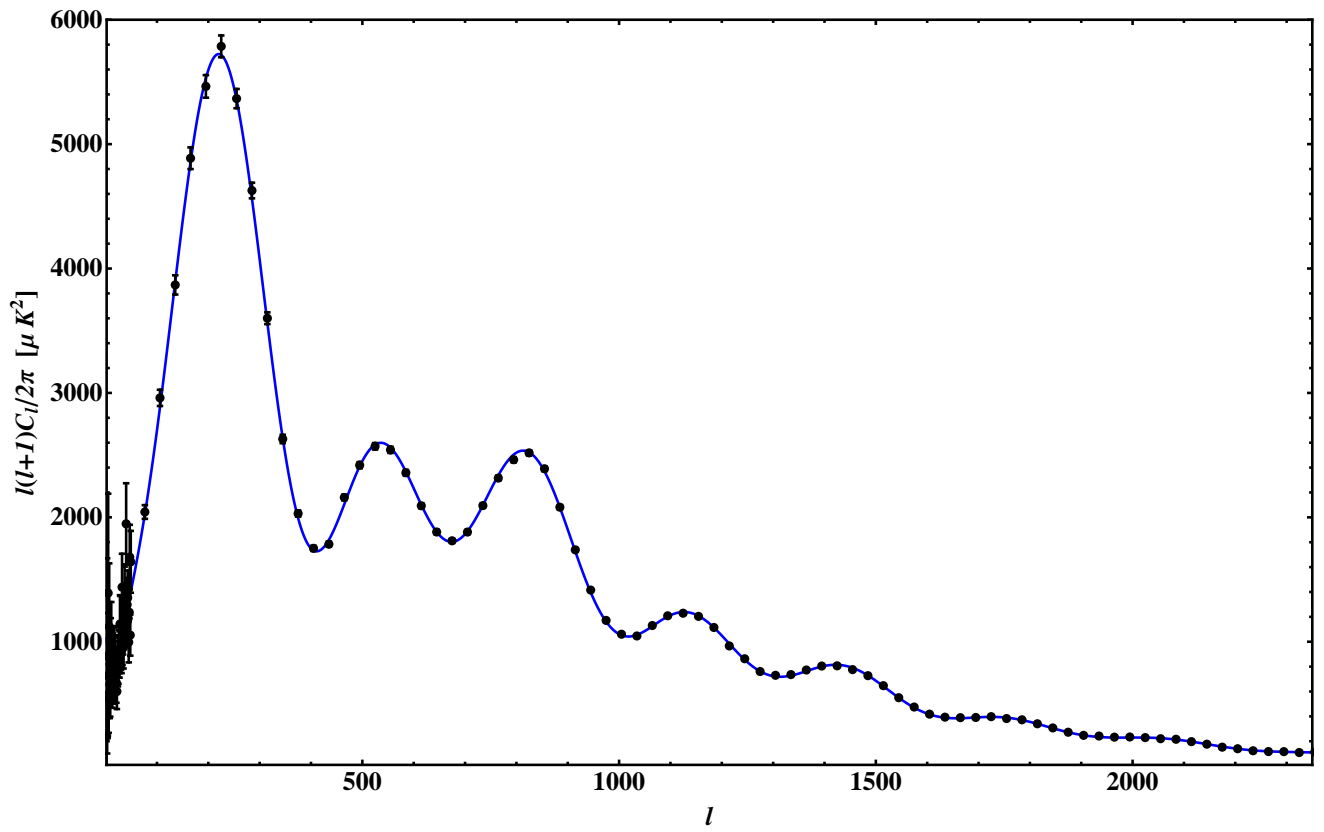
Figure 1.3: A sample plot of the fit of the Planck data to the ΛCDM model. The TT angular power spectrum is shown along with Planck error.

identical to TE. Signal in the BB channel will not be produced by scalar perturbations in the primordial power spectrum, but can be produced both by tensors and contaminants.

In addition to temperature and polarization data, Planck also produced a map of gravitational lensing, the distortions in the CMB due to the bending of light by gravity. This data is required for an accurate matching of observation to theory.

Other Measurements

Besides the satellite data, multiple ground based measurements provide additional constraints on the CMB parameters. One such measurement is of baryonic acoustic oscillations (BAO). This is an effect produced by sound waves through the baryons and photons in the early universe. At recombination, the baryons and photons loose contact, so the sound waves can no longer propagate and become frozen [42]. A characteristic sound horizon can be calculated based on speed of sound and the age of the universe when the sound waves stopped propagating. This is calculated to be about 150 Mpc. This produces characteristic peaks in both the CMB and the distribution of matter in the universe. Several ground-based measurements of BAO exist, measuring the distribution of matter in the universe, including the Sloan Digital Sky Survey in the US [43, 44, 45, 46], the 6dF Galaxy Survey in Australia [47], and the WiggleZ Dark Energy Survey in Australia [48].

Other teams have made independent measurements of various ΛCDM parameters. This includes measurements of the current Hubble constant [49, 50, 51], dark energy [52, 53, 54, 55], and the optical depth to reionization [26].

An additional dataset comes from a joint analysis by the BICEP2/Keck team and the Planck team [56]. This measured the contamination of the B-mode power spectrum by galactic dust. While in the CMB, only tensor modes will produce B-modes in the power spectrum, astrophysical sources such as dust can also produce them. In the BICEP2 analysis, B-modes had been detected in excess of the original dust models. Comparing this to Planck, however, revealed that this was dust contamination. This does provide an additional source of observational data for the match to theory, however.

1.4.3 Analysis

In order to calculate the predictions of a model, we need a few things. We need to calculate what a given realization of a model predicts for the observed data, and we need a means to find the best fit parameters for the model and their distribution to determine if the fit indicates viability of the model. For both these steps, we use the computer.

Boltzmann Equations

Our first tool will be a Boltzmann integrator. Here we use CAMB [57, 58, 59], which like all of these codes is based on CMBFAST [60, 61]. The goal is to calculate either backwards or forwards the expected distribution of matter now given a certain primordial power spectrum from the early universe and a number of parameters in our model. We will then need to put this in terms of what we can observe.

The initial conditions are given the primordial power spectrum. However, it turns out that the details of the evolution of matter can be calculated independently of the initial conditions, although the full predictions will require them.

The evolution is given by the Boltzmann equations, which are used to calculate non-equilibrium thermodynamics by keeping track of all interactions. The form of these equations are

$$\frac{df}{dt} = C\left[f\right],\tag{1.39}$$

where f is the distribution function of the particles in a system and C is a sum of collision terms. Both sides are calculated from the laws of nature governing the system.

For our case, we will use general relativity for the interactions between the metric and various energies, specifically linearized gravity over an FRW background metric as our perturbations are expected to be small. The case for which this is expected to be changed is for modified gravity theories as the approximation holds for all times of our analysis. In addition to this, we will need to account for electromagnetic interactions between electrons, protons and photons.

When we do this analysis, we need to ensure that we work in a unified gauge, although the gauge can be converted. CAMB uses the synchronous gauge in the cold dark matter rest frame. It also uses Fourier space as this simplifies the result. The result will be a system of differential equations, which can be solved numerically, although some fitting function approximations also exist.

Gravity is linearized by splitting the metric into a background $g_{\mu\nu}$ and its perturbations $h_{\mu\nu}$. In the synchronous gauge, $h_{00} = 0$ and $h_{0i} = 0$. The metric is defined by

$$ds^2 = a^2\left(\tau\right)\left[-d\tau^2 + \left(\delta_{ij} + h_{ij}\right)dx^i dx^j\right],\tag{1.40}$$

where h_{ij} is the metric of perturbations Fourier transformed to

$$h_{ij}\left(\vec{x}, \tau\right) = \int d^3k e^{i\vec{k}\cdot\vec{x}}\left[\hat{k}_i\hat{k}_j h\left(\vec{k}, \tau\right) + \left(\hat{k}_i\hat{k}_j - \frac{1}{3}\delta_{ij}\right)6\eta\left(\vec{k}, \tau\right)\right].\tag{1.41}$$

25

For matter and radiation, $\delta\left(\vec{k}, \tau\right)$ represents the Fourier transformed density perturbations, while $v\left(\vec{k}, \tau\right)$ represents the velocity perturbations. For radiation, we also have σ which represents the shear, and F_l for $l > 2$ represent the higher Legendre components averaged over momentum. We also define the conformal Hubble constant $\mathcal{H} = a^{-1}\frac{da}{d\tau}$

The equations are: [62] for photons

$$\dot{\delta}_\gamma = -\frac{4}{3}ikv_\gamma - \frac{2}{3}\dot{h}, \tag{1.42}$$

$$ik\dot{v}_\gamma = k^2\left(\frac{1}{4}\delta_\gamma - \sigma_\gamma\right) - \dot{\tau}_{od}\left(ikv_b - ikv_\gamma\right), \tag{1.43}$$

$$2\dot{\sigma}_\gamma \equiv \dot{F}_{\gamma 2} = \frac{8}{15}ikv_\gamma - \frac{3}{5}kF_{\gamma 3} + \frac{4}{15}\dot{h} + \frac{8}{5}\dot{\eta} + \frac{9}{5}\dot{\tau}_{od}\sigma_\gamma - \frac{1}{10}\dot{\tau}_{od}\left(G_{\gamma 0} + G_{\gamma 2}\right) \tag{1.44}$$

$$\dot{F}_{\gamma l} = \frac{k}{2l+1}\left[lF_{\gamma(l-1)} - (l+1)F_{\gamma(l+1)}\right] + \dot{\tau}_{od}F_{\gamma l} \tag{1.45}$$

$$\dot{G}_{\gamma l} = \frac{k}{2l+1}\left[lG_{\gamma(l-1)} - (l+1)G_{\gamma(l+1)}\right] - \dot{\tau}_{od}\left[-G_{\gamma l} + \frac{1}{2}\left(F_{\gamma 2} + G_{\gamma 0} + G_{\gamma 2}\right)\left(\delta_{l0} + \frac{\delta_{l2}}{5}\right)\right] \tag{1.46}$$

for matter and dark matter,

$$\dot{\delta}_c = -\frac{1}{2}\dot{h}, \tag{1.47}$$

$$\dot{\delta}_b = -ikv_b - \frac{1}{2}\dot{h}, \tag{1.48}$$

$$ik\dot{v}_b = -ik\mathcal{H}v_b + c_s^2k^2\delta_b + ik\dot{\tau}_{od}\frac{4\bar{\rho}_\gamma}{3\bar{\rho}_b}\left[v_b - v_\gamma\right]; \tag{1.49}$$

and for neutrinos,

$$\dot{\delta}_\nu = -\frac{4}{3}ikv_\nu - \frac{2}{3}\dot{h}, \tag{1.50}$$

$$ik\dot{v}_\nu = k^2\left(\frac{1}{4}\delta_\nu - \sigma_\nu\right), \tag{1.51}$$

$$2\dot{\sigma} \equiv \dot{F}_{\nu 2} = \frac{8}{15}ikv_\nu - \frac{3}{5}kF_{\nu 3} + \frac{4}{15}\dot{h} + \frac{8}{5}\dot{\eta} \tag{1.52}$$

$$\dot{F}_{\nu l} = \frac{k}{2l+1}\left[lF_{\nu(l-1)} - (l+1)F_{\nu(l+1)}\right] \tag{1.53}$$

An additional set of equations can be added for dark energy if it is not a cosmological constant. In CAMB, the equations for evolution are

$$\dot{\delta}_i + 3\mathcal{H}\left(1 - w_i\right)\left(\delta_i + 3\mathcal{H}\left(1 + w_i\right)v_i/k\right) + \left(1 + w_i\right)kv_i + 3\mathcal{H}\dot{w}_i v_i/k = -3\left(1 + w_i\right)\dot{h} \quad (1.54)$$

$$\dot{v}_i - 2\mathcal{H}v_i + kA = k\delta_i/\left(1 + w_i\right), \quad (1.55)$$

where A is the vector potential for the perturbed metric, giving $h_{ij}^{\perp} = \partial_i A_j + \partial_j A_i$, where $h_{ij}^{\perp}$ is the transverse component of the perturbation metric, given by $\partial_i \partial_j h_{ij}^{\perp} = 0$.

While it would seem that to solve these, we need to know the initial conditions, in practice we do not. These equations have several modes, for which the most important are the two adiabatic modes. Of these, there is a growing mode and a shrinking mode, and only the growing mode is relevant. We do need the Hubble constant $H\left(t\right)$ and the optical depth $\tau_{od}\left(t\right)$, however. $H\left(t\right)$ comes from the Friedmann equation. If we know H_0 and the various ρ_0s, we can calculate this using Equation 1.25. τ_{od} comes from our definition of optical depth, such that

$$\dot{\tau}_{od} = -n_e \sigma_T a. \quad (1.56)$$

This depends on time only through the scale factor a in a known way. The only complication in our model comes from the number density of electrons. We know that the CMB comes from the surface of last scattering which occurred when the electrons became bound in atoms. We know, however, that we have free electrons again after reionization. The time to reionization is unknown, but is given by the parameter for the optical depth to reionization.

Now that we have our perturbations, we can use this to calculate observation. We first calculate,

$$a_{l,m} = \int \frac{d^3 k}{\left(2\pi\right)^3} e^{i\vec{k}\cdot\vec{x}} \int d\Omega Y_{l',m'}^{*}\left(\hat{p}\right) \delta_\gamma\left(\vec{k}, \hat{p}, \tau\right), \quad (1.57)$$

then move to C_l space using the definition

$$\langle a_{lm} a_{l'm'}^{*}\rangle = \delta_{ll'}\delta_{mm'}C_l. \quad (1.58)$$

The Parameter Distribution

Now that we have a model which we can compare to data, we need to have a means of finding the best fit parameters of that model. One of the most computationally efficient methods of exploring a parameter space with a large number of parameters is randomly. This type of random simulation goes by the name of Monte Carlo Markov Chain or MCMC.

The standard such algorithm is called the Metropolis–Hastings algorithm [63, 64]. It is effectively a thermodynamic simulation, which will first approach the minimum value, then randomly explore that region of parameter space with a probability based on how likely the values of the parameters are when compared to data.

The output of such a method is a chain, a list of the sets of parameters and likelihoods of those parameters sampled in order, accompanied with the number of times the algorithm remained on that value.

The code we use for this exploration goes by the name of CosmoMC [65, 66]. It has the advantage of already being integrated with CAMB and being set up to use the cosmological data sets. It uses the Metropolis–Hastings algorithm adapted for separating out "faster" nuisance parameters from the "slower" model parameters. Once it constructs the chains using an MCMC simulation, it has another algorithm for processing the chains into a mean and standard deviation for each parameter, as well as being able to plot the distributions of likelihoods of various parameter values for either one or two parameters at a time.

If instead of a distribution, we just want the most probable set of parameters, we can use a minimizer algorithm. CosmoMC uses Powell's 2009 BOBYQA bounded minimization routine [67]. This algorithm converges faster, but only gives a better minimum than a full run of CosmoMC if it uses the mean calculated from CosmoMC as the starting point. This is probably due to getting stuck in local minimums, for which it is known to do when there is a large number of parameters over which to minimize.

The usefulness of this algorithm, thus, is not to get a fast convergence, but to find the best fit set of parameters after one gets the distribution. From this, one can calculate a value for the likelihood of the data given the model: $\mathcal{L} = -\log\left(likelihood\right)$. An alternative measure of this is $\chi^2 = 2\mathcal{L}$. If one takes the difference of this for two models, the square root $\sqrt{\chi_a^2 - \chi_b^2}$ gives the deviation. A difference of $< 1\sigma$ is considered insignificant, while a difference of $> 3\sigma$ can be considered to rule out the less likely model.

Bayesian Evidence

Bayesian evidence is an alternate method to likelihood of calculating how well a model fit the data. Instead of calculating the likelihood of the data given the model like χ^2 accounts for, Bayesian evidence uses Bayes' Theorem in order to estimate the probability of a model given the data. The advantage of this method is that it will naturally prefer models with fewer parameters, allowing for the easy comparison of models with an unequal number of parameters. The disadvantage is that the calculation is dependent on the choice of priors.

Bayes' Theorem inverts an event and its condition in a probability condition. When applied to a model and its data, it takes the form of

$$E = \int d\alpha_M P(\alpha_M) P(D|\alpha_M), \qquad (1.59)$$

where α_M is the set of parameters that specify the model and D is the data. Here, $P(D|\alpha_M)$ is the probability for obtaining the data D given parameters α_M, which is the same as the likelihood $\mathcal{L}(\alpha_\mathcal{M}) = \frac{\chi^2}{2}$ from the more typical χ^2 calculation. $P(\alpha_M)$ is the prior probability for the parameters.

Commonly, flat priors are used, assuming equal probability for all underlying models. This means $P(\alpha_M) = $ const. for all values of α_M which we consider viable, while it vanishes otherwise. Then, the evidence integral becomes

$$E = \frac{1}{\text{Vol}_M} \int_{\text{Vol}_M} d\alpha_M \mathcal{L}(\alpha_\mathcal{M}), \qquad (1.60)$$

where the integral is over the region of the parameter space in which the prior probability distribution is non-zero and Vol_M is the volume of this region.

A detailed exposition of this method can be found in [68, 69, 70] and references therein. To compute (1.60), MultiNest [71, 72, 73] was used.

1.5 Questioning the Orthodoxy: Alternative Explanations for the Early Universe

As described in Sections 1.3.4 and 1.3.5, although inflation has worked extremely well in order to predict observations, it appears to have many conceptual issues. To deal with this aspect, many have attempted to find alternative solutions which provide the same or similar calculations while providing a much different picture of the history of the universe. Hopefully such things will provide predictions to use in order to distinguish them from inflation.

1.5.1 What it Means to Question the Standard Model

In our search for the correct explanation of the universe, we need to try new alternatives, explore, and attempt to find our erroneous assumptions. We acknowledge all the strengths

of where we came from as we continue our explorations. We know in the past that we have reached the limits of our previous understandings and needed to find something new. Not everything we explore will work, but we keep looking for insights which may allow us to further understand the universe.

1.5.2 Lessons from the Development of Relativity

As referred to in Section 1.3.5, in the development of special relativity, the transformations Einstein developed were first developed earlier. Before special relativity, people believed in the existence of an aether through which light travelled. After the Michelson and Morley experiment in 1887 showed no aether wind [74], Lorentz and others developed a transformation which would allow for the speed of light to remain constant and explained it in terms a distortion in the forces between molecules [75]. In 1905, Einstein rederived these equations, this time using a less bulky explanation which allowed space and time to rotate into each other [9].

1.5.3 Bounce and Cyclic Models

The main category of theories alternative to inflation to describe the big bang and early universe are bounce models. The basic idea of a bounce model is that the initial singularity did not exist. Instead, the early universe began as the scale factor shrunk down to a minimum a_{min} before it started expanding again. If this process repeats, it can produce a cyclic model. While many conceptions of this now are based on quantum gravity considerations, it is possible to construct an FRW metric with this property. To do this, it is necessary to violate at least the strong energy condition [76].

However, the basic bounce and cyclic models were ruled out, or at least determined to be implausible, before dark energy was observed. For a bounce model, one has to account for an additional effective density term in the Friedmann equation relevant for anisotropic universes:

$$\rho_{aniso}\left(t\right) = \frac{\rho_{aniso}}{a^6}. \tag{1.61}$$

This term becomes irrelevant for expanding universes, but as the universe collapses, this will dominate over the other densities [40]. Its effect will cause the universe to stretch in some directions and collapse in others, creating a chaotic mixmaster behavior as the average scale factor goes to zero. Setting $\rho_{aniso} = 0$ exactly leads to the same questions of fine-tuning which inflation nominally avoid.

For a cyclic model, there was the question of entropy. Tolman's original cyclic model required each cycle to have more entropy than the previous, until it eventually couldn't contract any more. If this was examined in the opposite direction, each previous cycle would be shorter until it shrunk to nothing, beginning at a finite time in the past, preventing this model from solving the issue of requiring a beginning of time [77].

Now, however, they provide the leading contender to inflation and present a solution to the issues described in Section 1.3.4. A basic bounce will use the late phase dark energy we now observe to replace the inflaton in shrinking the Hubble horizon. This connects what we see now to explain what we observe in the past, and avoids quantum gravity and producing a scalar which would not be observable [41]. To deal with the issue of anisotropy in the scale factor, it is common to introduce an exotic matter with an equation of state $w > 1$ [78]. The density will vary with the scale factor as $a^{(-1-w)}$, disappearing in an expanding universe, but dominating over the anisotropic term in a contracting one.

1.5.4 Quantum Gravity

Inflation relies on semi-classical gravity where the metric is classical while the matter is not. Semi-classical gravity is probably not how the universe works, although it is used commonly as an approximation as we do not have a proven theory of quantum gravity. Since the mathematics of inflation appears to match observations very well, the calculation may be valid, although further analysis of the conceptions have questioned if there would be an issue of eternal inflation if the conceptions behind the calculations are valid.

As an alternative to semi-classical gravity, one may try to solve the candidate quantum gravity models and tools which do exist for what one would expect to observe in the early universe. At least some of these analyses imply a bounce rather than inflation.

1.6 Outline

This document covers four different classes of models on which I have worked which attempt to solve the issues solved by inflation while avoiding the issues of inflation. Each of these conceptions posit a different structure for the observable primordial power spectrum from the power law expansion. In working with these, I have used the described code to compare the new models to the standard power law expansion to determine their viability.

In Chapter 2, I discuss Holographic Cosmology. Holographic Cosmology uses the holographic principle to solve for the structure of space-time emerging from the early universe.

Because dualities, like those conjectured by the holographic principle, invert the coupling strength of a theory, the typical inflationary case would be representable by its holographic dual but unsolvable perturbatively. However, there is a solution which can be solved perturbatively without a well-defined space-time manifold at early times, for which I analyzed in CosmoMC.

Chapter 3 discusses my Periodic Time Cosmology model. By positing that our universe closes back on itself instead of going through an infinite cycle of expansion and collapsing, we can reuse the effects of matter and energy on the original primordial power spectrum to form the same power spectrum in the infinite future. A conformal rescaling to match the future and past allow for this structure to match observations.

For Chapter 4, I discuss a model based on the Holographic Big Bang model of R. Pourhasan, N. Afshordi, and R. B. Mann. In this, our universe exists on a 3-brane formed outside of a collapsing 5D star. Its travel through the star's atmosphere produces a calculable, approximately scale-invariant primordial power spectrum.

And in Chapter 5, I describe my work on the extension beyond quantum mechanics of an alternative, hidden variable model for quantum mechanics. Here, I show that the model will converge to quantum mechanics given reasonable deviations from it. The model has non-local, and therefore faster than light communication, which out of quantum mechanical equilibrium should allow for signalling. If this is correct, then this faster than light signalling could solve the horizon problem.

Chapter 2

Constraining holographic cosmology using Planck data

2.1 Introduction

Insight from the study of black hole entropy has long indicated that gravity might have a holographic nature [79, 80], *i.e.* that there is a dual quantum field theory (QFT) in one lower dimension without gravity. This principle, the holographic principle, should also apply to the early universe. Explicit examples of holographic dualities were found in string theory [81]. However, these cases tend to apply to theories with a negative cosmological constant, which is in contrast to cosmological observations.

The extension of the duality to de Sitter space-time and cosmology was considered soon after the initial work on Anti-de Sitter space [82, 83, 84, 85, 86]. In the cosmological context, the statement of the duality is that the partition function of the dual QFT computes the wave-function of the universe [86], using which, cosmological observables may be obtained. These dualities are less understood than the standard AdS/CFT duality, in part because we currently have no explicit realization in string theory. Nevertheless, one may set-up a holographic dictionary [87, 88, 89, 90, 91] using a correspondence [92] between cosmological accelerating solutions and holographic renormalization group (RG) flows, solutions that admit standard holographic interpretation.

In this duality, time evolution is mapped to inverse renormalization group flow and the physics of the early universe is mapped to the IR physics of the dual QFT. Thus, depending on the nature of the IR, we have different cosmological scenarios. Here we test theories for

the very early Universe against the cosmic microwave background (CMB) data, so more precisely we would like to know what the dual QFT is which is relevant at the energy scales probed by the CMB.

One of the main properties of the holographic dualities is that they are strong/weak coupling dualities. This means that when one of the two sides is strongly coupled, and therefore difficult if not impossible to solve, the other side is weakly coupled, and solvable perturbatively. Therefore a weakly coupled inflationary period is dual to a strongly coupled quantum field theory. While work has been done in using holography in this setting (see [93, 94, 95, 96, 97, 98, 99, 100, 101, 102, 103, 104, 105, 106, 107, 108, 109, 110] for a sample of works in this direction) we here mainly examine the opposite case. This is the case of a strongly coupled gravitational theory. In this case, the early universe does not have a well defined geometry. It can not be examined without quantum gravity. However, the dual QFT not only can be examined, but is weakly coupled and solvable perturbatively. This is the alternative model we examine, which we call the holographic model or holographic cosmology here.[1] In this case the dual QFT is a super-renormalizable three-dimensional QFT.[2] This model for the very early Universe was first proposed in [87] and it was subsequently analyzed in [88, 89, 90, 91, 114, 115]. A sketch of the Penrose diagram describing holographic cosmology is shown in Figure 1.

Previously, this holographic model had been compared to WMAP7. It was found to be viable [116, 117] but mildly disfavoured relative to ΛCDM. With the release of the Planck data, it is time to reexamine the viability of the holographic model for early universe cosmology. Our results were announced in [118] and the purpose of this work is to provide a more detailed and comprehensive discussion of their derivation.

The structure of this chapter is as follows. In Section 2.2, we describe the two models we are comparing. In Section 2.3, we find and explain the best fit model. Section 2.4 explains how well the two models fit the data and compare to each other. Finally, in Section 2.5 we present some concluding remarks.

---

[1]As inflation is also holographic, this is a potentially confusing terminology. Here we want to distinguish between a cosmology which has a conventional space-time description (inflation) and one without such description (holographic cosmology).

[2]An example of such QFT is the worldvolume theory of coincident D2-branes. The holography nature of this theory is well established [111, 112, 113].
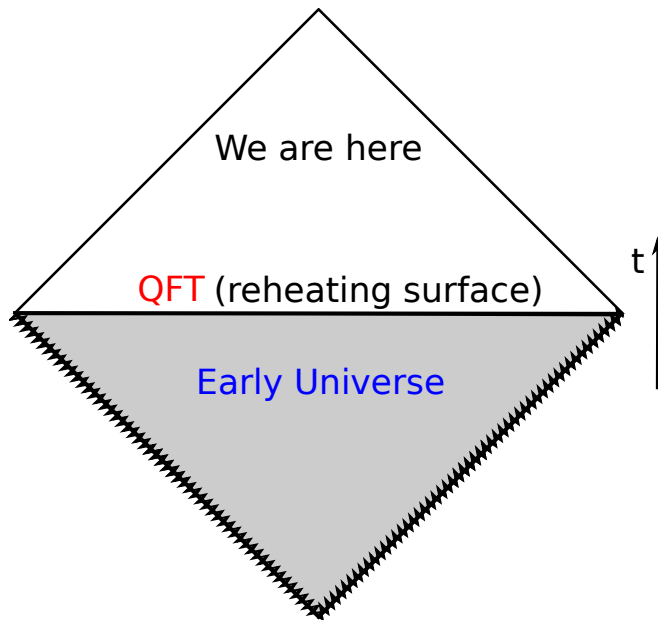
Figure 2.1: A sketch of the Penrose diagram describing holographic cosmology (HC). The early Universe is non-geometric and is described by a dual QFT, which is located at the end of the non-geometric phase.

2.2 Models

2.2.1 Holography for cosmology: basics

The idea of holography for cosmology is that the dual QFT computes the wavefunction of the Universe [86]. Schematically, this works as follows: The wavefunction is equal to the partition function of the dual QFT,

$$\psi(\Phi) = Z_{QFT}[\Phi], \tag{2.1}$$

where Φ on the left-hand side denotes collectively gravitational perturbations and on the right-hand side sources that couple to gauge invariant operators. Note that we consider the wavefunction of perturbations only here. Cosmological observables may be computed using standard quantum mechanics

$$\langle \Phi(x_1) \cdots \Phi(x_n) \rangle = \int D\Phi |\psi|^2 \Phi(x_1) \cdots \Phi(x_n), \tag{2.2}$$

where the correlators are evaluated at end of the early universe phase (for example, at the end of the inflationary phase, if inflation describes the very early universe). Using that $Z_{QFT}[\Phi]$ may be expressed in terms of correlation functions

$$Z_{QFT}[\Phi] = \exp\left(\sum_n \frac{(-1)^n}{n!} \langle O(x_1) \cdots O(x_n) \rangle \Phi(x_1) \cdots \Phi(x_n) \right), \tag{2.3}$$

where O denotes the gauge invariant operators to which Φ couples.[3] We now may express cosmological observables in terms of QFT correlation functions. If the QFT is strongly coupled, then the bulk is described by Einstein gravity and these results should match those coming from standard inflationary cosmological perturbation theory, while if the QFT is weakly coupled the bulk is non-geometric.

There is currently no first principles derivation of the QFT relevant for cosmology but one may use the domain-wall/cosmology correspondence [92] to map the cosmology problem to that of standard gauge/gravity duality, then use the QFT dual to the domain-wall and finally map the results back to cosmology [87, 88].[4] This leads to the following

---

[3]We take the QFT to be Euclidean, though this is not essential.

[4]There is a proposed duality [119] where the QFT is defined a priori (i.e. without the need to map the problem to the domain-wall first) but in this case the bulk involves Vasiliev's higher spin gravity instead of Einstein gravity.

holographic formulae for the scalar and tensor spectra, $\mathcal{P}$ and $\mathcal{P}_T$, respectively,

$$\mathcal{P}(q) = -\frac{q^3}{16\pi^2}\frac{1}{\mathrm{Im}B(q)}, \quad \mathcal{P}_T(q) = -\frac{2q^3}{\pi^2}\frac{1}{\mathrm{Im}A(q)}, \tag{2.4}$$

where A, B are extracted from the momentum space 2-point function of the energy momentum tensor T_{ij},

$$\langle\langle T_{ij}(q)T_{kl}(-q)\rangle\rangle = A(q)\Pi_{ijkl} + B(q)\pi_{ij}\pi_{kl}. \tag{2.5}$$

Here $\langle T_{ij}(q_1)T_{kl}(q_2)\rangle = (2\pi)^3\delta^3(q_1+q_2)\langle\langle T_{ij}(q_1)T_{kl}(-q_1)\rangle\rangle$, $\pi_{ij} = \delta_{ij} - q_iq_j/q^2$ is a transverse projector and $\Pi_{ijkl} = 1/2(\pi_{ik}\pi_{jl}+\pi_{il}\pi_{jk}-\pi_{ij}\pi_{kl})$ is a transverse-traceless projector. In other words, the scalar power spectrum is associated with the 2-point function of the trace of the energy-momentum tensor while the tensor power spectrum is related with the transverse-traceless part of the 2-point function. These formulae were derived for QFTs that admit a 't Hooft large N limit and they either become conformal in the UV or approach a QFT with a generalized conformal structure (where generalized conformal structure is explained in the next subsection). The imaginary part in (2.4) is taken after the analytic continuation,

$$q \to -iq, \quad N \to -iN, \tag{2.6}$$

where q is the magnitude of the momentum vector and we assume that we are dealing with an $SU(N)$ gauge theory coupled to matter in the adjoint representation, as is the case below.[5] Similarly, one can relate the bispectra with 3-point functions of the energy momentum tensor [89, 90, 91].

When the QFT is strongly coupled, the bulk is geometric and there is a conventional description in terms of quasi-de Sitter or power law inflation. In these cases, (2.4) correctly reproduces the results of cosmological perturbation theory [87, 88]. Here we focus on the opposite regime where the QFT is weakly coupled.

2.2.2 Non-geometric models

In non-geometric models, the theory is defined by giving the dual QFT. Here we analyze the model proposed in [87, 88], in which the QFT is an $SU(N)$ gauge theory coupled to scalars Φ^M and fermions ψ^L, where M, L are flavor indices. The action is given by

$$S = \frac{1}{g_{\mathrm{YM}}^2}\int d^3x\,\mathrm{tr}\left[\frac{1}{2}F_{ij}F^{ij} + \delta_{M_1M_2}\mathcal{D}_i\Phi^{M_1}\mathcal{D}^i\Phi^{M_2} + 2\delta_{L_1L_2}\bar{\psi}^{L_1}\gamma^i\mathcal{D}_i\psi^{L_2}\right.$$

$$\left.+\sqrt{2}\mu_{ML_1L_2}\Phi^M\bar{\psi}^{L_1}\psi^{L_2} + \frac{1}{6}\lambda_{M_1M_2M_3M_4}\Phi^{M_1}\Phi^{M_2}\Phi^{M_3}\Phi^{M_4}\right], \tag{2.7}$$

---

[5]In the case of a large N vector model, we need $N \to -N$.

37

where all fields, $\varphi = \varphi^a T^a$, are in the adjoint of $SU(N)$ and $\mathrm{tr} T^a T^b = \frac{1}{2}\delta^{ab}$. F_{ij} is the Yang-Mills field strength, and $\mathcal{D}$ is a gauge covariant derivative. The Yukawa couplings μ and the quartic-scalar couplings λ are dimensionless, while g_{YM}^2 has dimension 1.

This theory is superrenormalizable and has the important property that has a "generalized conformal structure." This means that if one promotes g_{YM}^2 to a new field that transforms appropriately under conformal transformation, the theory becomes conformally invariant [120, 113]. Related to this: if one assigns "4d dimensions" to the fields, $[A] = [\Phi^M] = 1, [\Phi^L] = 3/2$, then all terms in the action scale the same way. While this is not a symmetry of the theory, it still has implications.

In our case, the generalized conformal structure and the large N limit implies that the 2-point function takes the form

$$A(q, N) = q^3 N^2 f_T(g_{\mathrm{eff}}^2), \qquad B(q, N) = \frac{1}{4} q^3 N^2 f(g_{\mathrm{eff}}^2) \tag{2.8}$$

where $f_T(g_{\mathrm{eff}}^2)$ and $f(g_{\mathrm{eff}}^2)$ are (at this stage) general functions of their argument and $g_{\mathrm{eff}}^2 = g_{YM}^2 N/q$ is the effective dimensionless 't Hooft coupling constant. The factor q^3 reflects the fact that the energy momentum tensor has dimension 3 in three dimensions and the factor of N^2 is due to the fact that we are considering the leading term in the large N limit. The factor of $1/4$ in B is conventional.

Under the analytic continuation (2.6)

$$q^3 N^2 \to -i q^3 N^2, \qquad g_{\mathrm{eff}}^2 \to g_{\mathrm{eff}}^2, \tag{2.9}$$

so for this class of theories one may readily perform the analytic continuation and (2.4) becomes

$$\mathcal{P}(q) = \frac{q^3}{4\pi^2 N^2 f(g_{\mathrm{eff}}^2)}, \quad \mathcal{P}_T(q) = \frac{2 q^3}{\pi^2 N^2 f_T(g_{\mathrm{eff}}^2)}. \tag{2.10}$$

We have thus now arrived in a relation between cosmological observables and correlators of standard QFT.

Perturbation theory applies when $g_{\mathrm{eff}}^2 \ll 1$. Since $g_{\mathrm{eff}}^2 = g_{YM}^2 N/q$, $g_{\mathrm{eff}}^2 \to 0$, as $q \to \infty$, reflecting the fact that the theory is super-renormalizable. On the other hand the effective coupling grows in the IR, so the question of whether the theory is perturbative or not depends on the scales we probe. In the perturbative regime, the functions f and f_T up to 2-loops take the form

$$f(g_{\mathrm{eff}}^2) = f_0 \left(1 - f_1 \, g_{\mathrm{eff}}^2 \ln g_{\mathrm{eff}}^2 + f_2 \, g_{\mathrm{eff}}^2 + O(g_{\mathrm{eff}}^4) \right), \tag{2.11}$$

$$f_T(g_{\mathrm{eff}}^2) = f_{T0} \left(1 - f_{T1} \, g_{\mathrm{eff}}^2 \ln g_{\mathrm{eff}}^2 + f_{T2} \, g_{\mathrm{eff}}^2 + O(g_{\mathrm{eff}}^4) \right). \tag{2.12}$$

The coefficients f_0 and f_{T0} come from 1-loop and have been computed in [87, 88]. The 2-loop computation is discussed in detail in [121]. At 2-loops there are both UV and IR divergences and these induce the log terms. Both A and B suffer from UV divergences and these can be removed with a counterterm. If (some of) the scalars in (2.7) are non-minimally coupled scalars[6] then the B form factor (but not the A) also has an IR divergence. It is believed that this class of theories is non-perturbatively IR finite, with the Yang-Mills coupling effectively playing the role of an IR cut-off [122, 123]. In summary, f_1 and f_{1T} can be computed unambiguously in perturbation theory, while f_2, f_{2T} are scheme dependent and f_2 also has an IR ambiguity. As discussed in [118], we fix the scheme dependence by setting the RG scale μ equal to the pivot scale q_*, $\mu = q_*$, and the IR ambiguity of f_2 by setting the IR cut-off equal to g_{YM}.

Following [117], we define new dimensionless variables g, β, g_T, β_T via [7]

$$f_1 g_{\text{YM}}^2 N = g q_*, \quad \ln \beta = -\frac{f_2}{f_1} - \ln |f_1|, \qquad f_{1T} g_{\text{YM}}^2 N = g_t q_*, \quad \ln \beta_t = -\frac{f_{T2}}{f_{T1}} - \ln |f_{T1}| \tag{2.13}$$

In terms of new variables

$$\mathcal{P}(q) = \frac{\Delta_0^2}{1 + (g q_*/q) \ln |q/\beta g q_*|} \qquad \mathcal{P}_T(q) = \frac{\Delta_{0T}^2}{1 + (g_t q_*/q) \ln |q/\beta_t g_t q_*|} \tag{2.14}$$

where

$$\Delta_0^2 = \frac{1}{4\pi^2 N^2 f_0}, \qquad \Delta_{0T}^2 = \frac{2}{\pi^2 N^2 f_{T0}}. \tag{2.15}$$

We emphasize that these formulae were derived using perturbation theory, so our first task when fitting to data is to assess whether the perturbative expansion is justified at all scales seen by Planck. We use as an indication of the breakdown of perturbation theory the size of $g q_*/q$. Note that, unlike [117], we did not set $\beta = 1$. The theoretical computation [121] shows that generically $\beta \neq 1$, and furthermore, $\beta = 1$ provides a bad fit to the data (see Figure 2.6 or Table 2.2). We are thus forced to use 3 parameters to fit the primordial spectrum, one more than needed for ΛCDM in (1.1).

Note that the form of the power spectrum (2.14) is a universal prediction for this class of theories, so if this form is disfavoured by the data then it rules out this class of

---

[6]When non-minimal scalars are coupled to gravity, their action contains a coupling to curvature, $\int \xi R \Phi^2$. Correspondingly, their energy-momentum tensor contains a new term proportional to the so-called improvement term.

[7]This parametrization assumes that $f_1 \neq 0$, $f_{1T} \neq 0$. While generically this is true, there are also examples where this does not hold. For example, (2.7) with only scalars has $f_1 = 0$. These cases require a separate analysis.

holographic models. On the other hand, if (2.14) is consistent with data, one can further analyze whether the best fit values can be reproduced by a specific choice of QFT within this class.

2.2.3 Empirical models

To formalize the comparison we now define (following [117]) the empirical model of holographic cosmology (HC) to be the model parametrized by the seven parameters $(\Omega_b h^2, \Omega_c h^2, \theta, \tau, \Delta_0^2, g, \ln\beta)$, where $\Omega_b h^2$ and $\Omega_c h^2$ are the baryon and dark matter densities, θ is the angular size of the sound horizon at recombination and τ is the optical depth due to re-ionization.

This model is to be compared with ΛCDM, which is parametrized by six parameters, $(\Omega_b h^2, \Omega_c h^2, \theta, \tau, \Delta_0^2, n_s)$ and Δ_0^2, n_s are the parameters entering in (1.1).

We also compare HC with ΛCDM with running, which includes as a new parameter the running $\alpha_s = dn_s/d\ln q$. In this case the scalar power spectrum is given by

$$\mathcal{P}(q) = \Delta_0^2 \left(\frac{q}{q_*}\right)^{(n_s-1)+\frac{\alpha_s}{2}\ln\left(\frac{q}{q_*}\right)}. \tag{2.16}$$

The running is usually set to zero since it does not improve the fitting significantly. Here we include this model so that we can also compare HC to a model with the same number of parameters.

In inflationary models, n_s typically has weak dependence on q and it may be Taylor expanded around q_*. In ΛCDM, one keeps the leading order term in this expansion, while in ΛCDM with running one keeps in addition the sub-leading term. In slow-roll inflation, the running is second order in slow-roll parameters and higher order running is further suppressed [124]. The holographic power spectrum (2.14) can be rewritten in the form (1.1) with specific $n_s = n_s(q)$ when $gq_*/q \ll 1$. In this case, however, $\alpha_s/(n_s-1) = -1$, and higher order runnings are not suppressed [88, 117].

All the cosmological parameters other than those quantifying the primordial spectrum – i.e. those in the transfer function - are the same in all three models. In addition, all three models have a parameter Δ_0^2 which determines the overall amplitude of the power spectrum. These parameters are accounted for in the data analysis using CosmoMC by fitting for 100θ, τ, $\ln(10^{10}\Delta_0^2)$, $\Omega_b h^2$, and $\Omega_c h^2$. In addition, all the nuisance parameters of Planck are identical for both models. The values and details of these considered irrelevant for the analysis. For the parameters not shared by the models, ΛCDM uses n_s

Table 2.1: Priors for CosmoMC. The priors are the default for CosmoMC for the ΛCDM parameters. g and β ranges were chosen to ensure viability of the primordial power spectrum.

Parameter	Minimum	Maximum
$\Omega_b h^2$	0.005	0.1
$\Omega_c h^2$	0.001	0.99
100θ	0.5	10
τ	0.01	0.8
$\ln\left(10^{10}\Delta_0^2\right)$	2	4
n_s (ΛCDM)	0.8	1.2
α_s (ΛCDM running)	-0.05	0.05
g (HC)	-0.025	-0.001
$\ln\beta$ (HC)	-0.9	4

and α_s if running is included. Holographic cosmology uses g and $\ln(\beta)$. The priors used for the relevant parameters are in Table 2.1.

2.3 Matching the Model to Data

2.3.1 Best Fit Parameters

In order to determine how well the models fit to data, we started by finding the best fit parameters, median and expected ranges using CosmoMC [60, 61, 57, 66, 58, 65, 59]. Because we needed to compare models with no variations besides the primordial power spectrum, we ran not only holographic cosmology (for which we needed to modify the code to use our primordial power spectrum), but also ΛCDM using the same dataset. We ran ΛCDM both with and without running. Running was used to ensure the likelihoods were compared between models with the same number of parameters, while fitting to ΛCDM without running was done since running has previously been found to not make a significant difference [19].

We fit the models to two different sets of datasets. For both cases, the datasets used were identical for holographic cosmology and both ΛCDM models. The first case is marked as the standard, full Planck run, or is not indicated as special. The data sets used in this case were Planck 2015 (low TEB+high l [HM] TT) as well as lensing [19, 125, 126, 127, 29, 128, 129],

Table 2.2: Planck 2015 and BAO best fit parameters and 68% ranges for holographic cosmology and ΛCDM. Data for ΛCDM is from a separate run of CosmoMC, included to compare the χ^2 numbers.

	HC		ΛCDM		ΛCDM with running	
	best fit	68% range	best fit	68% range	best fit	68% range
$\Omega_b h^2$	0.02217	0.02215 ± 0.00021	0.02227	0.02225 ± 0.00020	0.02231	0.02229 ± 0.00022
$\Omega_c h^2$	0.1173	0.1172 ± 0.0012	0.1185	0.1186 ± 0.0012	0.1184	0.1186 ± 0.0012
100θ	1.04112	1.04115 ± 0.00042	1.04103	1.04104 ± 0.00042	1.04108	1.04105 ± 0.00041
τ	0.081	0.082 ± 0.013	0.067	0.067 ± 0.013	0.069	0.068 ± 0.013
$10^9 \Delta_0^2$	2.126	2.126 ± 0.058	2.143	2.143 ± 0.052	2.151	2.149 ± 0.054
n_s			0.9682	0.9677 ± 0.0045	0.9682	0.9671 ± 0.0045
α_s					-0.0027	-0.0030 ± 0.0074
g	-0.0070	$-0.0074^{+0.0014}_{-0.0013}$				
$\ln\beta$	0.88	$0.87^{+0.19}_{-0.24}$				
χ^2	11324.5		11319.9		11319.6	

as well as Baryonic Acoustic Oscillations (BAO) [47, 48, 45, 130, 46, 43, 131, 44] and BICEP2-Keck-Planck (BKP) polarization [56]. The second case, called the high-l run or the run without low ls, uses all the same data except does not use the portion of the Planck dataset corresponding to $l < 30$.

After running CosmoMC to get the distribution of parameters, we ran the minimizer [67] included with the code to find the best fit parameters as well as its likelihood.

This procedure leads to the parameter ranges in Table 2.2 for the best fit and 68% region of both models using the full Planck dataset. As can be seen, the difference in χ^2 is 4.81. This means the difference between the models is 2.2σ, favouring ΛCDM. The difference in likelihood between ΛCDM with and without running is less than 1, so the case with fewer parameters should be favoured. Our fit for ΛCDM is comparable to those found by the Planck team.

As mentioned earlier, the perturbative expansion (2.14) requires $|(gq^*)/q| \ll 1$. How large of values of $|(gq^*)/q|$ one is willing to accept depends on the error one is willing to tolerate. Certainly values of $|(gq^*)/q|$ which are of order 1 are outside the regime of validity of perturbation theory. In our case, as can be seen in Table 2.2, the best fit value is $g = -0.00703$ and one can check that $2 \times 10^{-3} \le |(gq^*)/q| \le 2.5$, for the multipoles $2500 \le l \le 2$ seen by Planck. Therefore, $|(gq^*)/q|$ is indeed very small for almost all

Table 2.3: Same as Table 2.2, but with $l < 30$ data removed for both holographic cosmology and ΛCDM.

	HC		ΛCDM		ΛCDM with running	
	best fit	68% range	best fit	68% range	best fit	68% range
$\Omega_b h^2$	0.02204	0.02202 ± 0.00022	0.02227	0.02224 ± 0.00020	0.02217	0.02212 ± 0.00024
$\Omega_c h^2$	0.1187	0.1187 ± 0.0014	0.1187	0.1188 ± 0.0013	0.1186	0.1188 ± 0.0013
100θ	1.04097	1.04099 ± 0.00042	1.04108	1.04104 ± 0.00043	1.04101	1.04100 ± 0.00041
τ	0.067	0.066 ± 0.017	0.0703	0.068 ± 0.016	0.0695	0.067 ± 0.016
$10^9 \Delta_0^2$	2.044	2.043 ± 0.074	2.158	2.151 ± 0.064	2.151	2.139 ± 0.066
n_s			0.9667	0.9660 ± 0.0048	0.9682	0.9666 ± 0.0047
α_s					0.0083	0.0090 ± 0.0094
g	-0.0130	$-0.0127^{+0.0042}_{-0.0038}$				
$\ln\beta$	1.01	$0.90^{+0.32}_{-0.16}$				
χ^2	824.0		824.5		823.5	

multipoles, but it does become large at very low multipoles (at $l = 30$ it is equal to 0.15, at $l = 20$ it is 0.25 and at $l = 2$ it is 2.5). It follows that perturbation theory is valid at all scales seen in Planck, except at very low multipoles. This is our first major conclusion: the data *a posteriori* justify the perturbative treatment for all multipoles but the very low ones.

At very low multipoles one cannot trust the model: a non-perturbative computation of the 2-point function of the energy-momentum tensor is needed in order to work out the predictions of this model for these multipoles. In order to stay within the regime of validity of the model, we therefore removed the low l data from our dataset and recalculated the parameters. The exact boundary at $l = 30$ was determined by the datasets we had from Planck, which offers the data already split between the $l < 30$ and $l \geq 30$ data and it is roughly in accordance with the estimate above. In [118] we further determined which model within the class of (2.7) reproduces the best fit values and within that model one can make a more precise estimate of the point where the perturbative treatment is not justified and this leads to $l \sim 35$.

Consequently, the results of the new fits can be found in Table 2.3 if we exclude $l < 30$. For this case, the difference in χ^2 is less than 1, indicating that the models are within 1.0σ of each other and that neither model is favoured. This is our second major conclusion: within their regimes of validity HC and ΛCDM fit the data equally well.

Figure 2.2 shows the shape and degeneracies of the most likely region of parameter
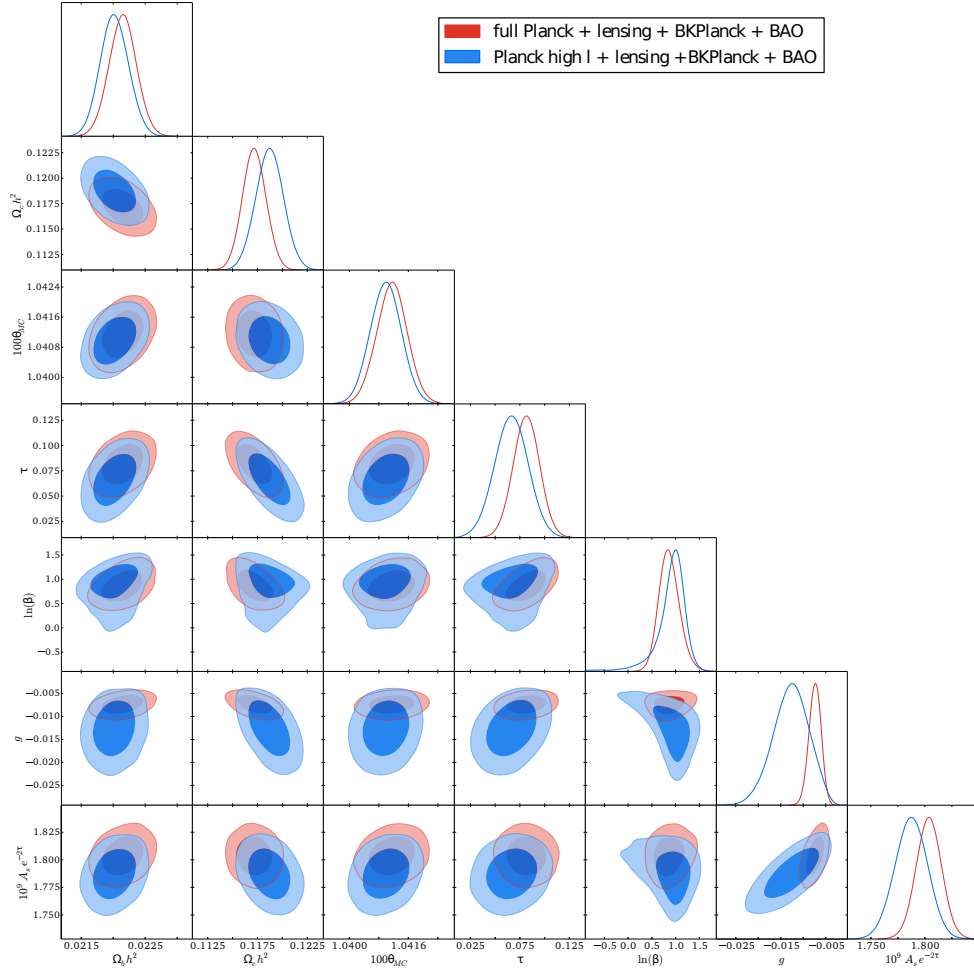
Figure 2.2: A triangle plot of the likelihoods of parameters for holographic cosmology. The blue plots showing the case without low ls is less symmetric than the red plots with the full data set due to the reduced amount of data. The contours show the 68% and 95% confidence levels.

space. The most obvious aspect of these figures is the irregular shape of $\ln(\beta)$ for the case when the low l data is removed. This is seen somewhat in the 1σ region, but more clearly in the 2σ region. This seems to imply that $\ln(\beta)$ becomes less constrained and potentially consistent with 0 when the low ls are removed. The rest of the figure is comparable to Figure 43 of [126], although the degeneracy between Δ_0^2 and g is in the opposite direction of that between Δ_0^2 and n_s in that figure.

Taking the parameters from the case with the low-l data removed, we show the TT angular power spectra in Figure 3.4 for Planck 2015 data, as well as ΛCDM and holographic cosmology. Both models appear to fit the data equally well, with the difference between them being within the 68% region of Planck. Small l's have the largest difference between the models, however the difference still remains within the error as low ls were not part of calculating the fit.

Similar plots for the TE and EE power spectra are shown in Figure 2.4. These plots do not include the low-l data however. The goodness of fit is similar to the TT case. The units for the C_l's match those used in [19].

2.3.2   Comparing Primordial Spectra

Now that we have the best fit parameters, we can examine the difference between the two primordial power spectra. This can be seen in Figure 2.5. We use the best fit parameters for holographic cosmology and ΛCDM without running found in Table 2.3. This means we again used the values for when the low l data was removed. The same plot with the best fit values from Table 2.2 or from much of either tables' indicated range for parameters would look similar to what is seen. The error is approximated by assuming the same relative error as the Planck TT power spectrum, using $l \approx q \times 14$ Gpc.

The biggest difference between the two is seen at low l values. The cutoff used of $l = 30$ is around $q = 0.002$ Mpc^{-1}. This removes much of the very low values of the holographic cosmology primordial power spectrum, but still occurs (in the middle of the insert) before the holographic cosmology's spectrum has become larger than that of ΛCDM. Despite being very similar in value for $q \gtrsim 0.002$ Mpc^{-1}, the HC and ΛCDM power spectra can be seen to have different shapes.

2.3.3   Comparison to Previous Results

Comparing the results for WMAP in [117] to the results for Planck here, it appears that g noticeably shifts to lower values, outside of the expected error. This shift remained when
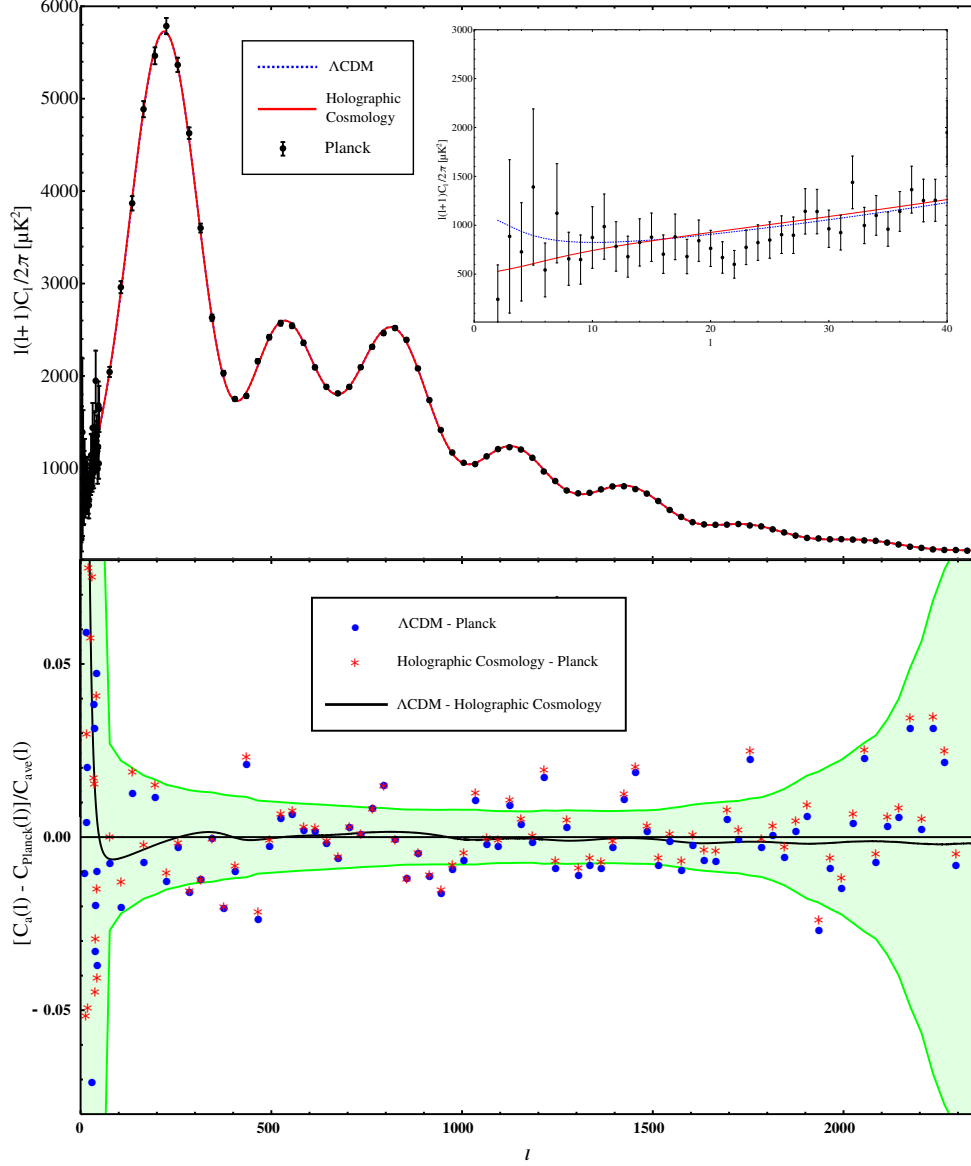
Figure 2.3: TT power spectra of Planck 2015, ΛCDM and HC. Error bars are shown for low l. In the insert ($l \leq 40$), the blue line (ΛCDM) is noticeably above the red one (HC). The green shaded region in the difference plot shows the Planck relative error.
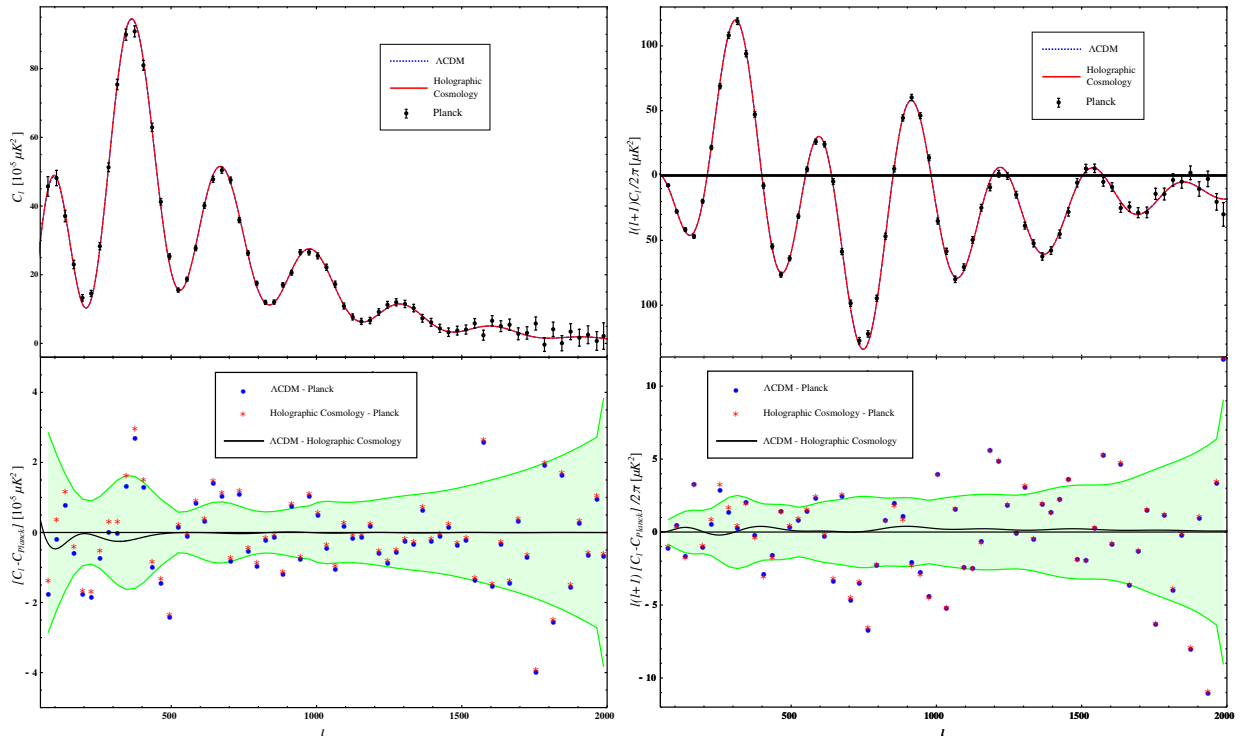
Figure 2.4: Plots of EE (left) and TE (right) polarization for Planck 2015 (black), ΛCDM (blue) and HC (red). The green shaded region in the difference plot shows the Planck error.

47
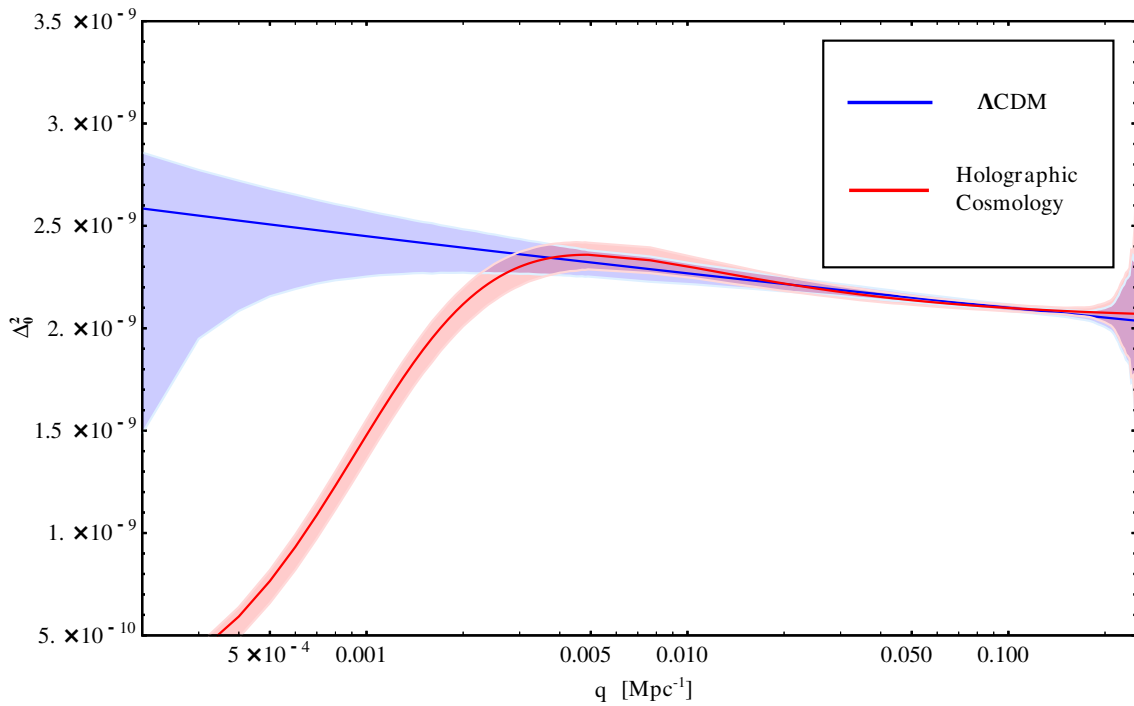
Figure 2.5: Plot of the primordial power spectrum for HC and ΛCDM. The parameters used to produce the curves are the best fit values in Table 2.3. The error (seen in the lighter shaded regions above and below the curves) is determined by assuming the same relative error as the Planck cls. It is included in order to give a sense of the error, not as the actual error. The red line indicating holographic cosmology starts significantly lower and increases rapidly at low q values.
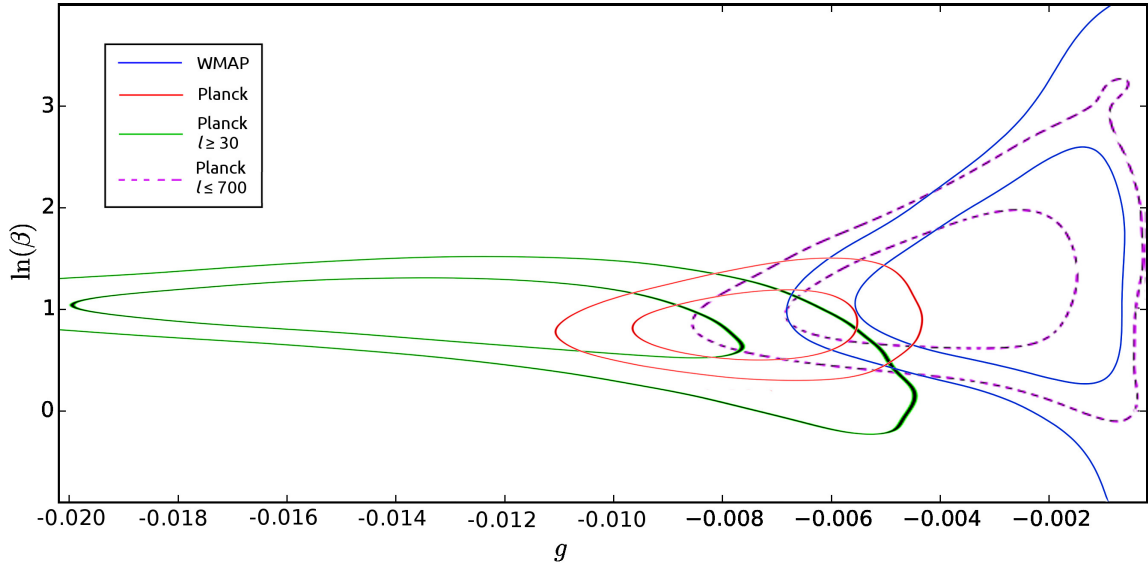
Figure 2.6: Plot of 1σ and 2σ regions in parameter space for holographic cosmology g and $\ln(\beta)$ values for WMAP (blue, right), Planck (red, middle), Planck with low l values removed (green, left), and Planck with high l values removed (purple, dashed).

we reran the code for WMAP, this time including β and the same external datasets as we used for Planck.[8] The trend towards more negative values of g continues when the low l dataset is removed from the data used to determine the parameters. This trend can be seen in Figure 2.6. While it is possible that this indicates an issue with the model, the theory, as stated previously, becomes non-perturbative when $|gq_*/q|$ becomes relatively large. This shift is believed to be compensating for the fact that the model is non-perturbative when using the full dataset. To test if the choice of range of ls is the reason for the shift in g, we also ran the Planck data without using any data for l above a chosen cutoff of $l = 700$ to mimic the uncertainty in the WMAP data for ls around that number. [9] Despite the differences in the sharpness of the cutoff, the values found are close to those from WMAP.

A similar analysis for ΛCDM is shown in Figure 2.7. For this case, there is no similar

---

[8]The parameter β was not used in [117] since it was (incorrectly) argued to be unimportant for the expected values of g. When we ran WMAP again using β (not setting it to 1), we got $\beta = 3.56$ and $g = -0.0027$. These values are used in Figure 2.6.

[9] Because the data for $l > 30$ is binned every 30 ls, the cutoff point is not exactly $l = 700$. The code is then told to ignore the data for ls above the cutoff. The data still remains available to be used, however. This makes the cutoff imprecise. It is, however, sharper than WMAP, which has data for larger ls, but with a very large error. See [132] for discussions on this type of cutoff.
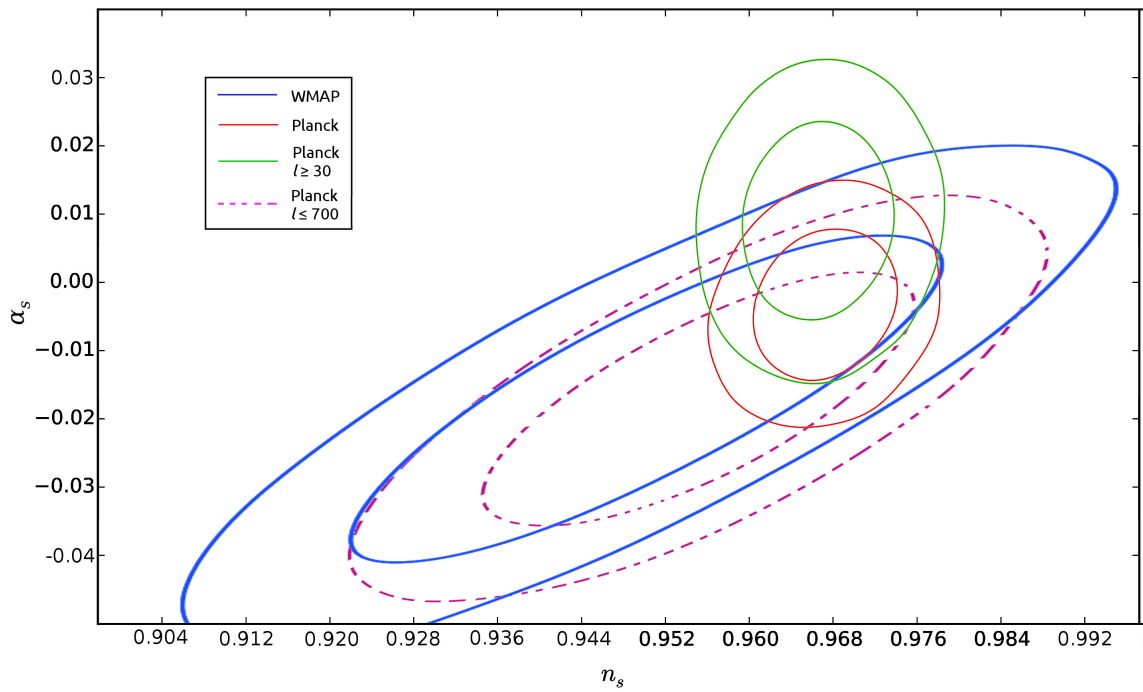
Figure 2.7: Plot of 1σ and 2σ regions in parameter space of ΛCDM n_s and α_s values for WMAP (blue, largest pair of curves), Planck (red, below the green), Planck with low l values removed (green, above the red), and Planck with high l values removed (purple, dashed).
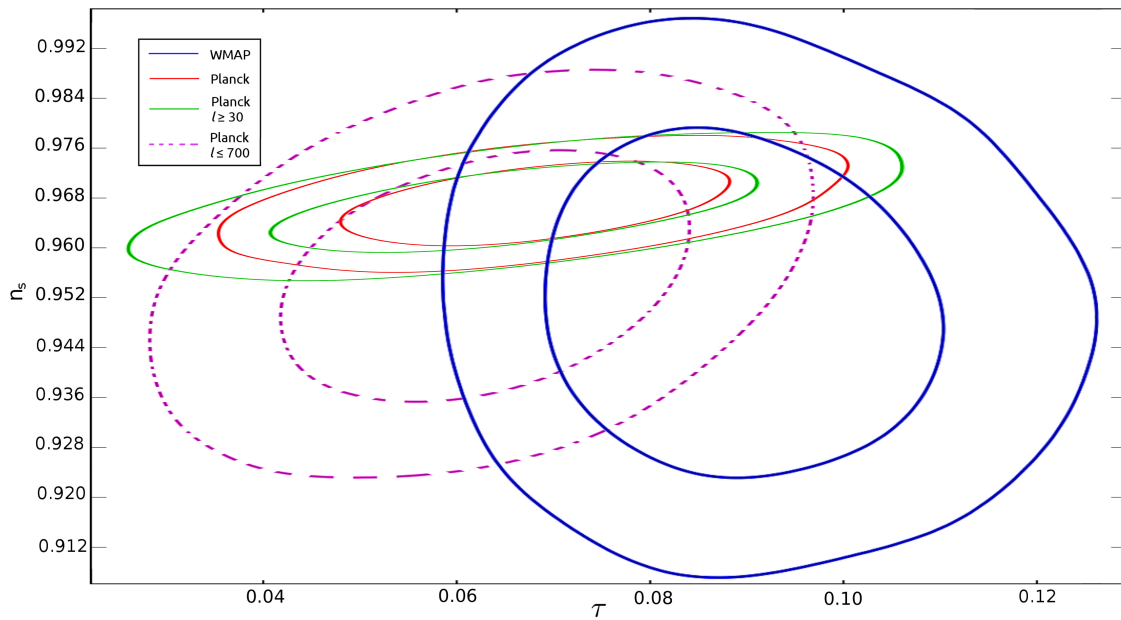
Figure 2.8: Plot of 1σ and 2σ regions in the parameter space of ΛCDM n_s and τ values for WMAP (blue, largest pair of circles), Planck (red, the smallest set of circles), Planck with low l data removed (green, slightly larger than the red), and Planck with high l data removed (purple, dashed).

shift in n_s and α_s. However, there is a known shift in τ from WMAP to Planck for the ΛCDM case: its best fit value went from 0.088 (WMAP) to 0.067 (Planck). Holographic cosmology with the full dataset gives $\tau = 0.081$ which goes down to 0.067 when we remove the $l < 30$ multipoles. The plot of n_s vs τ for ΛCDM is in Figure 2.8.

What we can see in these figures is that the shift in τ for ΛCDM appears due to Planck while the shift in g is at least partially due to the value of l. Since τ decreases to values similar to Planck when the low l data is removed (Table 2.3), it appears that τ is decreased by Planck, but increased to fit the erroneous holographic cosmology power spectrum to compensate for the drop in the low l primordial power spectrum. We suspect that the lower τ value is real.

All other common parameters between the two models are compatible with each other.

2.3.4 Tensors

As in slow-roll inflation, holographic cosmology allows for the production of tensors. There are also holographic cosmology models consistent with an absence of tensors. The tensor affects which holographic models are possible, so an analysis of the status of tensors is required.

In holographic cosmology, the power spectrum for tensors is given in (2.14). The upper limit for the ratio of tensors to scalars, $r = \Delta_{0T}^2/\Delta_0^2$, is 12.49% for 2σ and 17.12% for 3σ. The data is consistent with $r = 0$. Figure 2.9 shows the triangle plot of these three parameters, showing that $r = 0$ is consistent with the data and consistent with any value of g_t or β_t. The allowed value of r can be increased, but this requires the values of $|g_t|$ and β_t to be increased past the point for which the perturbative expansion would be valid.

2.4 Model Evidence

In order to compare different models, one needs to determine which model is more likely given the data. Typically one determines which models fit the data better, using for instance the value of χ^2 or its square root. While this has already been noted (in Tables 2.2 and 2.3), we examine these likelihoods further here. However, if what we want to know is the probability for the model given the data rather than the best fit of the model to the data we should use Bayesian Evidence. We emphasise that what we compare here are the empirical models introduced in Section 2.2.3.
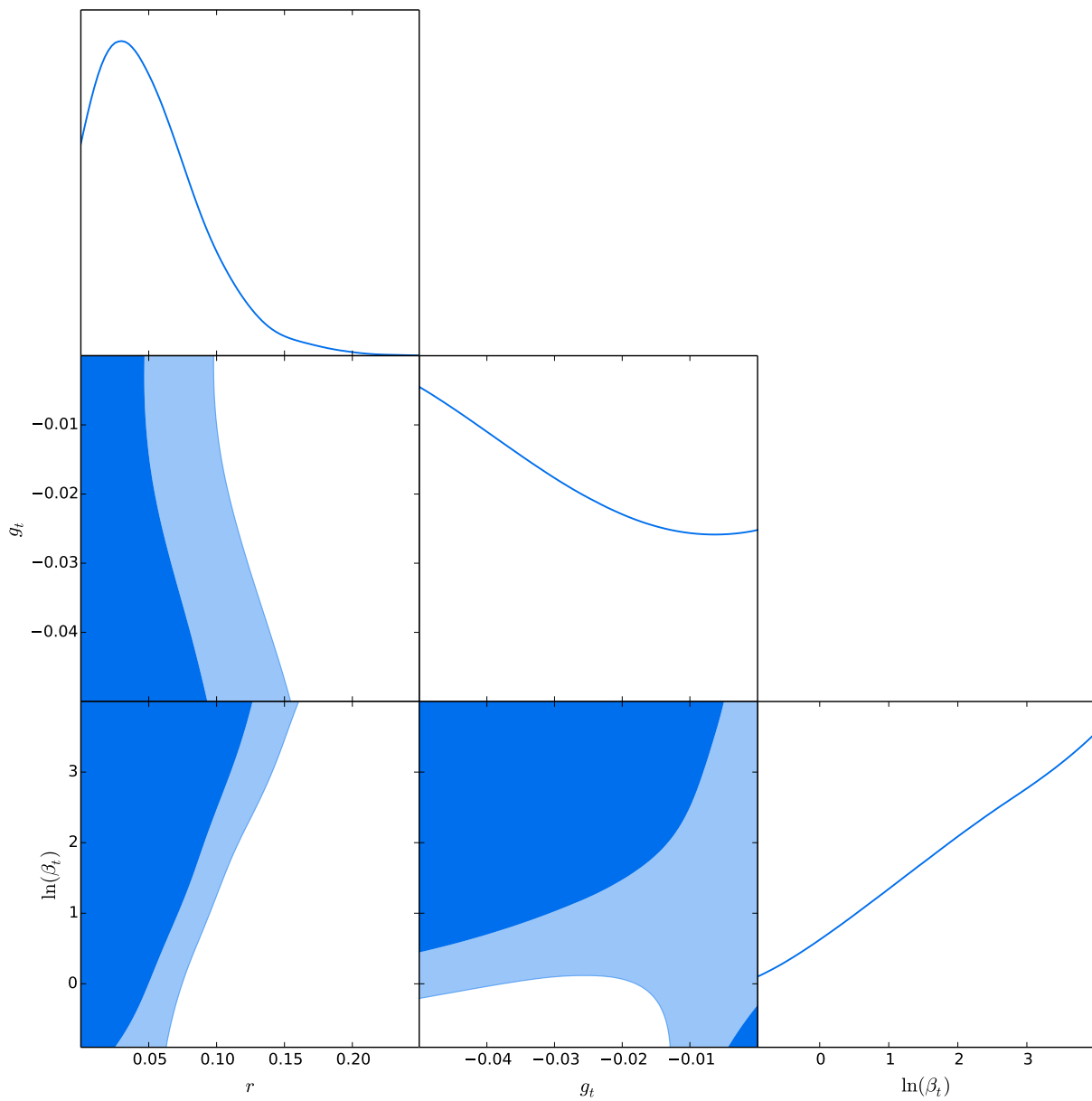
Figure 2.9: A triangle plot of the likelihoods of parameters for tensors in holographic cosmology. The contours show the 68% and 95% confidence levels.

Table 2.4: χ^2 breakdown for different runs of CosmoMC. The table shows the χ^2 values of the HC and ΛCDM with running from Table 2.2 (full Planck data) split by dataset. The χ^2's are split into contributions from the high l dataset ($l \geq 30$), the low l dataset ($l < 30$) and all other contributions to χ^2.

χ^2 breakdown for full Planck run (Table 2.2)	HC	ΛCDM with running
Contribution of high l data ($l \geq 30$)	767.4	766.6
Contribution of low l data ($l < 30$)	10498.2	10494.1
Contribution of other data	58.9	58.9
Total contribution	11324.5	11319.6

2.4.1 Likelihoods

In order to compare the best fits of the two models, we calculate the difference in χ^2. χ^2 is given by $\chi^2 = 2\left(-\ln \mathcal{L}\right)$, where $\mathcal{L}$ is the likelihood of the model. When we take the square root of the difference, $\sqrt{\Delta\chi^2}$, we can get the number of standard deviations one model is from the other. We interpret results within 1σ as insignificant, but a model is considered to be still viable at up to 3σ's.

However, the likelihood does not account for the number of parameters in the model. Since we had to include β in the holographic cosmology models, we have one more parameter than standard ΛCDM. Instead of adding a term to compensate for the different number of parameters as suggested in [117], we added running to ΛCDM so that it has the same number of parameters. Increasing the number of parameters decreases the minimum χ^2. Since this decrease, as seen in Table 2.2, is less than 1, the extra parameter is disfavoured in the model. It does, however, give us a model with the same number of parameters for comparison.

The χ^2 values given in Tables 2.2 and 2.3 are also presented here in Table 2.4 and 2.5 for holographic cosmology and ΛCDM with running. For the full Planck dataset, the difference in χ^2 is 4.81, corresponding to a difference of 2.2σ. However, as explained previously, our holographic model breaks down at low l values and cannot be trusted. Table 2.4 shows the breakdown in the source of χ^2 based on dataset. As can be seen, most of this difference comes from low l data, which we do not expect to be accurate. Comparing instead the model run without the unreliable portions of the data, $\Delta\chi^2 = 0.5$. This is within 1σ, indicating that neither model is statistically preferred to the other.

Table 2.5: χ^2's, excluding $l < 30$ data, using best-fit parameters from Tables 2.2 and 2.3.

	HC	ΛCDM with running
χ^2 for full Planck without low l data (from Table 2.4)	826.3	825.5
χ^2 total for $l \geq 30$ run (Table 2.3)	824.0	823.5

2.4.2 Bayesian Evidence

In the previous subsection, we added a parameter (running) to ΛCDM in order to have models with the same number of parameters when we use likelihood to compare them. In this subsection, we use a method that automatically accounts for the number of parameters: we compute the Bayesian evidence, the probability of each model given the data (rather than that of the data given the model). An explanation of this method was given in Section 1.4.3

Our aim is to compare the two empirical models introduced in Section 2.2.3 and in order to be maximally agnostic about the underlying physical models we proceed by using flat priors as described in Section 1.4.3. Alternatively, one could consider comparing physical models, for example a specific inflationary model versus the model specified by (2.7). In this case, the prior probabilities would (in principle) be theoretically computable from the underlying model. For the case of the holographic model in (2.7) the parameters g and β are related by a 2-loop computation to the parameters of the underlying model (the rank of the gauge group, the field content, the couplings etc.) and assuming that all perturbative models are *a priori* equally likely[10] one can, in principle, compute the prior probability for the parameters g and β by analyzing how often given values of g and β are realized. It would be interesting to see whether such analysis would lead to non-trivial prior distribution. We leave such analysis to future work and proceed with flat priors, as is common.

To compute (1.60), we used MultiNest [71, 72, 73]. The priors are determined from the previous fits of the same empirical models to data and are given in Table 2.6. These priors were chosen to be consistent with the choices in [117]. However, the range of 100θ needed to be increased to allow for the known best fit values. In addition, the range of g_{min} needed to be increased to match the lower values of g. The range of g was chosen to be $g_{min} < g < 0$, with g_{min} variable. The upper limit was set to 0 as g was found to be negative in [117] (and the theoretical computation [118, 121] also shows that g is

---

[10]Alternatively, one may use the partition function of the QFT (with no sources turned on) in order to assign different probabilities to different perturbative models.

Table 2.6: Priors used with MultiNest. g_{min} is variable and ranges from -0.009 to -0.65. The priors are identical to those used for WMAP [117] except for 100θ and g which needed to be expanded to accommodate the best fit results and β and α_s which were not used originally.

Parameter	Minimum	Maximum
$\Omega_b h^2$	0.02	0.025
$\Omega_c h^2$	0.09	1.25
100θ	1.03	1.05
τ	0.02	1.5
$\ln(10^{10} * \Delta_0^2)$	2.9	3.3
n_s (ΛCDM, asymmetric)	0.92	1.0
n_s (ΛCDM, symmetric)	0.9	1.1
α_s (ΛCDM running)	-0.05	0.05
g (HC)	g_{min}	0
$\ln\beta$ (HC, small)	0	2
$\ln\beta$ (HC, large)	-0.2	3.5

generically negative). The maximum $|g_{min}|$ reflects our expectation about the validity of the perturbative expansion. We allow for the possibility that the perturbative expansion is valid only for $l > 30$. We use as a rough estimate for the validity of perturbation theory that gq^*/q is sufficiently small, taking this to mean a value between 0.20 and 1 at $l = 30$.[11] This translates into $-0.009 < g_{\min} < -0.45$. The prior for β is fixed by using the results from (our fit to) WMAP data. We use two sets of priors: one coming from the 1σ range ($0 \leq \ln\beta \leq 2$) and the other from the 2σ range ($-0.2 \leq \ln\beta \leq 3.5$). The prior for the running was taken to be $|\alpha_s| \leq 0.05$. This contains the 1σ region of α_s for all 1σ values of n_s for WMAP. It also contains up to the 2σ region for α_s independent of other parameters. Both this and the case with no running were calculated for ΛCDM.

In Figure 2.10, we present the results for the Bayesian evidence using the data without the low multipole and for different choices of priors. We use the data without the $l < 30$ multipoles because only for this portion of the data the holographic model is perturbative. The shading around each line indicates the error. As a guide [69], a difference $\ln E < 1$ is insignificant and $2.5 < \ln E < 5$ is strongly significant. We can see that the difference in evidence between ΛCDM and holographic cosmology is insignificant.

---

[11]The momenta and multipoles are related via $q = l/r_h$, where $r_h = 14.2$ Gpc is the comoving radius of the last scattering surface.
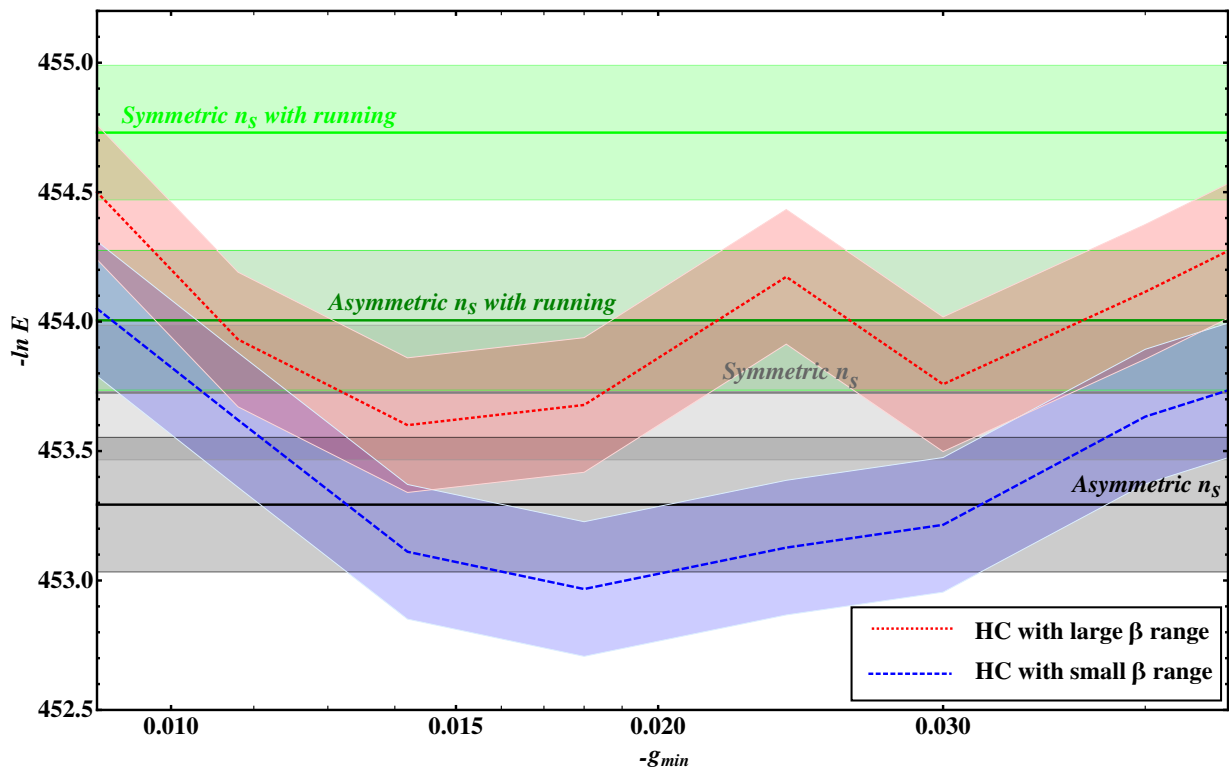
Figure 2.10: Plot of Bayesian evidence when $l < 30$ data is removed. Priors are given in Table 2.6.

2.5 Conclusion and outlook

Here we confronted holographic cosmology against Planck CMB anisotropy data, as well as other cosmological observations. In this work, holographic cosmology is the empirical model obtained by replacing the primordial power-law power spectrum assumed in ΛCDM by that obtained (holographically) by a perturbative computation in a three-dimensional superrenormalizbale QFT with generalized conformal structure. We found that the data *a posteriori* justifies the use of perturbation theory for all but the very low-multipoles ($l < 30$). Restricting to this part of the data, we further found that this theory fits just as well as ΛCDM. This follows both from the goodness of fit (the difference of χ^2 is less than 1) and Bayesian evidence (the difference in log Bayesian evidence is less than one). If we (incorrectly) use the holographic model over the entire data, then the model is viable but disfavoured.

In order to include in the analysis the low-multipole data one would need a non-perturbative evaluation of the 2-point function of the energy momentum tensor. One way to do this is to put the QFT on lattice and use the methods of lattice gauge theory; such computation is currently in progress. Such non-perturbative results would allow us to meaningfully compare this model with ΛCDM over the entire data, and may potentially explain the large angle anomalies in the CMB sky (e.g., [133]). A lattice computation would also allow us to formulate yet another new class of the holographic models, namely ones based on a QFT with a coupling constant of intermediate strength. Such models could potentially provide an even better fit than the models we analysed.

In this analysis we assumed an instant reheating: the data from the end of the very early universe phase were the initial conditions for hot big bang cosmology. It would be useful to develop a dynamical model describing the transition from the non-geometric phase to Einstein gravity. This may be achieved by adding irrelevant operators that would modify the UV sector of the QFT and induce an RG flow that would drive the theory to strong coupling. Such terms could modify the high l part of the spectrum, but our ability to fit the current data very well without such corrections suggests that that they are small. However, future results from the next generation stage IV CMB experiments [134], as well as future large scale structure surveys such as SPHEREX [135], are expected to reach up to much higher wavenumbers, potentially probing the holographic reheating phase in our model.

Chapter 3

Does History Repeat Itself? Periodic Time Cosmology

3.1 Introduction

All the typical cyclic models imagine the universe to repeat itself, potentially infinitely many times. However, the geometric structure of general relativity (GR) allows for another possibility: Since the spacetime manifold need not be flat globally, it is possible to construct a manifold for which, even without faster than light signalling, some events may be able to influence their own causal past [136]. These spacetimes are said to have closed timelike curves (CTC).

In such a spacetime manifold, it would not be possible to define generic initial conditions and simply evolve the system from the past to the future (i.e. solve a Cauchy problem in the standard way) as is typically done in physics. Because of this, regularly manifested by the "grandfather paradox", considering a universe with CTCs is often avoided. For instance, causal set theory [137] and shape dynamics [138] both state removing these as part of their strengths. In addition, with the standard energy conditions, added to require "reasonableness" and prevent runaway particle creation, CTCs cannot occur in general relativity [139].

However, it has been shown that when there is a CTC in a system, there exist self-consistent particle solutions for any choice of initial conditions before the CTC [140, 141, 142]. Moreover, solving dynamical equations based on an evolution from the past to the future is not the only way to do physics. The principle of least action, for instance, provides

a description of what happens between two points by fixing the beginning and the end, from which Novikov's self-consistency condition can be derived [143, 144].

So, if there is a repeating cosmic history, is it possible that the reason for this repetition is that the future is the past, and that we live on CTCs instead of time being infinite? Most cyclic models avoid this possibility for various reasons, one being that this constraint is difficult to work with. However, if a model is more constrained, it would potentially be more falsifiable. And if the model succeeds with the additional constraint, this would be more significant.

With this suggestion, we construct a cosmological model based on the constraint of temporal periodicity. We ask if we can take advantage of this constraint to construct a testable form of the primordial power spectrum.

It turns out we can. To do this, we take advantage of the concept of conformal matching of Penrose's conformal cyclic cosmology CCC. Penrose suggested that in the infinite future, most to all matter would evaporate to radiation. Without massive particles, time no longer has any meaning and the structure is conformally invariant, allowing an arbitrary rescaling. The big bang period was radiation dominated, and thus was also effectively scale invariant early on. Therefore, given the conformal invariance of our effective theories near big bang, and infinite future, these can be matched to each other, as the singularity only appears on the conformal factor [145].

As the superhorizon metric perturbations freeze at both big bang, and infinite future, they could be matched across the transition. If we match larger comoving scales from the previous cycle to smaller comoving scales in the next cycle, the metric power spectrum should transfer from one cycle to the next. Therefore, we do not need to construct a mechanism to produce metric fluctuations. Instead, as we shall see, the effects of matter transfer function from the previous cycle would produce a slight red tilt on an otherwise scale invariant power spectrum on large scales.

In this chapter, we examine if this power spectrum produces a satisfactory fit to observations such that a model which recycles its power spectrum at each cycle is viable. In Section 3.2, we develop the periodic time cosmology (PTC) model described here. In Section 3.3, we examine how well this model can fit the data, compared to the standard power-law power spectrum. In Section 3.4, we discuss the physical implications of our results, and Section 3.5 concludes the chapter.

3.2 Model Construction

3.2.1 Finding the Primordial Power Spectrum

We desire to construct a periodic model for which the condition of temporal periodicity will constrain the system, so that we can make predictions based on this construction. What can we observe from the previous cycle? In the cosmological data, we see the primordial power spectrum as what comes through from the earliest times, as an input to our model. It must have either come from the previous cycle or have been formed at early times. We will take it as coming from the previous cycle. This means that in the infinite future, there is a power spectrum of metric perturbations at some scale that transfers over into our past.

If the evolution of the universe *were not to affect the power spectrum*, there are two forms of solutions for which the matching of the infinite future to the early universe would preserve. First, if comoving scales are matched to themselves, any power spectrum would work. This produces no restriction on the form of the power spectrum, but would require any evolution of the power spectrum to either be periodic or to reverse itself. Since we do not expect this and are looking to restrict the form of the power spectrum, this case is uninteresting for our analysis.

Let us now define a general conformal rescaling across the infinite future/big bang transition, for the spatial metric g_{ij} of uniform density hypersurfaces:

$$g_{ij}(\alpha\mathbf{x})|_{\text{big bang}} \propto g_{ij}(\mathbf{x})|_{\text{infinite future}}, \tag{3.1}$$

where α is a constant factor. In this case, the power spectrum is matched across the transition with a fixed, non-unitary shift in the comoving scales. Any scale invariant primordial power spectrum would be preserved by any such matching. More generally though, a power spectrum periodic in $\ln\left(\frac{k}{k_*}\right)$ with a period of $\ln(\alpha)$ will match this condition, where k_* is an arbitrary pivot scale used to remove the dimension of k.

However, we know the power spectrum *does* evolve from its primordial shape as the universe evolves. For example, the CMB anisotropies we see now is determined by the power spectrum after it has lost power due to acoustic oscillations and Silk damping on small scales [146, 42]. This loss in power is defined by the transfer function $T(k, t)$, which can be calculated numerically [57, 58, 59, 60, 61], or approximated by a fitting function [147] in ΛCDM cosmology. It is defined such that it is normalized to

$$\lim_{k \to 0} T(k, t) \to 1. \tag{3.2}$$

To fit current observations, we only need to focus on the scalar adiabatic perturbations, which quantified by the Bardeen variable ζ [148], which quantifies the conformal fluctuations of the spatial metric on superhorizon scales in the uniform density gauge:

$$g_{ij}(\mathbf{x}) \propto [1 + 2\zeta(\mathbf{x})]\delta_{ij}, \tag{3.3}$$

which is related to the conformal Newtonian metric perturbations by

$$\zeta = \psi - \frac{H}{\dot{H}}\left(H\phi + \dot{\psi}\right). \tag{3.4}$$

In the Fourier space, the transfer function for linear perturbations at wavenumber k and time t is defined as:

$$T(k,t) \equiv \frac{\zeta_k(t)}{\zeta_k(t=0)}. \tag{3.5}$$

This function, for typical cosmological parameters and evolved from the early universe to the present, can be seen in Figure 3.1.

In order to determine what is passed from one cycle to the next, we need the transfer function at the infinite future:

$$T(k) \equiv \lim_{t\to\infty} T(k,t). \tag{3.6}$$

The cosmic future appears to be dark energy dominated. If the structure of dark energy is known, we can evolve the same equations we used to calculate the transfer function to today, into the future. Furthermore, if dark energy is just a simple cosmological constant, the transfer function no longer expected to evolve significantly after recombination, i.e. $T(k) \simeq T(k,t)|_{\text{present}}$. This is because the speed of sound of matter is close to zero and dark energy is non-dynamical.

With this introduction, the consistency condition (3.1) for primordial cosmological metric perturbations takes the form:

$$g_{ij}(\alpha\mathbf{x})|_{\text{big bang}} = T \star g_{ij}(\mathbf{x})|_{\text{big bang}}, \tag{3.7}$$

where $T\star$ denotes convolution with the linear transfer function $T(k)$. An example of this consistency under convolution+rescaling is depicted in Figure (3.2).

As convolution is a simple product in Fourier space, the primordial power spectrum (at the big bang) should satisfy the following simple consistency condition:

$$\mathcal{P}(\alpha^{-1}k) = \mathcal{P}(k)|T(k)|^2. \tag{3.8}$$
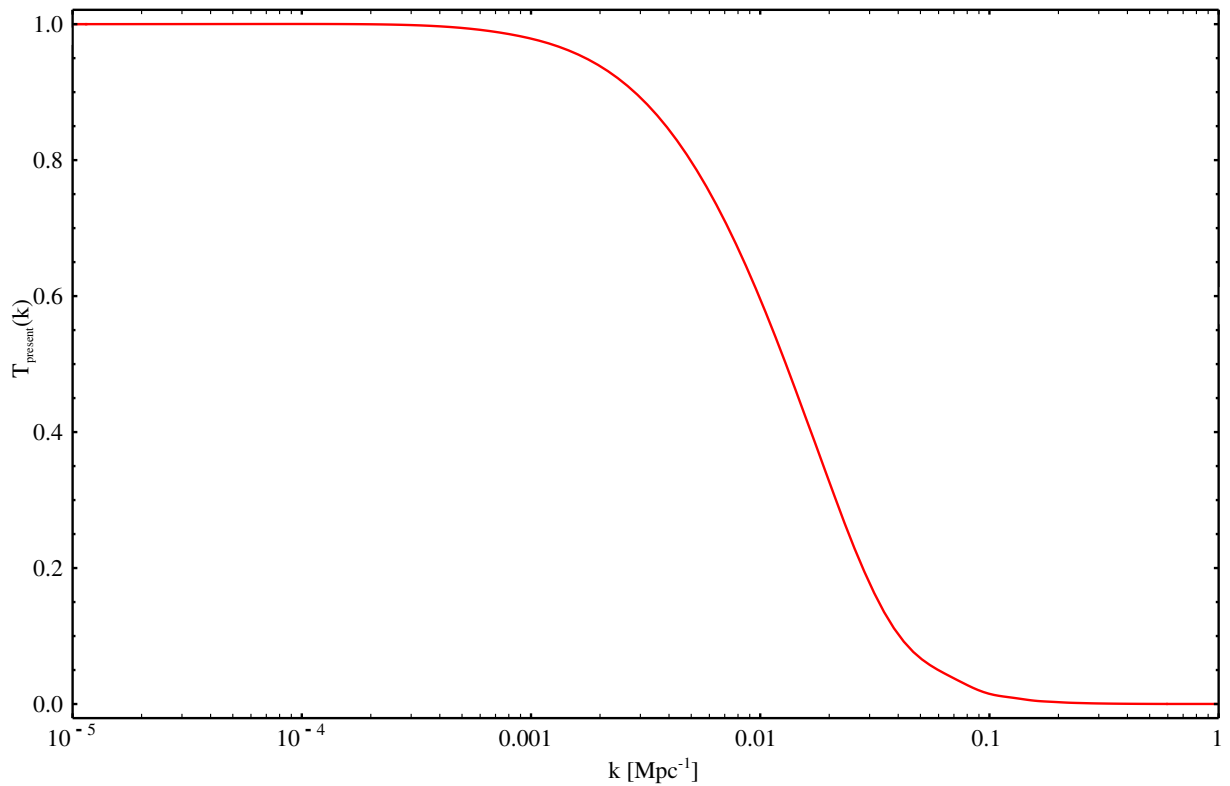
Figure 3.1: A plot of a sample transfer function evaluated at present time. The transfer function is normalized to one at the largest scales. This was calculated numerically in CAMB [57, 58] using values of Ω_b, Ω_c, τ and 100θ close to the best fit values for the standard ΛCDM fit to Planck [19, 132, 133, 125, 126, 127, 149, 150, 151, 29].
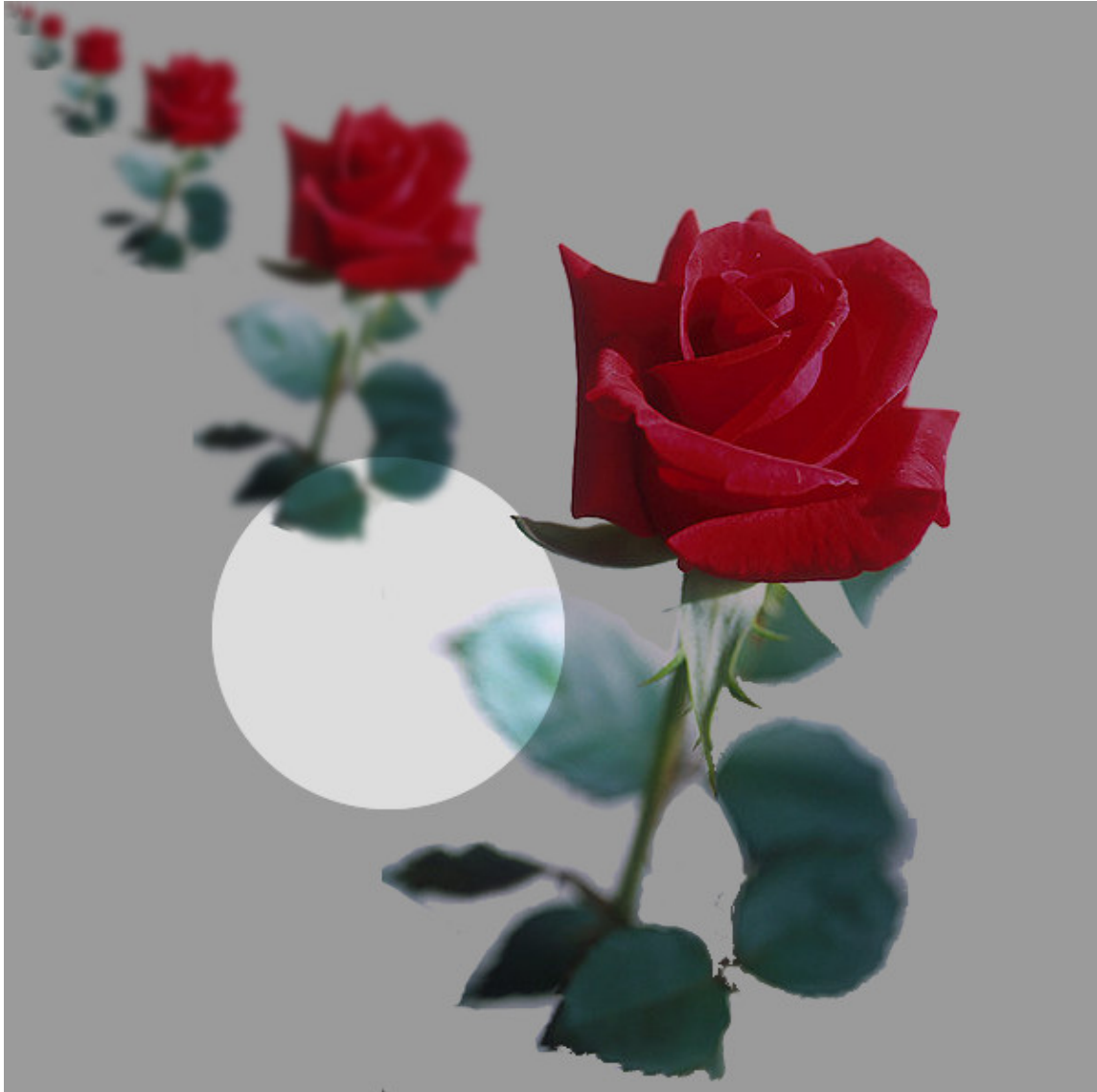
Figure 3.2: An image depicting a figure repeated over several cycles, each time shrunk and then convolved with a low-pass filter (or transfer function), as in Figure (3.1). This is an example of a pattern that satisfies the matching consistency condition (3.7) in PTC. In cosmology, what we see is limited by the Hubble horizon, depicted here as the boundary between the light and dark regions. As such, only the light region of the universe would be visible to us.

Given this condition, it is easy to see that the the power spectrum must be of the form

$$\mathcal{P}(k) = F\left(\ln \frac{k}{k_*}\right) \prod_{n=1}^{\infty} |T(\alpha^n k)|^2, \quad \text{for} \quad \alpha < 1, \tag{3.9}$$

where $F\left(\ln \frac{k}{k_*}\right)$ is periodic with a period of $\ln \alpha$: $F\left(\ln \frac{k}{k_*}\right) = F\left(\ln \frac{k}{k_*} + \ln \alpha\right)$. Here, for simplicity, we will just take $F\left(\ln \frac{k}{k_*}\right) = A_0$, a constant. This can be justified by requiring that on scales much bigger than all the physical length scales in the problem, physics *must* be conformal and thus the spectrum must be scale invariant, not just periodic. We thus posit that *only* the matter transfer function $T(k)$ breaks this symmetry.

Our resulting power spectrum is then

$$\mathcal{P}(k) = A_0 \prod_{n=1}^{\infty} |T(\alpha^n k)|^2, \quad \text{for} \quad \alpha < 1. \tag{3.10}$$

This function would be scale invariant if it were not for $T(k)$, as expected. However, $T(k)$ looks very unlike what we expect for the primordial power spectrum. In addition, the infinite product seems to push the power spectrum to zero on all scales. However, if we look at the large scales of $T(k)$, matter has very little effect, and it is nearly scale invariant. In addition, the tilt is red. If we choose $\alpha \ll 1$, we will have a power spectrum close to what we expect. In addition, since $\alpha^n k \to 0$ for large n, given Equation 3.2, the infinite product should have a finite, non-zero value at the scales of interest since the terms get closer and closer to one.

3.2.2 Approximating the Primordial Power Spectrum

Now that we have a potential primordial power spectrum, we need to test if this can fit the data. To do this, we use CosmoMC [65, 66]. However, while CosmoMC is easy to modify for a new power spectrum, our power spectrum is not in an analytic form. Fortunately the program already calculates the transfer function to the present time. As we discussed above, $T_{t\to\infty}$ is very close to $T_{present}$ for ΛCDM cosmology. Therefore, we use $T_{present}(k)$ instead of $T_{t\to\infty}(k)$ for the transfer function in Equation 3.10.

Given $T(k)$, in order to calculate $\mathcal{P}$, we need to know the limit of the infinite product. We start with the approximation $\alpha \ll 1$. From Equation 3.2, we know that $T(\alpha^n k)$ in Equation 3.10 will get closer and closer to one as $n \to \infty$. We will start with one factor of $|T(\alpha^n k)|^2$,

$$\mathcal{P}(k) \simeq A_0 |T(\alpha k)|^2, \tag{3.11}$$

and check whether our approximation is close enough.

We will start by determining if cutting off the product is a correct approximation. For the case when $\tilde{k} = \alpha^n k$ is sufficiently small, for $\tilde{k} \lesssim 10^{-4}$ Mpc^{-1}, from simple analyticity considerations, we expect the leading correction to the transfer function to look like

$$T\left(\tilde{k}\right) \simeq 1 - \epsilon\tilde{k}^2, \tag{3.12}$$

where ϵ is the inverse square of an appropriate comoving sound horizon. In this case, Equation 3.10 will become

$$\mathcal{P}\left(k\right) = A_0 \left[1 + \epsilon^2\alpha^4 k^4 - 2\epsilon\alpha^2 k^2 - 2\epsilon\alpha^4 k^2 + \mathcal{O}\left(\alpha^6\right)\right]. \tag{3.13}$$

This implies that to any finite order, Equation 3.10 can be approximated by a finite product, and Equation 3.11 is correct to $\mathcal{O}\left(\alpha^3\right)$ for low k.

Now that we know a finite product of transfer functions will work, we estimate α. We know our approximation, here Equation 3.11 is required to maintain a small spectral tilt throughout the relevant scales. We know this is sufficient since further factors of T will reduce the power of the smaller scales more than the larger ones, increasing the effective tilt. Using Figure 3.1, our first estimate for α is for it to be on the order of $k_{\text{inflection}}/k_{\text{max}} \sim 0.01$. With this shift, the successive factors of $T(\alpha^n q)$ will quickly approach unity to the relevant degree of precision. For relevant k ($k \leq 1$ Mpc^{-1}), $\alpha^2 k < 10^{-4}$, which is within the range approximated by Equation 3.12. In this case, each additional term corrects the previous by by a term of order $\alpha^2 = 10^{-4}$ relative to the previous, which is less than 1%. This means we can approximate Equation 3.10 by Equation 3.11.

However, the transfer function calculated by CosmoMC is calculated at only specific k values calculated by the program. In order to use this with a shift in the values of k, we will need an interpolation between points and an extrapolation function for low k values. For interpolation, we use linear interpolation. For extrapolation, we use Equation 3.12. We fit the smallest 30 k values to the function using a least squares fit, and use it in place of any value of k smaller than the 10th.

Now that we have our power spectrum, we need to estimate the value of α as well as the priors for this parameter. We will estimate this parameter by calculating the slope of $\mathcal{P}$ at the pivot scale $k_* = 0.05$ Mpc^{-1} and matching this to the ΛCDM known $n_s = 0.96$. Based on this our estimate is $\alpha \sim 0.007$.

We use as priors $0.0001 < \alpha < 0.1$. We do not expect that CosmoMC examines the whole range of this parameter space, however. Based on Figure 3.1, we expect the error in Equation 3.11 to be $< 1\%$ for $\alpha < 0.04$ for all the values of k within our range.

Table 3.1: The priors used for the parameters extending the ΛCDM astrophysics.

Parameter	Minimum	Maximum
N_ν	3	4
m_ν	0.05	0.5
w	-1.1	-0.9
w_a	-0.1	0.1
Ω_Λ	-0.01	0.02

3.2.3 Beyond ΛCDM

Since our model uses part of the transfer function in place of the primordial power spectrum, we know that any effect which affects the shape of the transfer function will change the primordial power spectrum. Thus, the extensions of ΛCDM which alter the shape of the transfer function will potentially be more relevant for our periodic model than they are for the standard power-law. Because of this, we will consider a variety of 7 and 8 parameter models in addition to the standard 6 parameter model when evaluating the viability of PTC as presented here.

We consider two potential such effects, that of neutrinos and that of dark energy. We do not consider curvature as the conformal matching requires a flat universe. We also, as is typical, use the Big Bang Nucleosynthesis constraints to determine the helium fraction, so this will not be treated as a free parameter. The parameters and their priors are in Table 3.1.

Our choice of priors was chosen to prevent the numbers from getting too large. However, Planck has presented a range of potential values for these variables based on an analysis of the extended ΛCDM models. We will leave for a future project a run CosomMC with an extended parameter range based on the maximum range the Planck team analysis has suggested.

Neutrinos

There are two standard parameters in the extended ΛCDM related to neutrinos. These are the sum of the neutrino masses m_ν and the effective number of neutrinos N_ν. Neutrino mass is typically taken to be minimum value possible based on our current observations.

It has a minor effect on the transfer function, but may effect the shape of the large scale spectrum which is relevant for our PTC.

The effective number of neutrinos is typically taken to be 3.046, which is calculated from the standard model. This parameter can also be taken to be a free parameter, calculated by fitting the data to the model. In this calculation, however, this parameter can be degenerate with H_0.

Dark Energy

Dark energy is an unknown factor in the evolution of the universe. Typically, dark energy is taken to be a cosmological constant. However, since the effects of dark energy are going to be significant for our model, we will examine a few simple possibilities.

Beyond a cosmological constant, the simplest model is for the case when dark energy has a constant equation of state. In this case, the equation of state is defined by a constant w, where $p = w\rho$, with p being the pressure and ρ being the density. $w = -1$ corresponds to the case when dark energy is a cosmological constant. We can vary w close to -1 and still fit our observations.

Since we are using the current transfer function as our infinite future transfer function, the real form of w we compare here is constant to now, then is set to -1 from now to the future. While this model is not what we expect, it will still determine if our model is viable when dark energy is not a cosmological constant. The case where we use the correct transfer function taken to the infinite future will have to wait for a future analysis. Moreover, a constant-w model is a toy model to begin with, even if it were taken to the infinite future.

To continue this examination, we also try a common extension to this model, w_a, which introduces a variation of w linear in a, the size of the universe. If w_a is taken alone without varying w, the present day w would be set to -1.

As another alternative model, we use early dark energy (+ a cosmological constant). This could, for example, appear for exponential quintessence potentials [152], or the quadratic cuscuton model [153]. This dark energy component will affect the early times, but will become irrelevant later. That means that the transfer function still stops changing by the present, so it does not need to be evolved to the infinite future.

The early dark energy component is assumed to be a constant fraction of the total density:

$$\Omega_{EDE} = \frac{\rho_{EDE}}{\rho_{tot}} = \text{const.}, \tag{3.14}$$

with

$$\rho_{tot} = \rho_m + \rho_r + \rho_{DE} \tag{3.15}$$

being the total energy density. In this case,

$$\rho_{DE} = \Lambda + \Omega_{EDE}\rho_{tot}. \tag{3.16}$$

If we solve this for the equation of state, w, we get

$$1 + w_{DE} = -\frac{\dot{\rho}_{DE}}{3H\rho_{DE}} = K\frac{3\Omega_{0m}a^{-3} + 4\Omega_{0r}a^{-4}}{\Omega_{0DE} - \Omega_{EDE} + \Omega_{EDE}\left(\Omega_{0m}a^{-3} + \Omega_{0r}a^{-4}\right)}, \tag{3.17}$$

where

$$K = \frac{\Omega_{EDE}\left(1 - \Omega_{EDE}\right)}{3}. \tag{3.18}$$

3.3 Comparing to Data

Now that we have our model set up, we can compare its predictions to data. As previously stated, we use CosmoMC in order to find a fit. In order to see how good of a fit this is, we will compare to the fit to the standard power-law primordial power spectrum given by Equation 1.1.

For both of these models and every choice of parameters to run, we find the best fit parameters as well as their medians and expected ranges. We first run CosmoMC to get the distribution using a Monte Carlo Markov Chain, then run the minimizer included in the CosmoMC code to get the best fit parameters. For the case of the power-law power spectrum, we also compare the results we got with those of the Planck team to see if they make sense.

The datasets we use are those supplied by the Planck team. For this, we include the $l \leq 30$ temperature and polarization data (low TEB), the $l > 30$ temperature and polarization data (TTTEEE) as well as the lensing data [19, 132, 133, 125, 126, 127, 149, 150, 151, 29, 129, 128]. In addition, we use BAO [43, 47, 44, 45, 46, 48, 131, 130], the BICEP2-Keck-Planck joint dust analysis [56] and an instantaneous reionization at $z_{re} > 6.5$ [26]. This last one was used since τ had been found to decrease for the best fit PTC model values.

To determine if our model is viable, for each run we compare the χ^2 for periodic time vs. power-law power spectrum with the same cosmological parameters. Our preliminary results are shown in Table 3.2. Due to an issue with CosmoMC, we were unable to run

Table 3.2: Minimum χ^2 values found for various runs of power-law and periodic time cosmology (PTC) power spectra with the full dataset used here in the CosmoMC minimizer, as well as the difference between these χ^2 values. The sigma value is calculated by the square root of the difference. A model is expected to be ruled out above 3σ.
This data is preliminary due to an issue with CosmoMC, although a full run is not expected to change the χ^2 values much except for the struck out data. The χ^2's that are struck out have not converged, are still bigger than the absolute minimum by $\sim 2-4$. The reason is due to an issue with the minimizer. The relevant effect of the additional parameters can still be seen, however.

	χ^2 for power-law power spectrum	χ^2 for PTC power spectrum	$\Delta\chi^2$	σ
ΛCDM	12995.3	13021.1	25.8	5.1
$+ N_\nu$	~~12997.2~~	13021.7	~~24.5~~	~~4.9~~
$+ m_\nu$	12995.0	~~13024.5~~	~~29.5~~	~~5.4~~
$+ w \neq -1$	12995.1	12998.5	3.4	1.8
$+ \Omega_{EDE}$	12995.8	13020.4	24.8	5.0
$+ N_\nu, m_\nu$	12995.2	13020.0	24.8	5.0
$+ w, N_\nu$	12995.0	12998.0	3.0	1.7
$+ w, m_\nu$	12995.8	~~13001.6~~	~~5.8~~	~~2.4~~
$+ w, w_a$	12994.7	12997.8	3.1	1.8

this code to the tolerance of the MCMC routine, so the true minimum may have not yet been found. Our results come from running CosmoMC to failure to get an estimate of the mean value for the parameters, then running the minimizer starting at those values until completion or failure. The results are not perfect, but are reasonably close to what we expect for χ^2 values for these models. Previous runs with less data and fewer combinations of parameters confirm this expectation. As can be seen from Table 3.2, PTC is ruled out at around 5σ for all $w = -1$ cases. This means our model requires non-trivial late-time dark energy.

A comparison of the primordial power spectra for a power-law, PTC with $w = -1$ and PTC with $w \neq -1$ can be seen in in Figure 3.3. Here we can see that $w \neq -1$ dark energy changes the shape of the primordial power spectrum, causing it to have a shape which matches the expected tilt. In a future analysis of this apparent tilt, we will examine the relationship between w and the apparent n_s.

The TT power spectrum for PTC with non-trivial dark energy can be seen in Figure
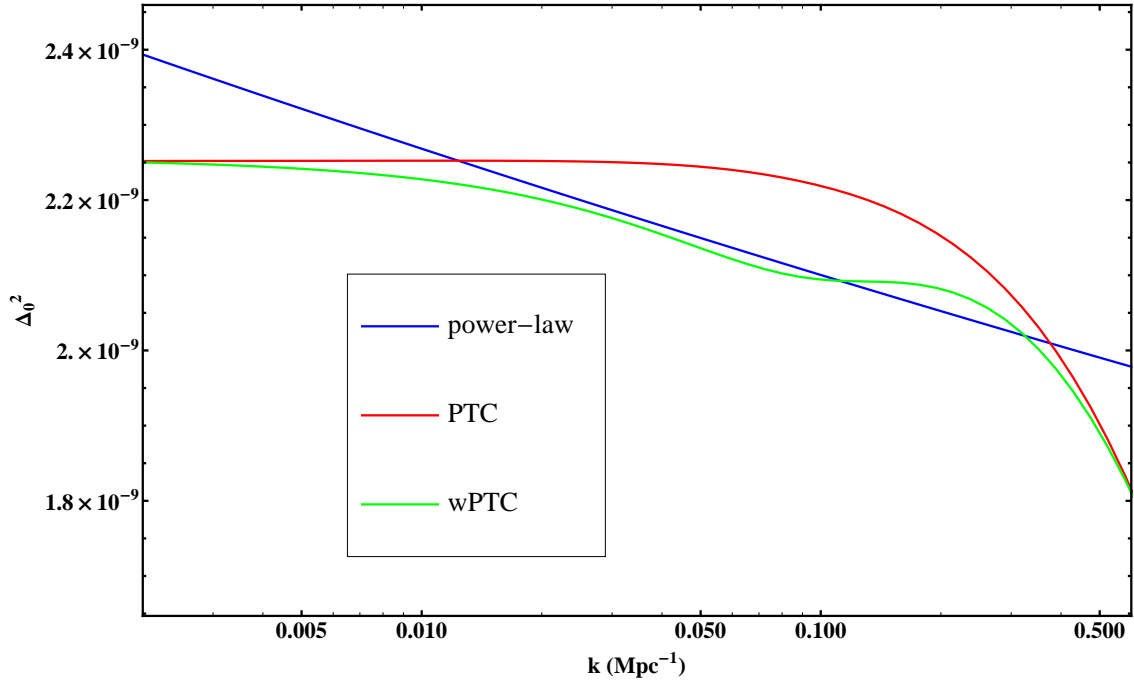
Figure 3.3: Best fit primordial power spectra for power-law power spectrum (blue), periodic time cosmology (red, PTC+ΛCDM), and PTC with $w \neq -1$ and the transfer function evolved to the present (green, PTC+wCDM). The portion of the transfer function for PTC+wCDM near the pivot scale $k_* = 0.05$ Mpc^{-1} can be seen to match the best-fit power-law. At larger scales, there is less power for PTC+wCDM compared to the power-law.

Table 3.3: Preliminary best fit parameters for periodic time cosmology (PTC) and power-law power spectra for the case when $w \neq -1$.

	power-law + wCDM	PTC + wCDM
$\Omega_b h^2$	0.02220	0.02225
$\Omega_c h^2$	0.1198	0.1184
100θ	1.04074	1.04094
τ	0.0527	0.0483
$10^9 \Delta_0^2$	2.0900	2.1779
w	-1.0364	-1.0238
n_s	0.9637	
α		0.01125

3.4. The fit seen here appears reasonably close to the Planck results.

Table 3.3 shows the best fit and 68% regions for both PTC and ΛCDM for the case when $w \neq -1$. From this we can see a drop in the value of τ.

3.4 Issues and Considerations

Now that we have seen that our model may fit the data reasonably well, we wish to ask what this fit means within the field of early universe cosmology. There are many aspects of periodic time cosmology to consider.

3.4.1 Phenomenology vs. Theory

As a phenomenological model, our model is based on testing the constraint of periodicity rather than developing an underlying theory. As such, it is a proof of principle that CTCs, often overlooked, could potentially provide a viable and consistent description of cosmic history. However, it does not give a reason for why the matching exists in the first place. It may be worth examining how this result fits in with CCC or the overall landscape of cyclic models, especially a microscopic mechanism for how such a matching could be produced in the context of a quantum theory of gravity.
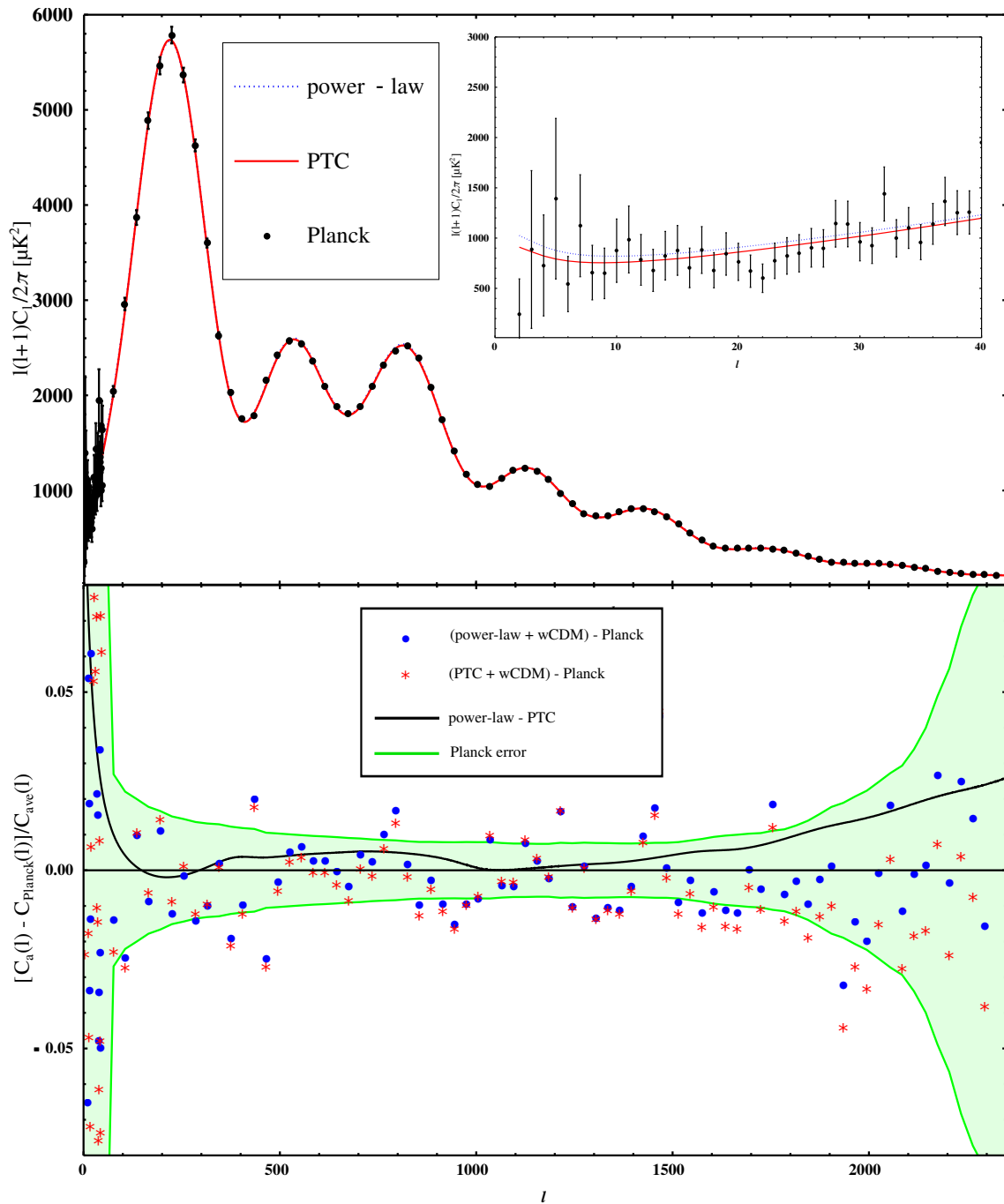
Figure 3.4: A plot of the differences in temperature power spectra between power-law+ΛCDM and PTC+wCDM power spectra (see Figure 3.3) .
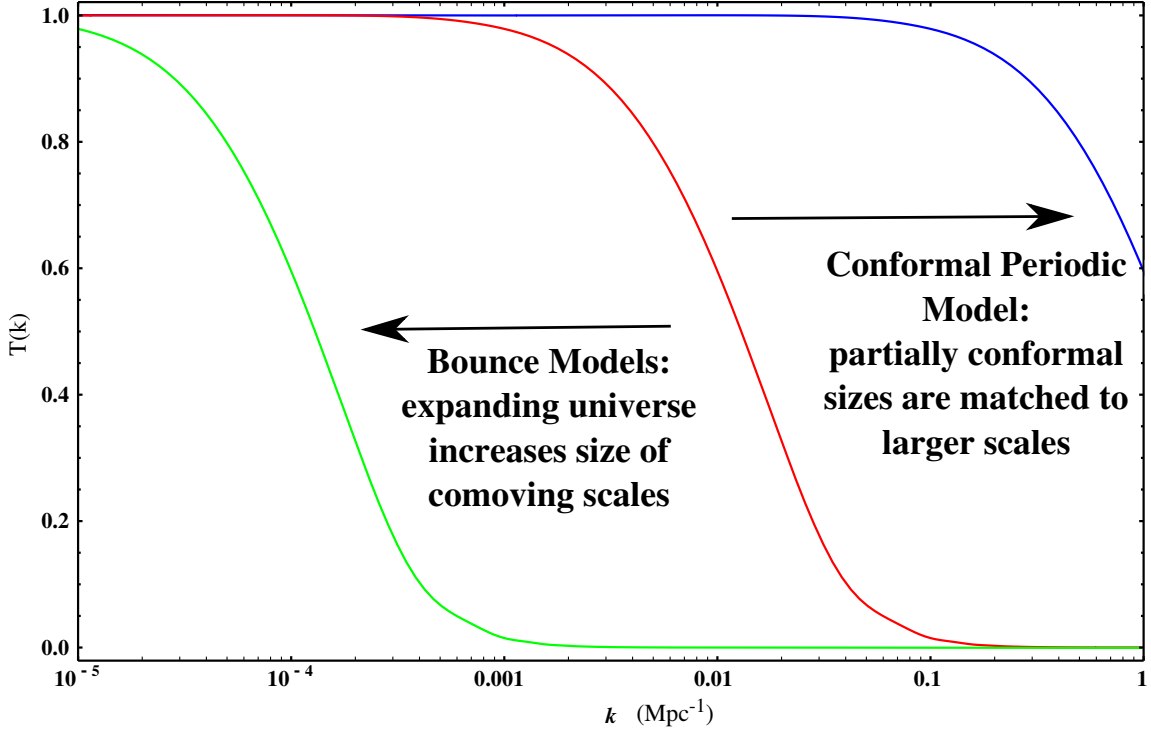
Figure 3.5: A plot of the transfer function with the shift in comoving scales of matching for our conformal periodic time cosmology model vs. the standard inflationary or bounce model expansions depicted. Our periodic time cosmology model shrinks large scales into small scales and recycles its power through each cycle, while most other models wash away the existing power spectrum to reform a new one.

3.4.2 The Creation of a Power Spectrum

Both inflation and the cyclic models will shift the small scale wavenumbers to larger scales, causing the visible power spectrum to be removed as the transfer function goes to zero at small scales. For inflation, the universe is inflated at early times, while bounce models do this at late times (during dark energy domination). This leaves an empty background on which a new nearly scale invariant power spectrum is constructed by some mechanism dependent on the model.

In part because of this trait, our model, despite using some of its conceptions, is not the same as Penrose's CCC. Not only was this original suggestion not exactly periodic, it also shifts the old power spectrum to zero and required a mechanism to reform the power

spectrum as other cyclic models. Our PTC model instead takes the shift of the power spectrum to be in the opposite direction. The reason for this is to allow for the periodicity to form a constraint on the new power spectrum instead of trying to conceive of a process to construct a new one. The comparison of these two mechanisms is shown in Figure 3.5.

In our model, we reuse (or recycle) the primordial power spectrum and everything else in the universe. In this way, it is unnecessary for us to create a mechanism for new matter to be created and a new primordial power spectrum to form. Typically the generation of the primordial power spectrum is required to predict something, but consistency in the context of PTC is enough to make testable predictions, without any generation mechanism.

3.4.3 Cyclic vs Periodic Models

Our model is designed on having exact periodicity to reduce the infinite series of universes required for cyclic models. We then use this exactness to construct a method to constrain the form of primordial power spectrum based on the required exact repetition. However, as stated, our model is phenomenological in nature, using the conditions of constraint to define the model instead of using a specific model to calculate the results. It is possible to therefore discuss the necessity of exact periodicity for this model to work. Without exact periodicity, this model would no longer have the conceptual niceties of not having a series of universes or the perfect constraint from our proposed model. However, the constraints would be loosened and the issues with having closed timelike curves would not be relevant.

A potential future examination of this may look at if this model is an attractor to determine if a series of universes would eventually lead to this type of thing.

3.4.4 Dynamical Dark Energy?

During our analysis, we found that non-trivial dark energy was required for our model to work. However, this may not be surprising. Modern cyclic universe models rely on the late time behaviour of the universe. And CTCs typically require matter violating the energy conditions to exist. Future precision tests of dark energy history (e.g., WFIRST, Euclid, LSST) will be able to test this prediction.

3.4.5 Closed Time Considerations

One of the big issues with this type of model is the consideration of the second law of thermodynamics. This may or may not be a real issue, as some have noted the fact that

this may only apply in an open system and not when considering the full universe [154]. Throughout previous sections, we have assumed this is not an issue. But let us consider here other solutions to this problem for cyclic universes. The original cyclic models had issues due to increasing of entropy at each cycle (which extended each cycle) [77]. The ekpyrotic model solves this issue by increasing the size of the universe each time, keeping a constant entropy density despite an increasing entropy [155]. CCC, the model closest to ours, uses black hole information loss to remove the increasing entropy [145]. Since our model decreases sizes instead of increasing them, no trick of increasing sizes to keep entropy density constant will work. The black hole case can work still, however.

Having an infinite space may prevent the entropy considerations from being relevant [154]. This would be required in order to have conformal symmetry at any time, as a finite spatial volume would create a preferred scale, removing the conformal symmetry required to make this work.

In talking about entropy, we left out consideration for the formation of an arrow of time. Having a time dimension which is not identical to the spatial ones is already known, both by having this dimension be the finite one as well as by the usage of FRW spacetime. FRW has a preferred time direction given that it lacks symmetry in that direction while maintaining symmetry for spatial directions. Future can be given by the direction of increasing universe size, which has relevance during times without conformal symmetry. While this doesn't solve all problems, anything further is beyond the scope of this chapter and probably unnecessary for our analysis.

3.4.6   Other Properties to Find

We also wonder if there are other observable signs of our proposed model. One proposal would be that there would be exact copies, and therefore an exactly fractal structure in the universe. Figure 3.2 shows what an image would look like if it were rescaled each cycle and passed through a low-pass filter like matter transfer function. If the universe were periodic, the fractal pattern produced would need to be exact. The rescaling would also create a preferred point. It might be possible to find signatures of these repeating rescaled structures in the large scale structure of the universe.

3.5 Conclusion

In this chapter, we developed a cosmological framework for periodic time dimension. This relies on the idea of matching infinite future and big bang, via conformal rescaling, following the original suggestion by Penrose [145]. We show that consistency fixes primordial power spectrum in terms of cosmic history, in the context of periodic time cosmology (PTC).

We then compared PTC predictions for standard cosmological histories to our current cosmological observations. We found that such a model can fit observations with a difference 1.8σ from the standard power law power spectra. While the data still favours the standard power-law, PTC model remains viable if a non-trivial dark energy equation of state is considered.

In our analysis, we found that having dark energy which is just a cosmological constant does not reproduce observations, being ruled out by 5.1σ. A further analysis indicates that the late time behaviour for dark energy is important. However, as discussed, this is expected for a cyclic model. These models are designed to take what will happen in the infinite future of our universe as a replacement for the effects which traditionally rely on inflation in the early universe.

Many questions still remain. For starters, the analysis presented is still preliminary. We need to rerun CosmoMC in order to get better fits. In addition, we need to evolve the transfer function into the infinite future to fit the data appropriately. Beyond this, we hope to find a better model for dark energy and to find a more physical origin of the matching condition. And many issues still remain unaddressed, like the issue of 2nd law of thermodynamics.

However, we end with a final question. Is it possible that we do not need to find a way to remove all the fluctuations from a former universe, and instead of trying to recreate them, perhaps we just need to recycle what is already there?

Chapter 4

Cosmological Perturbations in the 5D Holographic Big Bang Model

4.1   Introduction

Recently [156], a novel cosmological model was proposed in which our universe is a 3-brane emergent from the collapse of a 5-dimensional star. Motivated by the desire to see if a more satisfactory (or natural) understanding of these puzzles can emerge from an alternative description of the geometry, this model explains the evolution of our early universe whilst avoiding a big bang singularity. Furthermore, the model was shown to have a mechanism via which a homogeneous atmosphere outside the black hole generates a scale invariant power spectrum for primordial curvature perturbations, (nearly) consistent with current cosmological observations [157].

Our 5D holographic origin for the big bang is based on a braneworld theory that includes both 4 dimensional induced gravity *and* 5D bulk gravity: the Dvali-Gabadadze-Porrati (DGP) model [158], with action

$$
S_{DGP} = \frac{1}{16\pi G_5} \int_{\text{bulk}} d^5x \sqrt{-g} R_5 + \frac{1}{8\pi G_5} \int_{\text{brane}} d^4x \sqrt{-\gamma} K + \int_{\text{brane}} \sqrt{-\gamma} \left(\frac{R_4}{16\pi G_4} + \mathcal{L}_{\text{matter}} \right),
$$

(4.1)

where g and γ, G_5 and G_4, R_5 and R_4 are the metrics, gravitational constants and Ricci scalars of the bulk and brane respectively, while K is the mean extrinsic curvature of the

brane. Our universe, described by the metric

$$ds_4^2 = -d\tau^2 + \frac{a^2(\tau)}{\mathcal{K}}[d\psi^2 + \sin^2(\psi)(d\theta^2 + \sin^2(\theta)d\phi^2)]\,, \tag{4.2}$$

is represented by a hypersurface in a 5 dimensional Schwarzschild black hole spacetime

$$ds_5^2 = -\left(1 - \frac{\mu}{r^2}\right)dt^2 + \left(1 - \frac{\mu}{r^2}\right)^{-1}dr^2 + r^2 d\Omega_3^2\,, \tag{4.3}$$

located at $r = \frac{a(\tau)}{\sqrt{\mathcal{K}}}$. In this context, a pressure singularity is generically found when the energy density of the holographic fluid $\tilde{\rho}$ satisfies $\tilde{\rho} = \tilde{\rho}_s = \frac{3G_4}{16\pi G_5^2}$ [159]. The authors in [156] showed that the singularity happens at early times in the cosmic history as matter decays more slowly than a^{-4}. However, under the evolution from smooth initial conditions, the pressure singularity can occur before Big Bang Nucleosynthesis (BBN), and is generically inside a white hole horizon. Alternatively, the universe could have emerged from the collapse of a 5D star into a black hole, just before BBN, removing both pressure *and* big bang/white hole singularities. As advocated in the *fuzzball* program [160], the rate of this tunnelling is enhanced due to the large entropy of black hole microstates, which we speculate could match those of an expanding 3-brane thermal state. Our universe is represented by the boundary of a 5D spherically symmetric spacetieme with metric (4.3), in which we impose $\mathbb{Z}_2$ boundary conditions. This picture will be described in more detail in Section 4.2.

Interestingly, this model not only circumvents the singularity at the origin of time, but can also address other problems of cosmology that are typically solved by inflation. Because the collapsing star could have existed long before its demise, it had enough time to attain uniform temperature, thereby addressing the *Horizon Problem*. Furthermore, if we assume that the initial Hubble constant was of order of the 5D Planck mass, then the curvature density $-\Omega_k \sim (M_5 r_h)^{-2}$, where r_h is the radius of the black hole. Consequently $-\Omega_k \sim M_5/M_*$ could become very small for massive stars, thus solving the *Flatness Problem*. More generically, the *no hair* theorem ensures that a 3-brane nucleated just outside the event horizon of a massive black hole has a smooth geometry.

Yet another feature of the model is that a thermal atmosphere around the brane, composed of a gas of massless particles produces scale invariant curvature perturbations. In this work, we shall revisit this result, focusing our attention on the mechanism responsible for deviations from scale-invariance in the primordial curvature power spectrum in the context of the *5D Holographic origin of the Big Bang*. To this end, we consider a thin atmosphere that can be regarded as infalling matter, or the outer envelope of the collapsing

5D star, which resides in the 5D bulk and thus contributes to its energy momentum tensor. In this context, the DGP action Eq. (4.1) is modified to

$$S = S_{DGP} + \int_{\text{bulk}} d^5x \sqrt{-g} \mathcal{L}_{5,\text{atmosphere}} \tag{4.4}$$

where $\mathcal{L}_{5,\text{atmosphere}}$ accounts for the matter Lagrangian in the bulk. Consistency between cosmological phenomenology and the DGP model implies that the brane is expanding outwards, and thus eventually encounters this *atmosphere*. We then compute the resulting power spectrum of scalar curvature perturbations and the change of the Hubble parameter due to this encounter. We find that the best fit nucleation temperature of the 3-brane is considerably larger than the 5D Planck mass, perhaps indicating an origin in a 5D quantum gravity phase.

In Section 4.2, we discuss a possible mechanism for brane nucleation and the different scales involved in our problem, giving a qualitative description of the different physics processes. In Section 4.3, we solve Einstein equations with matter in the bulk, and the consequences that it has on the brane. In particular, we solve for the density profile of a 5D spherically collapsing atmosphere and compute the change on the Hubble parameter as it falls into our 3-brane. In Section 4.4, we study cosmological perturbations in the bulk and their projection onto the brane, making special emphasis on the curvature perturbation and its power spectrum. Section 4.5 compares our predictions against Planck data and contrasts it with the power-law power spectrum assumed in the ΛCDM model. We conclude our work with discussion of the limitations and prospects of our model in Section 4.6.

4.2   A 5D Holographic Big Bang

4.2.1   Brane Nucleation

As described in the introduction, we are working in the context of the 5D Holographic Big Bang model [156] where our universe is modelled as a hypersurface (the brane) in a 5-dimensional Schwarzschild space time according to the embedding $r = \frac{a(\tau)}{\sqrt{\mathcal{K}}}$. This construction is a solution of the DGP action (4.1) once we impose a $\mathbb{Z}_2$ boundary condition on the brane. As a consequence, via the embedding constraint the brane becomes an outward travelling boundary of the higher dimensional spacetime, an assumption that is necessary if we want our universe (represented by the brane) to be expanding.

From the perspective of an observer in the bulk, this setup is reminiscent of a construction proposed by Witten called the *'bubble of nothing'* [161], in which an interior region of

space is missing, with space ending smoothly at the surface of this bubble (the brane). One possible scenario in the 5D Holographic Big Bang model is that the brane was formed by the quantum tunnelling of a collapsing star in 5 dimensions, with all of the degrees of freedom of the inner part of the collapsing matter becoming degrees of freedom of the brane. This is analogous to the *fuzzball* paradigm, a model proposed to solve the information-loss paradox [162], which consists of the explicit construction of black hole microstates with no "dataless horizon region". The infalling matter can tunnel to a fuzzball state with amplitude [160]

$$\mathcal{A} \sim e^{-\frac{1}{G_5} \int R} \sim e^{-\alpha G_5 M^3} , \tag{4.5}$$

where $\alpha = \mathcal{O}(1)$ and we have used the length scale $r \sim G_5 M^2$ to estimate the Euclidean Einstein action for tunneling between two configurations that have the length and mass scales set to those of the black hole. Although this amplitude is very small, the number of fuzzball configurations that a black hole can tunnel to depends on the Bekenstein-Hawking entropy as

$$\mathcal{N} \sim e^{S_{BH}} \sim e^{G_5 M^3} \tag{4.6}$$

yielding a significant probability to form a fuzzball. In fact, the two exponentials exactly cancel each other [160]. We anticipate a similar principle operating here, in which collapsing matter at sufficiently high density – just prior to formation of a black hole horiozn– necessarily tunnels to a brane so as to avoid the ensuing quantum paradoxes that follow upon introducing an event horizon.

Since it is well established that BBN happened in the formation of our universe, and that in the 5D Holographic Big Bang (HBB) model [156] the pressure singularity generically forms before BBN, we consider a brane that must form before this. This means that the temperature of nucleation must be at most the temperature of BBN – $T_{\mathrm{BBN}} \sim 0.4\,\mathrm{MeV}$ [163]:

$$T_{\mathrm{nuc}} \geq T_{\mathrm{BBN}} \sim 0.4 \text{ MeV}. \tag{4.7}$$

Finally, let us mention that the DGP model possesses a scale $r_c = \frac{G_5}{G_4}$, above which 5-dimensional gravity dominates over 4-dimensional gravity. Constraints on the normal branch of the DGP model [164] give [1]

$$r_c \gtrsim 3H_0^{-1} \quad \rightarrow \quad M_5 < (H_0 M_4^2/12)^{1/3} \quad \rightarrow \quad M_5 < 9\,\mathrm{MeV}. \tag{4.8}$$

where $M_4 = \frac{1}{(8\pi G_4)^{1/2}}$ is the reduced 4D Planck mass.

---

[1]Planck 2015 constraints on the dark energy equation of state roughly imply $|1 + w| < 0.11$ at 95% level, at the pivot redshift of $z \simeq 0.23$ (Fig. 5 in [165]), which provides a similar bound on r_c, using the DGP Friedmann equation with a cosmological constant.
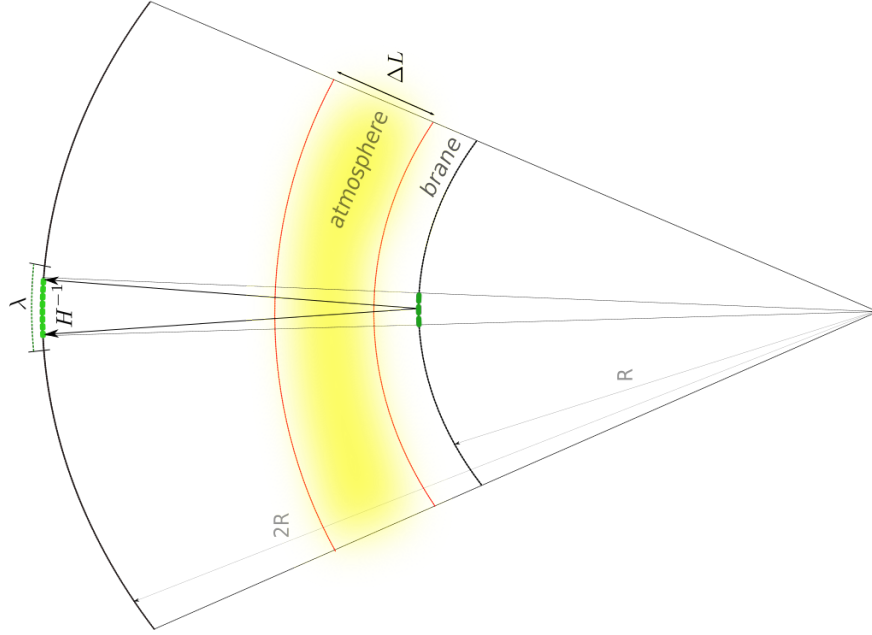
Figure 4.1: Cartoon of the different scales treated in this problem, in the black hole rest frame. The inner black circular arc represents the brane with radius R and the outer black circular arc represents the brane with radius $2R$. H^{-1} is estimated by tracing light rays on the brane after it has doubled it size; it is small if the brane is traveling near the speed of light. The atmosphere is shown in yellow sitting in between the two red arcs with length ΔL.

4.2.2 The Atmosphere: Setup and Scales

In this scenario, we are interested in the effects of a thin atmosphere located just outside the brane. Although the brane forms a $\mathbb{Z}_2$ boundary, excluding the event horizon in Eq. (4.3), we shall refer to the metric in Eq. (4.3) as the black hole metric.

In order to organize the different assumptions, we will review the implied hierarchy of the scales present in this problem. If we assume that the Hubble patch of our universe, at/near brane nucleation, is small enough to be insensitive to the curvature of the black hole spacetime, we can assume that the atmosphere is just a perturbation around a Minkowski background. This limit implies $H^{-1} \ll R$ where R is the radius of the black hole, or brane upon nucleation. This assumption is also observationally motivated, since today we

measure $(HR)^{-2} \ll |\Omega_k| \ll 1$ and thus our observable Hubble patch is approximately flat. In our model, if the brane is moving very close to the speed of light, $H^{-1} \ll R$. This will allow us to define metric perturbations in Section 4.4. We will then be interested in finding the behaviour of the power spectrum of curvature perturbations for modes of wavelength λ, that are of super-horizon size before BBN, but are now observable in the CMB sky. This restricts $R \gg \lambda \gg H^{-1}$.

Finally, we would like to understand the behaviour of different physical quantities of the brane, such as the behaviour of the Hubble parameter before and after the encounter with the atmosphere. Assuming it can be considered to be a thin atmosphere in the 5 dimensional space time, the width ΔL of the atmosphere needs to be smaller than R for the brane to cross the atmosphere completely in less than a Hubble time. We then get the following hierarchy of different scales

$$H^{-1} \ll \lambda \ll R, \text{ and } \Delta L \ll R \text{ (black hole frame)}, \tag{4.9}$$

$$\lambda \lesssim \Delta L \text{ (atmosphere frame)}. \tag{4.10}$$

As we shall in Section 4.4, the latter inequality is the key ingredient that leads to a near scale-invariant spectrum of primordial curvature perturbations for large scales. This hierarchy of scales is illustrated in Fig. 4.1.

4.3 Homogeneous brane meets thin atmosphere

4.3.1 Einstein Equations

We want to study the influence of an atmosphere that is falling into the black hole as shown in in Fig. 4.2. For this, we assume that the brane is moving supersonically (in fact, almost with the speed of light) into the atmosphere, and thus bulk metric perturbations do not react to the brane's presence until it runs into them.

The Einstein equations on the brane that follow from the action (4.4) are:

$$G_{\mu\nu} = 8\pi G_4 \left(T_{\mu\nu} + \tilde{T}_{\mu\nu} \right) \tag{4.11}$$

where the two different components of the energy-momentum tensor are $T_{\mu\nu}$, the matter living on the brane, and $\tilde{T}_{\mu\nu}$ the *holographic fluid* that is induced on the brane via the junction conditions described below. Due to the symmetry of the (unperturbed) FRW spacetime, $T_{\mu\nu}$ has the form of a perfect fluid

$$T_{\mu\nu} = (P + \rho) u_\mu u_\nu + P\gamma_{\mu\nu} , \tag{4.12}$$

83
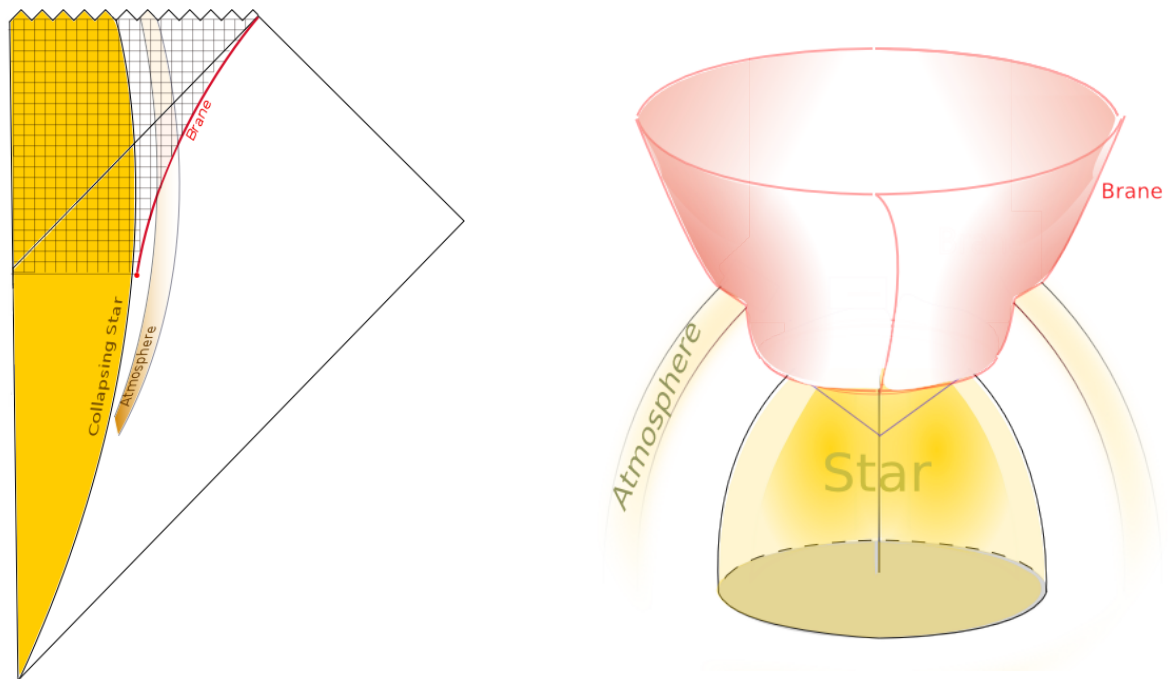
Figure 4.2: Penrose diagram (left), and cartoon of the 5D star collapse (right), followed by the nucleation of a 3-brane (our universe). The star (in yellow) that is collapsing (nearly) forms a black hole, but the 3-brane (red) will nucleate just prior to the formation of the event horizon, and traverses a thin atmosphere of infalling matter or atmosphere (cross-section shown in the cartoon at right).

where u^μ is the 4-velocity of the fluid normalized such that $u^\mu u_\mu = -1$.

The holographic fluid is the Brown-York stress tensor induced on the brane once Einstein equations are imposed on the bulk

$$\tilde{T}_{\mu\nu} = \frac{1}{8\pi G_5} \left(K\gamma_{\mu\nu} - K_{\mu\nu} \right), \tag{4.13}$$

where $K_{\mu\nu} \equiv \nabla_\alpha n_\beta e_\mu^\alpha e_\nu^\beta$ is the extrinsic curvature of the brane whose unit normal is n^α. Here $e_\nu^\alpha \equiv \frac{\partial \hat{x}^\alpha}{\partial x^\nu}$, where we have associated the set of coordinates $\{\hat{x}^\alpha\}$ and $\{x^\nu\}$ with the bulk and the brane respectively. In addition to the Einstein equations (4.11), the continuity equations for the total matter living on the brane arising from the Bianchi identities are:

$$\nabla^\mu \left(T_{\mu\nu} + \tilde{T}_{\mu\nu} \right) = 0. \tag{4.14}$$

The Gauss-Codazzi equations constrain the geometric quantities of the brane with the matter present in the bulk

$$\nabla^\mu \left(Kg_{\mu\nu} - K_{\mu\nu} \right) = 8\pi G_5 T_{\alpha\beta}^5 e_\nu^\alpha n^\beta, \tag{4.15}$$

$$R^4 + K^{\mu\nu} K_{\mu\nu} - K^2 = -16\pi G_5 T_{\alpha\beta}^5 n^\alpha n^\beta, \tag{4.16}$$

where $R^4 = -8\pi G_4 \left(T + \tilde{T} \right)$ is the Ricci scalar of the brane. $T_{\alpha\beta}^5$ is the energy momentum tensor of the bulk which satisfies the Einstein's equations on the bulk $G_{\alpha\beta} = 8\pi G_5 T_{\alpha\beta}^5$. Note that the first of the Gauss-Codazzi equations (4.15) reduces to the conservation of the holographic fluid $\tilde{T}_{\mu\nu}$ in the case that $T_{\alpha\beta}^5 = 0$. If the bulk matter flows into the brane, the holographic fluid is not conserved and the effect of the continuity equation (4.14) is to change the matter on the brane through the holographic fluid in order for the sum of both to be conserved.

In the same way, as a result of the symmetries of FRW spacetime, the holographic fluid must have the form of a perfect fluid. Moreover, the 4-velocity of this fluid must coincide with the 4-velocity of the normal matter on the brane:

$$\tilde{T}_{\mu\nu} = \left(\tilde{P} + \tilde{\rho} \right) u_\mu u_\nu + \tilde{P} \gamma_{\mu\nu}. \tag{4.17}$$

Combining Eqs. (4.13) and (4.17) we get:

$$K_{\mu\nu} = -8\pi G_5 \left[\left(\tilde{P} + \tilde{\rho} \right) u_\mu u_\nu + \frac{1}{3} \tilde{\rho}_{\mu\nu} \right]. \tag{4.18}$$

4.3.2 Shift in the Hubble

The rate of expansion described by the Hubble parameter will change as the brane goes through the atmosphere and we can find a general expression for H by studying the Einstein equations and junction conditions for the DGP brane in the general case. This general case treats the bulk as a 5-dimensional Schwarzschild black hole (4.3) and the brane as a hypersurface parametrized by $r = \frac{a(\tau)}{\sqrt{\mathcal{K}}}$, as detailed in the Introduction.

From Equations (4.11) and (4.14-4.16) we obtain

$$H^2 + \frac{\mathcal{K}}{a^2} = \frac{8\pi G_4}{3}\left(\tilde{\rho} + \rho\right) \tag{4.19}$$

$$\dot{\rho} + \dot{\tilde{\rho}} + 3H\left(\rho + \tilde{\rho} + P + \tilde{P}\right) = 0 \tag{4.20}$$

$$\dot{\tilde{\rho}} + 3H\left(\tilde{\rho} + \tilde{P}\right) = T^5_{\alpha\beta}e^\alpha_\tau n^\beta \tag{4.21}$$

$$0 = T^5_{\alpha\beta}e^\alpha_i n^\beta \tag{4.22}$$

$$(\rho + \tilde{\rho}) - 3\left(P + \tilde{P}\right) + \frac{8\pi G_5^2}{G_4}\left(\frac{2}{3}\tilde{\rho}^2 + 2\tilde{P}\tilde{\rho}\right) = -2\frac{G_5}{G_4}T^5_{\alpha\beta}n^\alpha n^\beta \tag{4.23}$$

The quantity $T^5_{\alpha\beta}$ is the stress-energy of the atmosphere outside the black hole. This atmosphere will have two effects on the brane. It will induce metric and matter perturbations in our universe, which we shall use to compute the curvature perturbation in Sec. 4.4 below. However it will also make the Hubble parameter change its value as the brane crosses the atmosphere: the brane will expand more slowly due to an extra source of infalling matter. Combining Eqs. (4.19) and (4.20) and ignoring the curvature term we get

$$\Delta H = -4\pi G_4 \int \left(P_T + \rho_T\right) d\tau, \tag{4.24}$$

where the integral is performed in the proper time of the brane and $P_T = P + \tilde{P}$, $\rho_T = \rho + \tilde{\rho}$.

Let's first look at the behavior of the holographic fluid $\tilde{P}$ and $\tilde{\rho}$. From Equation (4.23) we have

$$\tilde{P} + \tilde{\rho} = \frac{1}{3\left(\frac{\tilde{\rho}}{\tilde{\rho}_s} - 1\right)}\left[-2\frac{G_5}{G_4}T^5_{nn} - 4\tilde{\rho} + 2\frac{\tilde{\rho}^2}{\tilde{\rho}_s} + T\right], \tag{4.25}$$

where $T = 3P - \rho$, $T^5_{nn} = T^5_{\alpha\beta}n^\alpha n^\beta$ and $\tilde{\rho}_s = \frac{3G_4}{16\pi G_5^2}$. In order to avoid the pressure singularity we require $\tilde{\rho} \gg \tilde{\rho}_s$ and in this limit the last equation becomes

$$\tilde{P} + \tilde{\rho} = \frac{1}{3}\left[-2\frac{G_5}{G_4}T^5_{nn}\frac{\tilde{\rho}_s}{\tilde{\rho}} + 2\tilde{\rho} + T\frac{\tilde{\rho}_s}{\tilde{\rho}}\right]. \tag{4.26}$$

Now let's analyze the behavior for the the matter on the brane P and ρ. Combining Eqs. (4.20) and (4.21) and assuming an equation of state $P = w\rho$ the fluid on the brane satisfies

$$\dot{\rho} + 3H\left(\rho + P\right) = -T^5_{\alpha\beta}e^\alpha_\tau n^\beta \Rightarrow \frac{d}{d\tau}(\rho a^{3(w+1)}) = -T^5_{\alpha\beta}e^\alpha_\tau n^\beta a^{3(w+1)} \,. \tag{4.27}$$

If we now assume that the atmosphere is thin enough so that we can approximate the matter distribution as a delta function (i.e. $H\Delta\tau \ll 1$, during the impact time $\Delta\tau$), we see that the last equation will give a jump in the density (and hence in the pressure) proportional to a step function. In fact, if we consider the system of equations (4.19-4.23), with $P = w\rho$, and a delta function $T^5_{\alpha\beta}$, the only consistent solution would have a delta function in $\tilde{P}$, with step function jumps in other variables. As such, the biggest contribution in Eq. (4.24) is given by the first term on the right hand side of Eq. (4.26):

$$\Delta H = \frac{G_4}{2G_5} \int \frac{T^5_{\alpha\beta}n^\alpha n^\beta}{\tilde{\rho}} d\tau \left[1 + \mathcal{O}(H\Delta\tau)\right] \,. \tag{4.28}$$

We shall see in Sec. 4.4 below that the amplitude of curvature perturbations depends on $\Delta \ln H = \frac{\Delta H}{H}$. To compute this, we note that from Eq. (4.19) we can write $H^2 \approx \frac{8\pi G_4}{3}(\tilde{\rho} + \rho) \approx \frac{8\pi G_4}{3}\rho$ in the regime where $\rho \gg \tilde{\rho}$. Then

$$\Delta \ln H \approx \frac{G_4}{2G_5}\sqrt{\frac{3}{8\pi G_4}}\frac{1}{\sqrt{\rho\tilde{\rho}}} \int T^5_{\alpha\beta}n^\alpha n^\beta \, d\tau \,, \tag{4.29}$$

We can now use the solution in vacuum for $\tilde{\rho}$ found in [156]

$$\tilde{\rho} = \tilde{\rho}_s\left(1 + \sqrt{1 - \frac{2(\rho_{BH} - \rho)}{\tilde{\rho}_s}}\right) \,, \tag{4.30}$$

where $\rho_{BH} = \frac{3\Omega^2_k H^4_0 r^2_h}{8\pi G_4 a^4}$. In the approximation where $\rho \gg \rho_{BH}$ and $\rho \gg \tilde{\rho}_s$ we find

$$\tilde{\rho} \approx \rho\sqrt{\frac{2\tilde{\rho}_s}{\rho}} \tag{4.31}$$

and then Eq. (4.29) reads

$$\Delta \ln H \approx \frac{1}{2\rho} \int T^5_{\alpha\beta}n^\alpha n^\beta d\tau \,, \tag{4.32}$$

implying that the relative jump in the Hubble parameter due to a thin atmosphere is the ratio of the work done by the pressure of the atmosphere to the energy of the brane.

4.3.3 Profile of the atmosphere

So far we have considered a general energy momentum tensor on the bulk responsible of dynamic features on the brane. Let's now consider that the bulk is filled with a relativistic spherically symmetric, collapsing 5D radiation atmosphere ($P_5 = \frac{1}{4}\rho_5$) that represents the atmosphere whose energy momentum tensor is

$$T^5_{\alpha\beta}(w) = \rho_5(w)\left[\left(1 + \frac{1}{4}\right)\delta^0_\alpha\delta^0_\beta + \frac{1}{4}\eta_{\alpha\beta}\right].$$

(4.33)

In order to study the effect of this atmosphere we need to introduce scalar homogeneous perturbations in the bulk. A generalization of 4D perturbation theory allows us to write the perturbed metric of the bulk in the Newtonian gauge in 5D as

$$ds^2_{\text{bulk}} = -[1 + 2\Phi_5(x^\alpha)]dt^2 + [1 - 2\Psi_5(x^\alpha)][dx^2 + dy^2 + dz^2 + dw^2].$$

(4.34)

where Φ_5 and Ψ_5 represent the scalar perturbations of the bulk and x^α are bulk coordinates. Our universe is represented as a hypersurface in the 5D bulk, whose trajectory is given by the constraint $w = f(x^\mu)$. In this setup, the brane will inherit three bulk coordinates $\{t, x, y, z\}$ and will respond to perturbations that are just functions of the bulk time via the relation $w = f(x^\mu)$. Consider that the metric perturbations and the brane position are homogeneous:

$$\Phi_5 = \epsilon\Phi^0_5(w), \quad \Psi_5 = \epsilon\Psi^0_5(w), \quad f = f_0(t),$$

(4.35)

where $\epsilon \ll 1$ is a parameter that controls the homogeneous metric perturbations. Assuming hydrostatic equilibrium in the (infalling) rest frame of the atmosphere, the Einstein Equations in the bulk for the metric (4.34) leads to the relativistic Poisson and Euler equations:

$$\nabla^2\Phi^0_5 = \frac{8\pi G_5}{3}\rho_5,$$

(4.36)

$$\nabla\Phi^0_5 = -\frac{1}{4}\frac{\nabla\rho_5}{\rho_5}.$$

(4.37)

These equations can be solved exactly in Minkowski background:

$$\rho_5(w) = \bar{\rho}_5\left\{1 - \tanh^2\left[\bar{\gamma}\left(\frac{w}{\bar{w}} - 1\right)\right]\right\},$$

(4.38)

where $\bar{\rho}_5 \equiv \frac{3}{16\pi G_5}\frac{\bar{\gamma}^2}{\bar{w}^2}$, while $\bar{\gamma}$ and $\bar{w}$ are constants of integration.

The relationship between the energy density and the temperature of the atmosphere can be computed by integrating the Bose-Einstein distribution in 4+1 dimensions

$$\rho_5(w) = \int \frac{d^4k}{(2\pi)^4} \frac{\omega}{\exp\left[\omega/T_5(w)\right] - 1} = \frac{3\zeta_R(5)}{\pi^2} T_5(w)^5 \,, \tag{4.39}$$

where $\omega^2 = k_\alpha k^\alpha$. The above expression allows us to write

$$T_5(w) = \left(\rho_5(w)\frac{\pi^2}{3\zeta_R(5)}\right)^{\frac{1}{5}} = 1.26 \, \rho_5(w)^{1/5} \,. \tag{4.40}$$

Note that the characteristic thickness of the atmosphere is given by

$$\Delta L = \frac{\bar{w}}{\sqrt{2}\bar{\gamma}} \,. \tag{4.41}$$

We are now in position to compute Eq. (4.32) and we will do so in the reference frame of the atmosphere. In this frame ρ_5 does not depend on time, but the normal to the brane n^α will depend on the relative velocity of the brane and the atmosphere. First consider the fluid velocity $u^\alpha = (1, \mathbf{v})/\sqrt{1 - v^2}$, where $\mathbf{v}$ is the relative 3 velocity between the brane and the atmosphere. If we now require $n_\alpha n^\alpha = 1$ and $n^\alpha u_\alpha = 0$ we have $n^\alpha = (v, \mathbf{v}/v)/\sqrt{1 - v^2}$. With this we can write $T^5_{\alpha\beta} n^\alpha n^\beta = \rho_5(w)(1 + 4v^2)/4(1 - v^2)$ and the RHS of Eq. (4.32) reads

$$\begin{aligned}
\Delta \ln H &= \frac{1}{2\rho} \int T^5_{\alpha\beta} n^\alpha n^\beta d\tau = \frac{1}{2\rho} \int_0^\infty T^5_{\alpha\beta} n^\alpha n^\beta \sqrt{1 - v^2} dt \,, \\
&= \frac{1}{2\rho} \int_0^\infty T^5_{\alpha\beta} n^\alpha n^\beta \sqrt{1 - v^2} \frac{dw}{v} \,, \\
&= \frac{(1 + 4v^2)}{v\sqrt{1 - v^2}} \frac{\bar{\rho}_5}{8\rho} \frac{\bar{w}}{\bar{\gamma}} \left[1 + \tanh(\bar{\gamma})\right] \,.
\end{aligned} \tag{4.42}$$

4.4 Cosmological perturbations

As discussed in the last section, if the velocity of the brane is near the speed of light we can assume that the Hubble patch of the universe will be smaller than the curvature radius of the black hole spacetime. In this regime it is safe to approximate the bulk as Minkowski spacetime and analyze the perturbations around it. In the last section we have briefly introduced the homogeneous scalar perturbations and in Appendix A.1 we present

the anisotropic perturbations. The curvature perturbation can be written as function of the scalar gauge invariant quantities (A.8)

$$\zeta = \Psi_4 - \frac{H}{\dot{H}}\left(H\Phi_4 + \dot{\Psi}_4\right). \tag{4.43}$$

Note that in our framework the Hubble constant is of first order in the perturbation (see Eq.(A.9)) as the brane crosses the atmosphere, and thus the term $H\Phi_4$ can be neglected. With this we have

$$\zeta \approx \Psi_4 - \frac{\Delta\Psi_4}{\Delta \ln(H)}, \tag{4.44}$$

where $\Delta\Psi_4 = \Psi_{4_f} - \Psi_{4_i}$. Here $\Psi_{4_{i(f)}}$ stands for the metric perturbation in 4D right before (after) the brane crossed the atmosphere, and we assume that ζ evolves continuously. We are interested in the value of the curvature perturbation after the brane has passed through the atmosphere where the metric perturbation $\Psi_{5_f} = 0$, which makes $\Psi_{4_f} = 0$. In this regime the curvature perturbation becomes

$$\zeta = \zeta_f \approx \frac{\Psi_{4i}}{\Delta \ln(H)}. \tag{4.45}$$

We are now ready to analyze the behaviour of the curvature perturbation power spectrum

$$P_\zeta(k) = \int d^3\mathbf{x}\, e^{i\mathbf{k}\cdot\mathbf{x}}\langle\zeta(x)\zeta(0)\rangle. \tag{4.46}$$

If the atmosphere is not in thermal equilibrium, we can relate the 2-point correlation function of the thermal fluctuations in 5D energy density to the temperature profile of the atmosphere:

$$\langle\rho_5(y_1)\rho_5(y_2)\rangle = \alpha\,(T_5(y_1))^6\delta^4(y_1 - y_2). \tag{4.47}$$

To proceed, we notice that in [156] it was found that the 5D energy density correlation function due to a thermal gas is

$$\langle\rho_5(y_1)\rho_5(y_2)\rangle \simeq \frac{5}{8}\left[\int\frac{d^4k}{(2\pi)^4}\left[\frac{1}{\exp(\omega/T_5) - 1} + \frac{1}{2}\right]\omega\exp[ik_a(y_1^a - y_2^a)]\right]^2. \tag{4.48}$$

This expression can be approximated as a delta function $\langle\rho_5(y_1)\rho_5(y_2)\rangle \simeq \alpha(T_5(y_1))^6\delta^4(y_1 - y_2)$, where $\alpha = \frac{5}{8}\left[\frac{1}{\pi^2 63}(945\zeta_R(5) - \pi^6)\right]$, while we have dropped the power-law UV divergence and ζ_R is the Riemann zeta function. Note, that (4.48) can be approximated by a 4 dimensional delta function on length scales larger than the thermal wavelength T_5^{-1}.

With the use of the Poisson equation in 5D

$$\nabla^2 \Psi_5(y) = \frac{8\pi G_5}{3}\rho_5(y)\,,\tag{4.49}$$

we can find the power spectrum for the curvature perturbation to be (see Appendix A.2 for details)

$$\mathcal{P}(k) = \frac{k^3}{2\pi^2}P_\zeta(k) = \beta\,k\int_0^\infty dw\,e^{-2|w|k}\,(T_5(w))^6 \tag{4.50}$$

$$= \Delta_0^2\,k\int_0^\infty dw\,e^{-2|w|k}\,\left\{1 - \tanh^2[\bar{\gamma}(w/\bar{w} - 1)]\right\}^{6/5} \tag{4.51}$$

where $\Delta_0^2 = \beta\,[\bar{T}_5]^6$, $\beta = \frac{\alpha}{2}\left(\frac{G_5}{6\Delta\ln H\,\pi^3}\right)^2$ and we have used Eqs.(4.39) and (4.40) of Sec. 4.3.3 to write the temperature of the brane. The power spectrum predicted by our model is characterized by 3 free parameters $\bar{\gamma}, \bar{w}, \Delta_0^2$ which we are going to fit to Planck data in the next section.

4.5 Observational constraints on 5D holographic big bang

The standard model of cosmology, ΛCDM, is described by 6 parameters $(\Omega_b h^2, \Omega_c h^2, \theta, \tau, \Delta_0^2, n_s)$, the baryon density, dark matter density, angular size of the sound horizon at recombination, the optical depth to reionization, amplitude of the scalar power spectrum and its tilt respectively. This model characterizes early universe cosmology via the power spectrum of the curvature perturbations

$$\mathcal{P}(k) = \Delta_0^2\left(\frac{k}{k_*}\right)^{n_s-1}\,,\tag{4.52}$$

where $k_* = 0.05/\text{Mpc}$ is the comoving pivot scale. This form of the power spectrum, expected in slow-roll inflationary models, best fits the CMB data with parameter values [157]

$$\Delta_0^2 = (2.196 \pm 0.059) \times 10^{-9} \qquad n_s = 0.9603 \pm 0.0073\,. \tag{4.53}$$

We would like to compare this model with the HBB model (Eq. 4.51) that strictly is represented by the seven parameters $(\Omega_b h^2, \Omega_c h^2, \theta, \tau, \bar{\gamma}, \bar{w}, \Delta_0^2)$. In order to compare models with the same number of parameters, will also include ΛCDM with running $\alpha_s = dn_s/d\ln q$.

Table 4.1: Planck 2015 and BAO best fit parameters and 68% ranges for HBB and ΛCDM models. The last row indicates the χ^2 for each of the models. Note that $\bar{w}_c$ corresponds to the comoving value of the position of the centre of the atmosphere and its related to the physical $\bar{w}$ via $\bar{w} = \bar{w}_c \frac{2.3 \times 10^{-10} \text{MeV}}{T_{\text{nuc}}}$.

	HBB		ΛCDM		ΛCDM with running	
	best fit	68% range	best fit	68% range	best fit	68% range
$\Omega_b h^2$	0.02212	0.02210 ± 0.00023	0.02227	0.02225 ± 0.00020	0.02231	0.02229 ± 0.00022
$\Omega_c h^2$	0.1172	0.1169 ± 0.0012	0.1185	0.1186 ± 0.0012	0.1184	0.1186 ± 0.0012
100θ	1.04113	1.04116 ± 0.00042	1.04103	1.04104 ± 0.00042	1.04108	1.04105 ± 0.00041
τ	0.081	0.083 ± 0.014	0.067	0.067 ± 0.013	0.069	0.068 ± 0.013
$10^9 \Delta_0^2$	5.79	0.793 ± 0.021	5.798	5.798 ± 0.019	5.82	5.82 ± 0.020
n_s			0.9682	0.9677 ± 0.0045	0.9682	0.9671 ± 0.0045
α_s					-0.0027	-0.0030 ± 0.0074
$\bar{\gamma}$	0.513	0.525 ± 0.053				
$\bar{w}_c\,[\text{Mpc}]$	275	297^{+39}_{-77}				
χ^2	11327.4		11319.9		11319.6	

We have performed the comparison by running the CosmoMC code [166, 167, 168, 169, 170, 171, 172] with Planck 2015 data, Barionic Acoustic Oscillations (BAO) [173, 174, 175, 176, 177, 178, 179, 180] as well as lensing data [125, 181, 127, 182, 183]. Finally, to determine the best fit parameters and the likelihood, we run the minimizer expressing our results Table 4.1. Comparing best-fit χ^2 of HBB and ΛCDM (with running), we see that HBB is disfavoured at roughly 2.7 2.8σ (2.8σ). The Planck angular TT spectrum together with the best fit curves and residuals for HBB and ΛCDM are shown in Fig. 4.3. The best fit primordial scalar power spectrum in both models are also contrasted with a non-parametric reconstruction from Planck 2015 data [184]. We note that the difference between the two models (mostly) lies within the 68% region and the largest disagreement of the models is at low l's or k's.

We are now going to analyze the physical implications of the best fit parameters $\{\bar{\gamma}, \bar{w}_c, \Delta_0^2\}$. In particular, we are interested in the temperature and position of the atmosphere and the change on Hubble constant of the brane when crossing the atmosphere. All of these physical quantities are related to the fitted parameters, and also to the temperature of the brane at nucleation T_{nuc} and the Planck mass in the bulk M_5. Using $\bar{w} = \bar{w}_c \frac{2.3 \times 10^{-10} \text{MeV}}{T_{\text{nuc}}}$ and Eqs. (4.38), (4.39) and (4.41) we can find the values for the amplitude of the energy density, the temperature and the width of the atmosphere respectively. We have summarized our results in Table 4.2.

The model still allows freedom for the parameters $\{T_{\text{nuc}}, M_5, v\}$. These can be con-
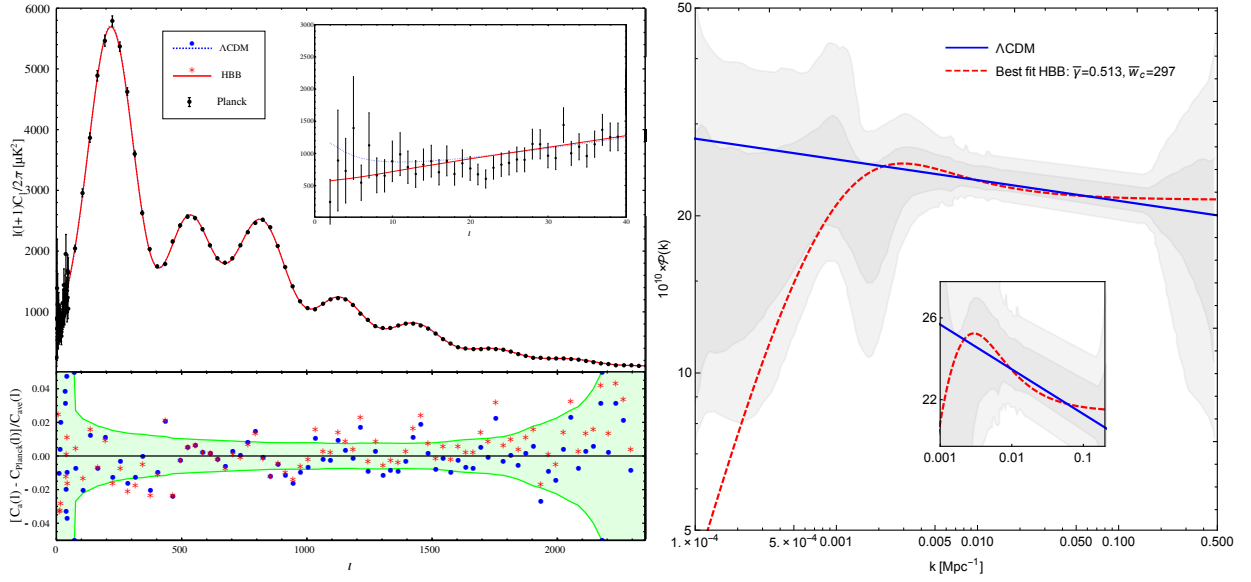
Figure 4.3: Left-Top: angular power spectrum of CMB temperature anisotropies, comparing Planck 2015 data (black dots) with best HBB model (solid/red) for all l. Left-Inset: angular power spectrum of CMB temperature anisotropies, comparing Planck 2015 data with ΛCDM (dotted/blue) and HBB (solid/red) for $l < 40$. Left-Bottom: relative residuals and difference between ΛCDM and HBB (black solid) where the green shaded region indicates the 68% region of Planck 2015 data. Right: Best fit of the primordial power spectrum as predicted by HBB (dashed-red) in comparison with the best fit of ΛCDM model (blue). The grey regions are the $\pm 1\sigma$ and $\pm 2\sigma$ constraints from a non-parametric reconstruction using Planck 2015 data [184].

Table 4.2: Physical characteristics of the HBB model using the best fit parameters presented in Table 4.1. The first column shows the relevant physical parameters and their definitions in terms of the best fit parameters and related quantities. The second column shows the numerical values and scaling with M_5 and $T_{\rm nuc}$. Finally, in the last column we show the limits necessary for the thin atmosphere condition (4.61). The 5th and 6th rows show the shift in the Hubble constant when crossing the atmosphere computed using perturbations and bulk background information, respectively. The 7th row presents a function constraining the velocity of the atmosphere in the bulk that can be computed by equating the results of rows 5 and 6. Note that $T_{\rm nuc} \geq 0.4\,{\rm MeV}$ in order for the BBN constraint to be valid.

Quantity	Value	Thin atmosphere bound $M_5 \leq 8.56 \times 10^{-4} \left(\frac{\rm MeV}{T_{\rm nuc}}\right)^{5/21} T_{\rm nuc}$ (4.61)
$\bar{w} = \bar{w}_c \frac{2.3 \times 10^{-10}\,{\rm MeV}}{T_{\rm nuc}}$	$9.872 \times 10^{27}\, \frac{1}{T_{\rm nuc}}$	$9.872 \times 10^{27}\, \frac{1}{T_{\rm nuc}}$
$\bar{\rho}_5 = \frac{3}{16\pi G_5} \frac{\bar{\gamma}^2}{\bar{w}^2}$	$1.62 \times 10^{-56}\, M_5^3\, T_{\rm nuc}^2$	$\leq 1.02 \times 10^{-65} \left(\frac{\rm MeV}{T_{\rm nuc}}\right)^{5/7} T_{\rm nuc}^5$
$\bar{T}_5 = 1.26\, \bar{\rho}_5^{1/5}$	$8.75 \times 10^{-12}\, (M_5^3\, T_{\rm nuc}^2)^{1/5}$	$\leq 1.26 \times 10^{-13} \left(\frac{\rm MeV}{T_{\rm nuc}}\right)^{1/7} T_{\rm nuc}$
$\Delta L = \frac{1}{\sqrt{2}} \frac{\bar{w}}{\bar{\gamma}}$	$1.35 \times 10^{28} \frac{1}{T_{\rm nuc}}$	$1.35 \times 10^{28} \frac{1}{T_{\rm nuc}}$
$\Delta \ln H = \frac{G_5 T(0)^3}{6\pi^3 \Delta_0} \left(\frac{\alpha}{2}\right)^2$ Eq. (4.56)	$4.54 \times 10^{-35} \left(\frac{T_{\rm nuc}}{M_5}\right)^{6/5}$	$\geq 2.18 \times 10^{-31} \left(\frac{T_{\rm nuc}}{\rm MeV}\right)^{2/7}$
$\Delta \ln H = f(v) \frac{\bar{\rho}_5}{8\rho} \frac{\bar{w}}{\bar{\gamma}} [1 + \tanh(\bar{\gamma})]$ Eqs. (4.57) and (4.42)	$1.62 \times 10^{-29} \left(\frac{M_5}{T_{\rm nuc}}\right)^3 f(v)$	$\geq 2.18 \times 10^{-31} \left(\frac{T_{\rm nuc}}{\rm MeV}\right)^{2/7}$
$f(v) = \frac{(1 + 4v^2)}{v\sqrt{1-v^2}}$	$2.8 \times 10^{-6} \left(\frac{T_{\rm nuc}}{M_5}\right)^{21/5}$	$\geq 2.14 \times 10^7 \frac{T_{\rm nuc}}{\rm MeV}$

94

strained using observational bounds for DGP model and by requiring consistency of our approximations. In particular, we have modelled the atmosphere as being thin, which is equivalent to the requirement that the time it takes the brane to cross it is less than a Hubble time:

$$\Delta L \frac{\sqrt{1-v^2}}{v} \leq H^{-1} = \left(\frac{3}{8\pi G_4 \rho}\right)^{1/2} \quad \Rightarrow \quad T_{\text{nuc}} \leq \frac{v}{\sqrt{1-v^2}} 2.33 \times 10^{-7} \, \text{MeV}\,, \quad (4.54)$$

employing the fact that the energy density on the brane at nucleation time is $\rho = \frac{\pi}{30} g_* T_{\text{nuc}}^4$, for g_* effective relativistic degrees of freedom. The above bound is consistent with the BBN constraint ($T_{\text{nuc}} \geq T_{\text{BBN}}$) for velocities near the speed of light. On the other hand, as discussed in Section 4.3.2 when the brane encounters the atmosphere its Hubble parameter will change as predicted by Eq. (4.42). Since this quantity enters in the amplitude of the power spectrum Eq. (4.51) we can write

$$\Delta_0^2 = \beta \, \bar{T}_5^6\,, \qquad \beta = \left(\frac{G_5}{6\pi^3 \Delta \ln H}\right)^2 \tag{4.55}$$

and thus

$$\Delta \ln H = 4.54 \times 10^{-35} \left(\frac{T_{\text{nuc}}}{M_5}\right)^{6/5}. \tag{4.56}$$

We also get a constraint on $\Delta \ln H$ from the bulk atmosphere using Eq. (4.42)

$$\Delta \ln H = 1.62 \times 10^{-29} \frac{(1+4v^2)}{v\sqrt{1-v^2}} \left(\frac{M_5}{T_{\text{nuc}}}\right)^3, \tag{4.57}$$

Using Eqs. (4.56) and (4.57) we can constrain the velocity and the speed of sound of the brane

$$f(v) = \frac{(1+4v^2)}{v\sqrt{1-v^2}} = 2.8 \times 10^{-6} \left(\frac{T_{\text{nuc}}}{M_5}\right)^{21/5}. \tag{4.58}$$

From the above equation we notice that in order to have a real brane velocity we need to satisfy

$$T_{\text{nuc}} \geq 30 \, M_5\,. \tag{4.59}$$

We can obtain a constraint for $\{T_{\text{nuc}}, M_5\}$ by combining expressions (4.58) and (4.54) and noting that in the large velocity limit $\frac{v}{\sqrt{1-v^2}} \approx \frac{1}{\sqrt{1-v^2}} \approx \frac{f(v)}{5}$

$$T_{\text{nuc}} \leq 1.31 \times 10^{-13} \left(\frac{T_{\text{nuc}}}{M_5}\right)^{21/5} \text{MeV}\,. \tag{4.60}$$

Inverting this we find

$$M_5 \leq 8.56 \times 10^{-4} \left(\frac{\text{MeV}}{T_{\text{nuc}}} \right)^{5/21} T_{\text{nuc}} \,. \tag{4.61}$$

This bound represents the maximum allowed value of M_5 in order for the thin atmosphere condition to be satisfied. In the third column of Table 4.2 we list the values for the physical quantities allowing M_5 to saturate the above bound. This constraint must be combined with the physical constraint (4.7)

$$T_{\text{nuc}} > T_{\text{BBN}} \sim 0.4 \text{ MeV} \tag{4.62}$$

as well as with the constraint (4.8)

$$M_5 < 9 \text{ MeV} \,, \tag{4.63}$$

on the normal branch of DGP in order to get the allowed region in parameter space for $\{T_{\text{nuc}}, M_5\}$ – depicted in Fig.4.4 (blue shaded region).

It is interesting to compare the thermal entropy of our brane to the holographic bound expected from its surface area in 5D. The entropy for the 5D black hole is $S_{BH} = \frac{A}{4G_5}$, while the entropy density in a universe dominated by relativistic particles $s(T) = \frac{4\pi^2}{90} g_* T_{\text{nuc}}^3 \simeq 4.71 \times T_{\text{nuc}}^3$, for $g_* = 10.75$ effective relativistic degrees of freedom, prior to electron/positron annihilation [185]. This puts a lower bound

$$M_5 > 0.23 \left(\frac{T_{\text{nuc.}}}{0.4 \text{ MeV}} \right) \text{ MeV} \qquad \text{(holographic bound)} \tag{4.64}$$

on the 5D Planck mass $M_5 = \frac{1}{(32\pi G_5)^{1/3}}$, where $T_{\text{nuc.}}$ is the nucleation temperature of the brane. We show the Holographic bound allowed region in parameter space in Fig. 4.4 (orange shaded region). Eqs. (4.64)-(4.8) constrain the 5D Planck mass to be within 1.5 decades in energy:

$$0.23 \text{ MeV} < M_5 < 9 \text{ MeV}, \tag{4.65}$$

a range that will inevitably shrink with future observations that better constrain BBN, and late-time cosmic expansion history. As we see in Fig.4.4, the best-fit value for $T_{\text{nuc.}}$ from cosmological observations (assuming the thin atmosphere condition) does violate the holographic bound (4.64) by at least 2.5 orders of magnitude, which would decrease the lower limit on M_5 in Eq. (4.65) by the same factor[2].

---

[2] Note that the exact saturation of the holographic bound predicts a brane velocity that is not real.

Is this a "show-stopper"? While the holographic bound on entropy remains a very well-motivated conjecture, it is not clear how firm it might be as objects that get close to crossing it are already in the quantum gravity regime where the classical description of spacetime physics fails. One may argue that since the degrees from responsible for thermal entropy of our brane are on scales much smaller than the 5D Planck length, they are not accessible by a 5D bulk observer, and thus are not limited by the 5D holographic bound.

4.6   Summary and Discussion

The 5D Holographic Big Bang (HBB) is a novel proposal for a holographic origin of our universe as a 3-brane with induced gravity, out of the collapse of 5D star that can address the traditional problems of big bang cosmology. The main goal of this study was to provide detailed and concrete predictions for this proposal, and to see whether it can serve as a possible competitor to slow-roll inflationary models to explain cosmological observations.

We first focused our attention on a possible mechanism for the nucleation of our 3-brane in which the quantum degrees of freedom of the bulk tunnel into a fuzzball configuration reminiscent to the *bubble of nothing* model. This mechanism not just provides a possible scenario of brane nucleation but also constrains the Planck mass in the bulk.

Previous work has shown that the presence of uniform thermal gas in the 5D bulk leads a scale-invariant primordial power spectrum for cosmological scalar perturbations. To formalize this result and search for mechanisms that could potentially explain deviations from scale-invariance (observed in the CMB data), we studied cosmological perturbations induced by a thin infalling atmosphere. This atmosphere is composed of a spherically symmetric thermal relativistic gas that the brane encounters after nucleation. We showed that this atmosphere induces a change in the Hubble parameter and also scalar cosmological perturbations on the brane. The power spectrum is scale invariant for large k's and scales as k for small k's.

We then tested this prediction for power spectrum against the cosmological observations. The transition is characterized by a decay of $1/k$ for scales where the power spectrum is highly constrained by data [184] as shown in Fig. 4.3 (right). We found that our model is broadly consistent with non-parametric reconstruction of primordial power spectrum, but is disfavoured compared to a pure power-law at 2.7σ level. We finally outlined various theoretical constraints on the nucleation temperature and 5D Planck mass in the HBB model, and found that the best fit nucleation temperature of the 3-brane was at least 3 orders of magnitude larger than the 5D Planck mass.
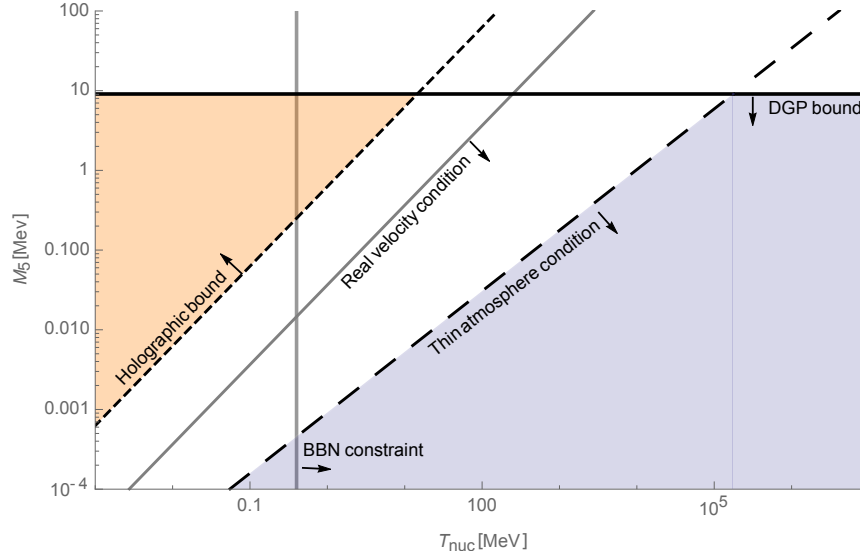
Figure 4.4: Theoretical and empirical bounds for the Holographic Big Bang model. The DGP bound Eq.(4.63) (thick-black) and the holographic bound Eq.(4.64) (black, thin dashed), together with the BBN bound Eq.(4.62) (vertical black) constitute the theoretical bounds of the model. The top shaded area (orange) is the allowed region for these three bounds to be satisfied. The real velocity bound Eq.(4.59) (thick, grey) and the thin atmosphere condition (4.60) (black, thick dashed) constitute the empirical bounds that HBB must satisfy. The bottom shaded area (blue) is the allowed region of $\{M_5, T_{\mathrm{nuc}}\}$ parameter space satisfying the empirical bounds, and the arrows indicate the directions in which the different bounds apply. It is clear that the empirical bounds violate the holographic bound for all possible allowed pairs $\{M_5, T_{\mathrm{nuc}}\}$ by at least 2.5 orders of magnitude. The least severe violation of the holographic bound is for parameters at the bottom left of the plot: for T_{nuc} being the minimum allowed value by BBN and M_5 the maximum allowed by the thin atmosphere condition (third column of Table 4.2).

This first attempt to understand the detailed consequences of the HBB model for cosmology relies on several simplifying assumptions that can be relaxed in future work. Some of the issues that remain to be tackled are:

1. Perhaps our most perplexing finding was that our best-fit model violated the holographic entropy bound by 8 orders of magnitude. It is not yet clear whether this is a feature or a bug!

2. It would be interesting to study how brane cosmological perturbations will be affected by the large-scale curvature of the bulk (in a 5D Schwarzschild of Kerr spacetime).

3. Other observables that remain to be computed are the amplitude of tensor modes and the non-gaussianity, although we do not expect them to be significant.

4. Given that the speed of sound for a relativistic 5D atmosphere is $c_s = c/2$, one expect $\mathcal{O}(0.2)$ relativistic corrections to the atmosphere profile, which we have ignored. This could affect the functional shape of the power spectrum at a similar level, potentially improving (or worsening) the fit to the data. A related issue is whether the hydrostatic equilibrium profile for the relativistic thin atmosphere is stable.

To conclude, while we believe the 5D holographic big bang remains an intriguing possibility for the origin of our universe, there remain empirical and theoretical challenges to its status amongst various scenarios for the early universe cosmology that should be addressed in future work.

Chapter 5

A Non-Local Reality: Is there a Phase Uncertainty in Quantum Mechanics?

5.1 Introduction

In his ground-breaking 1964 paper, John Bell demonstrated that the correlations predicted for quantum mechanical observables can never be fully replicated in *local hidden variable* theories [186]. The empirical success of quantum mechanics over the past 50 years would thus only be consistent with a hidden variable theory with superluminal (in fact, instantaneous) communication. However, experimental verification of Lorentz invariance (or equivalence principle) at extreme precisions (e.g. [187]) has nearly vanquished any (empirical) motivation for such a possibility.

Surprisingly though, a motivation for this possibility may come form cosmological observations: If quantum mechanics is given by a hidden variable theory, that theory could have a non quantum mechanical extension with quantum mechanics as an equilibrium fixed point. Then, non-local signalling [188] may be possible *before* the universe enters the quantum mechanical "equilibrium", and could be imprinted in the initial conditions of the universe. Therefore, one might be able to replicate the correlations observed in the cosmic microwave background (CMB) (e.g. [189]) using the non-local signalling in the pre-quantum mechanical universe [188], as they cannot otherwise be explained in the standard Big Bang theory (so-called horizon problem).

Another motivation for instantaneous signalling comes from a power-counting renormalizable approach to 3+1d geometrodynamics, known as Horava-Lifshitz gravity [190] which, violates foliation invariance (and thus relativistic locality) of general relativity. At high energies, the speed of propagation for excitations in this theory approaches infinity, amounting to non-local (though causal) instantaneous signalling.

A real ensemble model is a non-local hidden variable theory, as an alternative to quantum mechanics, and so can potentially possess this type of non-local signalling. In order for this theory to be viable, however, quantum mechanics must be an attractor, such that the non-quantum mechanical theory becomes quantum mechanics at later times, consistent with present-day experiments. Valentini shows this is the case for Bohmian mechanics [191, 192] using a coarse-grained H-theorem as in statistical mechanics, so that one can see there are regimes which approach quantum equilibrium [193]. The proof applies to the coarse-grained case for a model with a real wave-function and independent probability.

In this chapter, we focus on a different hidden variable model, the so-called "real ensemble" model recently introduced by Smolin [194]. The model focuses on an object described in quantum mechanics by a wavefunction $|\psi\rangle$, which could be a particle, field, composite system of many particles, etc. We will refer to this as the system. It puts all systems that would be in the same state in quantum mechanics into an ensemble. One would then examine this system in a given eigenbasis for the observable of interest. There are two beables[1] for each such system – the value of the observable in question and the phase of the component of the wavefunction in the eigenstate corresponding to the observable value would possess in quantum mechanics. All these systems are spread out across the universe, interacting non-locally as governed by the rules of interaction of members of the ensemble. The systems then evolve according to two rules: *i)* The continuous evolution rule states that the phase of the systems evolves according to some equation, and *ii)* The copy rule states that there is a finite probability for one system in the ensemble to change its observable and phase values to match those of another system's. This then can be used to determine the evolution of the probability that a system would be in a given state as well as the phase associated with that state.

The model is called "real ensemble" since all the systems can exist in the same universe and their Hamiltonians which determine their local interactions can, in principle, include the influence of other members of the ensemble. This conception is in contrast to

---

[1]Beables generally refer to properties innate to the system rather than determined by observation. This term is used in hidden variable theories to give a name to the properties of the system which actually exists and are subject to the laws of evolution of the system. It typically includes both the observables and the hidden variables.

the "many-worlds interpretation", where the ensemble is effectively over multiple parallel "universes" (or rather separate portions of the wave-function), but for what would be considered the same system in each.

Since in Smolin's real ensemble model the phases (of the wave function) are the additional hidden variables, the non-equilibrium behaviour is different. While we do not have a coarse-grained H-theorem, we have examined the convergence numerically and analytically to determine not only that there are regimes for which the model converges, but also the rate of convergence is dependent on *absolute energy*.

The outline of the chapter is as follows: We begin in Sec. 5.2 by developing a non-equilibrium real ensemble model, which admits quantum mechanics (Eqs. 5.1-5.2) as an equilibrium limit. We also study the dynamics close to the equilibrium. In Sec. 5.3, we study the stability properties of the non-equilibrium model numerically for simple spin$-\frac{1}{2}$ systems, and in particular examine the stable parameter-space of the theory. In Sec. 5.4, we provide an analytic perturbative study of near-equilibrium behaviour, which is roughly consistent with the numerical results. Finally, Sec. 5.5 puts the real ensemble framework, along with our findings, into some physical context, and Sec. 5.6 concludes the chapter.

5.2   Real Ensemble Theory: the framework

We begin by introducing the equilibrium real ensemble model which reproduces quantum mechanics. In the case of equilibrium, there is one phase per observable value. For this case, the number of systems, N, is sufficiently large such that there is a large enough number of systems per distinct sets of beables (phases AND observable values), so that they can be treated as continuous numbers. We define the probability for a system to have a given value a for the observable of interest as $\rho_a(t)$. The phase associated with this observable value is defined as $\phi_a(t)$. The equations which reproduce quantum mechanics are then [194]:

$$\dot{\phi}_a\left(t\right) = \sum_b \sqrt{\frac{\rho_b\left(t\right)}{\rho_a\left(t\right)}}\, R_{ab} \cos\left[\phi_a\left(t\right) - \phi_b\left(t\right) + \beta_{ab}\right], \tag{5.1}$$

$$\dot{\rho}_a\left(t\right) = \sum_b 2\sqrt{\rho_a\left(t\right)\rho_b\left(t\right)}\, R_{ab} \sin\left[\phi_a\left(t\right) - \phi_b\left(t\right) + \beta_{ab}\right], \tag{5.2}$$

where the evolution $\dot{\phi}$ comes from the continuous evolution rule and the evolution $\dot{\rho}$ from the copy rule [2]. R and β in this equation are real, non-negative numbers defined by the particular system. This case is identical to the quantum mechanical system with the wavefunction given by

$$|\Psi\rangle = \sum_a \sqrt{\rho_a\left(t\right)}\, e^{-i\phi_a} |a\rangle , \tag{5.3}$$

and Hamiltonian given by

$$H = \hbar \sum_{a,b} R_{ab} e^{i\beta_{ab}} |a\rangle \langle b| . \tag{5.4}$$

Equation 5.1 is equivalent to equation 31 in [194], equation 5.2 to equation 30.

In order to determine the non-equilibrium forms of the equations, we need to remember that the calculation of the two Equations 5.1 and 5.2 starts with the assumption that ϕ is a function of the value of the observable rather than the system, defined as the equilibrium condition. The goal is to extrapolate these equations to non-equilibrium equations, one which has ϕ different for different systems even if the value of the observable is the same, using the known equilibrium equations. $\dot{\phi}$ and $\dot{\rho}$ must reduce to those shown in Equations 5.1 and 5.2 when there is only one potential phase per value of the observable, as this will reproduce quantum mechanics when the function achieves equilibrium. We will retain the large N limit assumption.

5.2.1 Allowing for Multiple Phases per Value of Observable

The number of cases for a given value of the observable can be represented as a sum of the number of systems with a given set of beables for all beable sets with the given observable value a. Working in probabilities since the number of systems N is large, this can be replaced by a weight function w which determines the probability of the system with a given value of an observable having a given phase. As a probability function,

$$1 = \sum_\phi w\left(a, \phi, t\right) \tag{5.5}$$

for every a and t. We will label a system type – all systems which share phase and observable value – by the labels i, j, k, etc., rewriting a as a_i, ρ_a as ρ_{a_i}, and ϕ_a as ϕ_{a_i}.

---

[2]In order to match quantum mechanics, one needs to include a factor of 2 that was missing from Equation 30 from [194]. This correction, however, will not effect any later conclusions, and it was fixed in the published version. The other change in this from Smolin's notation is the replacement of δ with β to prevent confusion with the Kronecker δ-function.
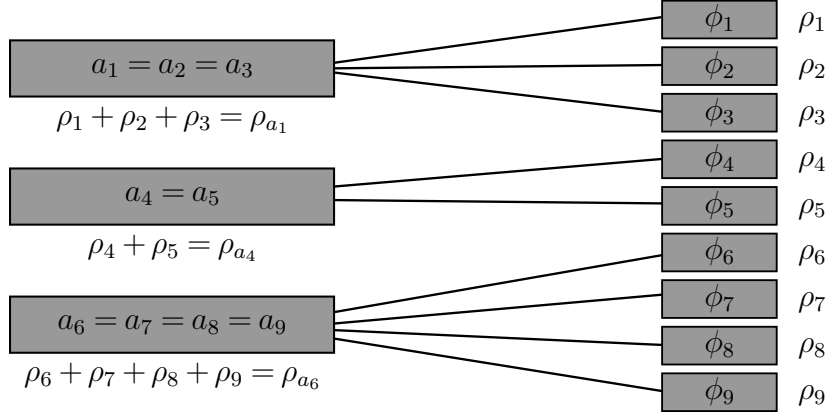
Figure 5.1: A pictorial depiction of an out of equilibrium real-ensemble system: Each value of observable, a_i, has multiple potential values of phase, ϕ_i. ρ_i on the right is the probability for a particle to have both an observable value a_i and a phase ϕ_i. In contrast, ρ_{a_i} on the left is the probability of having a_i but with any phase. The sum of a given quantity over all i can either be determined by taking the sum over all indices i, or by taking the sum over all observable values and all phases with non-zero probability for each observable value. In equilibrium, there is only one ϕ for each a_i, i.e. $\phi_i = \phi_{a_i}$.

In the non-equilibrium case, ρ_{a_i} becomes ρ_i and ϕ_{a_i} becomes ϕ_i. Note that ρ_{a_i} still has meaning out of equilibrium as $\sum_j \rho_j \delta_{a_i a_j}$. δ here is the Kronecker delta. A depiction of this expansion of the number of distinct pairs of beables and the labelling is shown in Figure 5.1. Using w, $\rho_i = \rho_{a_i} w_i$. Since a_j is no longer the only quantity the terms in the sum are dependent on, $\sum_{a_j} \cdots$ becomes

$$\sum_{a_j} \sum_{\phi_j} w\left(a_j, \phi_j, t\right) \cdots \equiv \sum_j w_j \ \cdots \,, \tag{5.6}$$

where $\cdots$ is whichever expression the sum is taken over in the equations of evolution. The process of converting from a double sum to a single sum is a simplification of the notation determined by recognizing there are multiple values of j with the same a_j, each with different ϕ_j. This can be seen in Figure 5.1 where it is a sum over three a_j, and for each a_j, a sum over two to four ϕ_j converted to a sum over nine values of j.

However, there is a less obvious place in which this weight function is needed. Underneath the square roots ρ_{a_j} may not be independent of phase anymore. It is uncertain if it only depends on the probability of a value of the observable or on the probability of a

given beable pair. This is dealt with by adding in an arbitrary real function $F(a, \phi_1, \phi_2)$ for which $F(a, \phi_1, \phi_1) = 1$ and $F(a, \phi_1, \phi_2) \geq 0$ everywhere. This function determines the contribution to the density functions under the square root of systems with different phases but the same value of the observable. We must then replace ρ_a by

$$\tilde{\rho}_{a_i} \equiv \rho_{a_i} \sum_j w_j \delta_{a_i a_j} F(a_i, \phi_i, \phi_j) \tag{5.7}$$

$$\equiv \sum_j \rho_j \delta_{a_i a_j} F(a_i, \phi_i, \phi_j). \tag{5.8}$$

F must be periodic with respect to $\phi_1 - \phi_2$, but might have additional dependence on a and ϕ_1. Since this is an extension beyond quantum mechanics, we have no guide to determine what form this extension should take, but we can examine several different models to test for convergence. We will minimize the symmetries broken when leaving equilibrium since there is no reason to suspect that they are broken and this reduces the potential forms of F. A ϕ_1 dependence could introduce a dependence on absolute phase, while a dependence on a may remove certain quantum mechanical symmetries from some systems when leaving equilibrium. These additional dependencies will not be considered here since there is no reason to believe that such dependencies exist nor any need to consider them. In addition, only the case for which $F(\phi_1 - \phi_2) = F(\phi_2 - \phi_1)$ will be considered. If this does not hold, time reversal invariance will no longer hold: Since under time reversal in this model, $\phi \to -\phi$, $t \to -t$, $\rho \to \rho$, $R \to R$, and $\delta \to -\delta$[194], applying time reversal to Equations 5.11 and 5.12 (the final equations, later) will only give $\dot{\rho} \to -\dot{\rho}$ and $\dot{\phi} \to \dot{\phi}$ for all a, ϕ, and $\rho(a, \phi, t)$ if $F(\phi_1 - \phi_2) = F(\phi_2 - \phi_1)$.

We further exclude the possibility that F is 1 when $\phi_1 = \phi_2$ and 0 otherwise, because then transferring a large number of systems from $\phi_1 \neq \phi_2$ to $\phi_1 = \phi_2$ continuously will result in a discontinuity in the function $\dot{\phi}$ and $\dot{\rho}$ from the discontinuity in $\rho(a, t) \sum w(a, \phi_j, t) F(a, \phi_i, \phi_j)$. Other functions which similarly produce a discontinuity when going to equilibrium will be problematic.

The resulting evolution equations are

$$\dot{\phi}_i(t) = \sum_j w_j(t) \sqrt{\frac{\rho_{a_j}(t) \sum_k w_k(t) \delta_{a_j a_k} F(\phi_j - \phi_k)}{\rho(a_i, t) \sum_k w_k(t) \delta_{a_i a_k} F(\phi_i - \phi_k)}} \times R_{a_i a_j} \cos\left[\phi_i(t) - \phi_j(t) + \beta_{a_i a_j}\right] \quad \text{and} \tag{5.9}$$

$$\dot{\rho}_i\left(t\right) = w_i\left(t\right) \sum_j w_j\left(t\right) \sqrt{\rho_{a_i}(t)\left[\sum_k w_k(t)\delta_{a_i a_k}F(\phi_i-\phi_k)\right]\rho_{a_j}(t)\left[\sum_k w_k(t)\delta_{a_j a_k}F(\phi_j-\phi_k)\right]}$$

$$\times 2R_{a_i a_j}\sin\left[\phi_i\left(t\right)-\phi_j\left(t\right)+\beta_{a_i a_j}\right]. \quad (5.10)$$

Equivalently, we can define the probability for a given value of the observable and phase, $\rho_i \equiv \rho_{a_i} w_i$, yielding:

$$\dot{\phi}_i = \sum_j \frac{\rho_j}{\sum_k \rho_k \delta_{a_j a_k}} \sqrt{\frac{\tilde{\rho}_{a_j}}{\tilde{\rho}_{a_i}}} \times R_{a_i a_j}\cos\left[\phi_i-\phi_j+\beta_{a_i a_j}\right], \quad (5.11)$$

$$\dot{\rho}_i = \frac{\rho_i}{\sum_k \rho_k \delta_{a_i a_k}}\sum_j \frac{\rho_j}{\sum_k \rho_k \delta_{a_j a_k}} \sqrt{\tilde{\rho}_{a_i}\tilde{\rho}_{a_j}} \times 2R_{a_i a_j}\sin\left[\phi_i-\phi_j+\beta_{a_i a_j}\right]. \quad (5.12)$$

Here, as in equation 5.8,

$$\tilde{\rho}_{a_i} \equiv \sum_k \rho_k \delta_{a_j a_k}F\left(\phi_j-\phi_k\right). \quad (5.13)$$

First note that R_{ab} and β_{ab} are symmetric and anti-symmetric, respectively, due to the hermiticity of the Hamiltonian. Therefore, summing Eq. (5.12) above over a_i and ϕ_i, we end up with terms that are completely symmetric under $i \leftrightarrow j$, with the exception of the sine factor, which is anti-symmetric. As a result, the sum vanishes and thus the total probability remains conserved.

5.2.2 Other Changes When Leaving Equilibrium

While they will not be covered here, there are a few other additions to this equation which might be examined. The first is the addition of terms which go to zero for the large N equilibrium case. There is nothing to indicate what form these terms might take, except that they must go to zero for either the large N limit or the quantum mechanical limit, and they can't cause any probabilities to not behave as probabilities. Other possibilities include adding a ϕ dependence into R and β. This would have to take a form in which the quantum mechanical limit still holds, say by taking the difference between the mean phase and ϕ, or the spread of phases as influencing R.

5.3 Discrete Systems: Spin-$\frac{1}{2}$ with Finite Number of Phases per Value of Observable

In this section, we numerically study the evolution of simplest possible systems, i.e. spin-$\frac{1}{2}$'s or qubits, and investigate whether/how their evolution approaches the quantum mechanical equilibrium.

5.3.1 The Model

This case involves two possible values of a, spin up or spin down, simplifying the analysis since there are only two potential values of the observable to sum over. The input to the algorithm will determine the R and β parameters by using the sum of Pauli matrices to define a Hamiltonian, $H = c_t I + c_x \sigma_x + c_y \sigma_y + c_z \sigma_z$. The R and β functions are determined by the Hamiltonian in equation 5.4 using

$$R_{12} = R_{21} = \sqrt{c_x^2 + c_y^2}; \; R_{11} = |c_t + c_z|; \; R_{22} = |c_t - c_z| \tag{5.14}$$

$$\beta_{12} = -\beta_{21} = \arg\left(c_x - i c_y\right); \; \beta_{11} = \arg\left(c_t + c_z\right); \; \beta_{22} = \arg\left(c_t - c_z\right). \tag{5.15}$$

The function F will have one of a few predefined values constructed as sample functions using the limitations in previous section. The first possibility is a constant F, $F(\Delta\phi) = 1$. This corresponds to the case when the densities under the square roots are independent of phase.

The smooth cosine type function is a simple solution to account for the phase differences as being important while still creating an influence from the variation in the phases of the different systems. This would appear as

$$F(\Delta\phi) \equiv \frac{1}{2} + \frac{1}{2}\cos\left(\Delta\phi\right) = \cos^2\left(\frac{\Delta\phi}{2}\right). \tag{5.16}$$

This definition can be generalized to model a sharper dependence on phase difference. One such function is

$$F_c(\Delta\phi) \equiv \cos^2\left(\frac{c\,\Delta\phi}{2}\right)\Theta[\cos(\Delta\phi) - \cos(\pi/c)], \tag{5.17}$$

for a constant c, where $\Theta[x]$ is the step function that vanishes for $x < 0$ and is 1 otherwise. We note that $F_1 = F$ defined in Eq. (5.16). Moreover, for completeness, we define $F_0(\Delta\phi) \equiv 1$.

For our numerical studies below, unless noted otherwise, we focus on three possibilities: $F(\Delta\phi) = F_0, F_1,$ and F_{100}.

5.3.2 Results and Plots

We numerically evolve Eqs. (5.11-5.12) with either two or three different phases per each potential value of s_z. The results can be seen in Table 5.1, as well as in the appendix. In the plots, spin up is represented by the blue colours (dotted black line, dashed blue line, thin purple line), while spin down by the red colours (wide dashed red line, dot-dashed orange line, solid pink line). The plots in Table 5.1 are representative of all the cases run with similar initial differences in the phases of the same value of s_z. In each case, the sum of the probabilities of measuring a specific value of s_z follow an evolution indistinguishable within the expected error from the quantum mechanical case.

For the two cases of functions which are flat or close to flat within this region, they start with the same behaviour, but the kernel that slightly deviates from flat (i.e. F_1) is stable and fully approaches equilibrium, while the other case, F_0 does not and diverges from equilibrium. The third case, F_{100}, which which has the narrowest domain causes the system to approach equilibrium in a different way: Instead of the probability for certain pairs of beables to be present dropping to zero, the difference between the phases of the beable pairs with the same observable value goes to zero.

One subtlety to note for the F_0 case is that the values given do go below the expected error threshold for the numerical simulation. This, however, does not nullify the results which are seen - the fact that this is unstable remains, but the values after the point in which the model decreases below the error threshold can not be trusted.

For both the F_0 and F_1 cases, the very low probabilities could approach the levels in which the discreteness of the set are relevant and the large N approximation breaks down for that particular beable pair. This possibility could alter the evolution of these beable pairs, and more interestingly potentially cause one of the potential pairs of beables to completely empty, removing it from the ensemble. This could possibly cause the F_0 case to become quantum mechanical, despite the instability, or the F_1 case to become exactly equilibrium.

For the evolution with greater initial difference in the phases, the cases with a phase difference of 0.1 still go to equilibrium for those F functions which approached equilibrium

Table 5.1: Plots of the evolution of spin-$\frac{1}{2}$ systems in the non-equilibrium real ensemble model. Each case has three different phases for each of the two potential values of s_z. The initial conditions are $\rho(0) = \{\{0.16, 0.08, 0.06\}, \{0.23, 0.3, 0.17\}\}$ and $\phi(0) = \{\{0, 0.001\pi, 0.002\pi\}, \{\frac{\pi}{2} + 0.001\pi, \frac{\pi}{2}, \frac{\pi}{2} + 0.0005\pi\}\}$. The Hamiltonian is $H = \omega_0\hbar(2\sigma_z)$. $\hbar \equiv 1$ and ω_0 determines the units for t. From top to bottom, the functions F within equations 5.11 and 5.12 for the plots are $F = 1$, $F = \cos^2\left(\frac{\Delta\phi}{2}\right)$, and F given by equation 5.17 with $c = 100$.
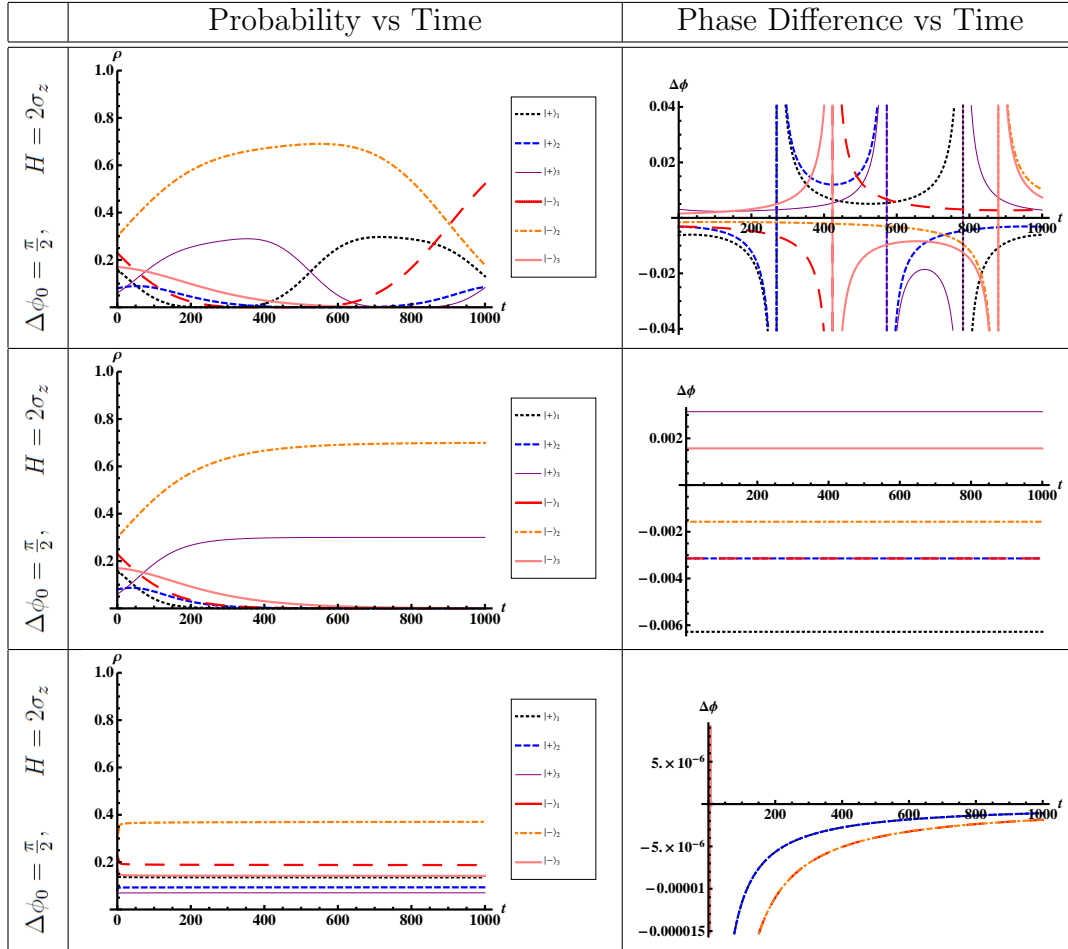
for smaller initial angle difference, while the cases with a relatively large phase difference do not. At the start, however, the evolution of the sum of all probabilities of measuring one of the two values of s_z is not necessarily quantum mechanical for even the moderate phase difference. Sample plots for the F_1 and F_{100} cases are given in Tables B.1 and B.2 in the Appendix.

5.3.3 Rate of Convergence

In an examination of the small phase difference for which shape converges fastest, one must first develop a measure for the rate of convergence. A simple such definition would be to use the standard deviation, as it approaches zero for either method of approaching equilibrium. Table 5.2 shows the distance from quantum mechanics using this measure vs. time. Note that the F_{100} case here is log-log, showing an approximate $\sim t^{-1}$ decay, while the F_1 case is logarithmic only on the y-axis, showing an exponential decay/convergence.

It can be seen that with this measure of convergence, the F function given by a spike ($c = 100$) converges to quantum mechanics faster within the given time, than that given by a cosine function ($c = 1$). This indicates a faster rate of convergence at early times, for a sharper F-kernel. The flat F function ($c = 0$) approaches equilibrium in a similar rate as the cosine function, until it jumps away from equilibrium.

For the case of $H = 2\sigma_z$, Figure 5.3 shows if the distribution converges to quantum mechanics for a given width c of the F function in equation 5.17 and initial phase separation $\Delta\phi_0$ for $\rho(0) = \{\{0.16, 0.08, 0.06\}, \{0.23, 0.3, 0.17\}\}$ and $\phi(0) = \{\{0, \alpha, 2\alpha\}, \{\frac{\pi}{2} + \alpha, \frac{\pi}{2}, \frac{\pi}{2} + \frac{\alpha}{2}\}\}$. The case for $c = 0$, equivalent to $F = 1$, is not shown on the plot, and does not converge. The convergence can be seen for an initial phase separation less than $\frac{\pi}{10}$, while for values above $\Delta\phi_0 \sim 1$, the system *does not* approach quantum mechanics. Convergence here is defined as having the variance decrease faster than approximately $t^{-0.2}$ by $t = 1000$, however most cases are obvious with a variance either oscillating around unity, or decreasing as t^{-n} with $n > 1$ (or exponentially for $c = 1$) by $t = 1000$ (see Fig. 5.2). The cases which converge slowly (slower than $t^{-0.5}$) as well as those that converge late (after $t = 500$) are in the purple zone (the region in the center with mostly diamond shaped points for those viewing without colour).

5.4 Perturbation Theory near Equilibrium
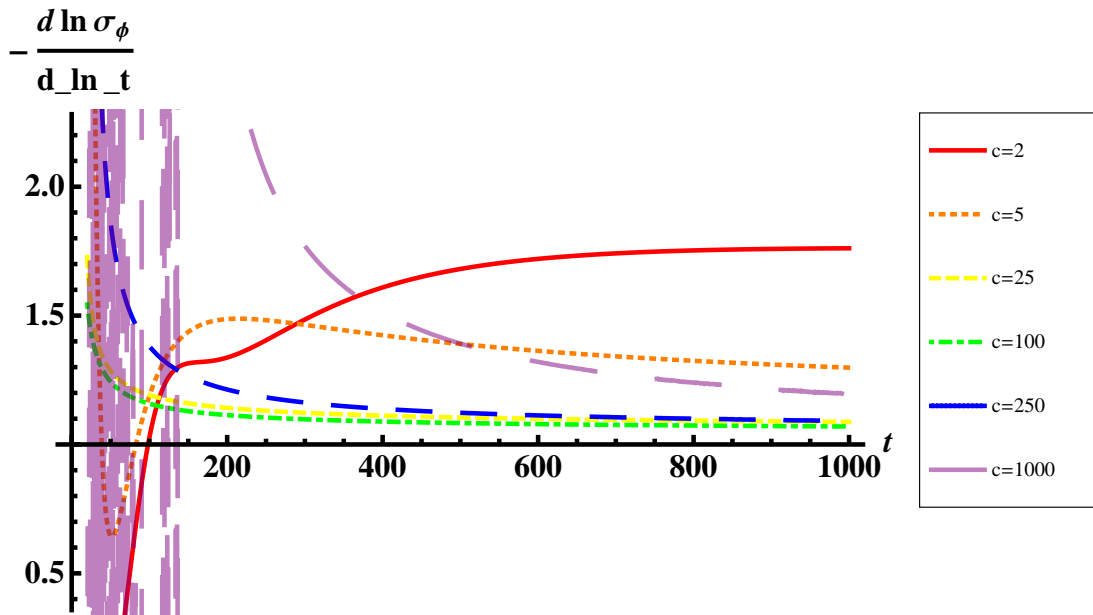
Figure 5.2: This plot shows the asymptotic behaviour of the rate of convergence, which we quantify as the logarithmic time derivative of the standard deviation of the phase: $n = \frac{d \ln \sigma_\phi}{d \ln t}$. Shown is the plot of $-n$ vs t. The colours red (solid line), orange (dotted line), yellow (dashed line just above the green/dot-dashed line), green (dot dashed line), blue (wide dashed line) and purple (dashing wider than blue case, consists of spike behaviour before $t = 200$) correspond to $c = 2, 5, 25, 100, 250$ and 1000 respectively. We see that convergence is always faster than $\sigma_\phi \propto t^{-1}$. The case $c = 1$ is not plotted here, as it decays exponentially $n \to -\infty$.

As we saw above, by construction, the quantum mechanical equations are approximately recovered, when the spread in phases, specified by $w(a, \phi, t)$ for a given value of the observable a, $\Delta\phi_a$, satisfies:

$$\Delta\phi_a \ll \pi, \text{ and } \Delta\phi_a \ll \Delta\phi_F, \tag{5.18}$$

where $\Delta\phi_F$ characterizes the phase spread/width of the kernel F. These conditions ensure that different coefficients in the sums: $\sum_\phi w(a, \phi)$ in Eqs. (5.9-5.10) factor out, which then let us replace the sums with unity. In other words, for narrowly-spread phases per observable value, one can combine Eqs. 5.9-5.10 (or 5.11-5.12) for systems, to evolution equations for mean phase and total probability *per observable value* to approximately recover quantum mechanics (5.1-5.2).

In order to examine the next order approximation to compare this evolution to quantum mechanics, we examine the analytical case for a diagonal Hamiltonian. The reason for this choice is that the diagonal case is simple enough to do this calculation analytically, and still can represent any quantum mechanical system (assuming unitary equivalence, which we discuss in the next section). For a diagonal Hamiltonian, Eqs. (5.9)-(5.10) separates for different observable values, and can be written as:

$$\dot{\phi}_i = \sum_j w_j \cos(\phi_i - \phi_j) \sqrt{\frac{\sum_k w_k F(\phi_j - \phi_k)}{\sum_k w_k F(\phi_i - \phi_k)}}, \tag{5.19}$$

$$\dot{w}_i = 2w_i \sum_j w_j \sin(\phi_i - \phi_j) \sqrt{\sum_k w_k F(\phi_j - \phi_k) \times \sum_k w_k F(\phi_i - \phi_k)}, \tag{5.20}$$

where we have suppressed the dependence on a for brevity, and chosen R_{aa}^{-1} as unit of time. Furthermore, as we saw above, in the regime close to quantum mechanics we can assume $\Delta\phi \ll \pi, \Delta\phi_F$, thus we can Taylor expand both F and cosine:

$$\cos(\phi - \phi') \simeq 1 - \frac{(\phi - \phi')^2}{2}, \tag{5.21}$$

$$F(\Delta\phi) \simeq 1 - \frac{\Delta\phi^2}{\Delta\phi_F^2}, \tag{5.22}$$

where $\Delta\phi_F^{-2} \equiv -\frac{1}{2}F''(0)$ here. For example, $\Delta\phi_F = 2c^{-1}$ for systems studied in the last section (Eq. 5.17). In this limit, the evolution for ϕ_i and w_i can be approximated as:

$$\dot{\phi}_{im} = \frac{\lambda}{2}\left[(\phi_i - \langle\phi\rangle)^2 - (\phi_m - \langle\phi\rangle)^2\right] + \mathcal{O}(\Delta\phi^4), \tag{5.23}$$

$$\dot{w}_i = 2w_i(\phi_i - \langle\phi\rangle) + \mathcal{O}(\Delta\phi^3), \tag{5.24}$$

112

where

$$\lambda \equiv \Delta\phi_F^{-2} - 1, \tag{5.25}$$

$$\phi_{im} \equiv \phi_i - \phi_m, \tag{5.26}$$

$$\langle\phi\rangle \equiv \sum_i w_i \phi_i. \tag{5.27}$$

We now notice that Eq. (5.23) can be written as:

$$\frac{d}{dt}(\phi_i - \langle\phi\rangle) - \frac{\lambda}{2}(\phi_i - \langle\phi\rangle)^2 = G(t), \tag{5.28}$$

where $G(t)$ is a yet to be determined function of time. In particular, combining Eqs. (5.27-5.28) yields:

$$G(t) = -\frac{(\lambda+4)}{2}\langle\Delta\phi^2\rangle = -\frac{(\lambda+4)}{2}\sum_i w_i(\phi_i - \langle\phi\rangle)^2. \tag{5.29}$$

The advantage of Eq. (5.28) is that it decouples the evolution for different phases, and thus reduces to a first order ODE for a given $G(t)$. Unfortunately, the solution cannot be written in closed form for arbitrary $G(t)$.

5.4.1 Power Law Convergence: $\lambda > 0$

We first introduce an ansatz, which, as we see below, is applicable for $\lambda > 0$, or equivalently $\Delta\phi_F < 1$ (implying $c > 2$ for the models of Sec. 5.3).

To proceed, we next notice a scaling symmetry of the Equations (5.23-5.24), which remain invariant under:

$$\phi_{im} \to A \times \phi_{im}, \quad t \to A^{-1} \times t, \tag{5.30}$$

for arbitrary A. Therefore, we postulate an ansatz: $G(t) \propto \langle\Delta\phi^2\rangle \propto t^{-2}$. With this assumption, it is convenient to define:

$$\tilde{\phi}_i \equiv \lambda t(\phi_i - \langle\phi\rangle), \tau \equiv \ln(t), G(t) = -\frac{\sigma^2 - 1}{2\lambda t^2}, \tag{5.31}$$

which let us write Eq. (5.28) as

$$\tilde{\phi}_i' = \tilde{\phi}_i + \frac{1}{2}\tilde{\phi}_i^2 - \frac{\sigma^2 - 1}{2} = \frac{1}{2}(\tilde{\phi}_i + \sigma + 1)(\tilde{\phi}_i - \sigma + 1). \tag{5.32}$$

$$w_i' = 2\lambda^{-1}w_i\tilde{\phi} \tag{5.33}$$

113

Note that σ is an arbitrary constant, with $\sigma > 1$ for $\lambda > 0$ and $0 < \sigma < 1$ for $\lambda < 0$, which is set by the variance of $\tilde{\phi}$, by combining Eqs. (5.31) and (5.29):

$$\langle \tilde{\phi}^2 \rangle = \frac{\sigma^2 - 1}{1 + 4/\lambda}. \tag{5.34}$$

Moreover, $'$ denotes derivative with respect to τ.

Interestingly, both the variance of $\tilde{\phi}$ (Eq. 5.34) and its equations of motion (5.32-5.33) become time-independent, which potentially admit steady state distributions. In particular, Eq. (5.32) has two fixed points at

$$\tilde{\phi}_{\pm} = -1 \pm \sigma. \tag{5.35}$$

The fixed point $\tilde{\phi}_+$ is an unstable fixed point, while $\tilde{\phi}_-$ is stable. For positive λ, it turns out that phases approach infinity (in the perturbative equations) within a finite time in the interval $(\tilde{\phi}_+, \infty)$, which given the periodic nature of phase, puts them within $(-\infty, \tilde{\phi}_-)$. For negative λ, the stability and evolution for $\tilde{\phi}$ is identical to that for positive λ, but this is not the case for ϕ. Since $\frac{\partial \tilde{\phi}_i'}{\partial \tilde{\phi}_i} = 1 + \tilde{\phi}_i = \pm\sigma$, near the fixed point $\tilde{\phi}_i - \tilde{\phi}_{\pm} \propto t^{\pm\sigma}$ which is equivalent to $\Delta\phi \propto t^{\pm\sigma-1} + C\tilde{\phi}_{\pm}t^{-1}$, where C is an unknown constant. Since $\sigma < 1$ for negative λ, this is stable for both fixed points. Therefore, given that we would like to study small phase variances, it stands to reason that we focus on the $(\tilde{\phi}_-, \tilde{\phi}_+)$ interval. Now, defining $w(\tilde{\phi})$ as the weight (or probability) density in the $\tilde{\phi}$ space, we can write the *steady-state* continuity equation:

$$\cancel{\frac{\partial w}{\partial \tau}} + \frac{\partial}{\partial \tilde{\phi}} \left[w(\tilde{\phi}) \tilde{\phi}' \right] = w'(\tilde{\phi}), \tag{5.36}$$

which, plugging from Eqs. (5.32-5.33), becomes:

$$\frac{\partial}{\partial \tilde{\phi}} \left[w(\tilde{\phi}) \left(\tilde{\phi} + \frac{1}{2}\tilde{\phi}^2 - \frac{\sigma^2 - 1}{2} \right) \right] = 2\lambda^{-1} w(\tilde{\phi}) \tilde{\phi}, \tag{5.37}$$

which can be integrated to give:

$$w(\tilde{\phi}) \propto (\tilde{\phi}_+ - \tilde{\phi})^{\alpha_+} (\tilde{\phi} - \tilde{\phi}_-)^{\alpha_-},$$

$$\alpha_{\pm} = -1 + \frac{2}{\lambda} \mp \frac{2}{\lambda\sigma}. \tag{5.38}$$

We notice a few interesting properties of this solution:

114

1. For $\lambda > 0$, $\alpha_\pm > -1$, which ensures that the probability $= \int w(\tilde{\phi})d\tilde{\phi}$ is finite. This is not the case for $\lambda < 0$, implying that the steady-state solution is non-existent. We can thus consider:

$$\lambda = \Delta\phi_F^{-2} - 1 = -\frac{1}{2}F''(0) - 1 > 0,$$
$$\Rightarrow \quad -F''(0) > 2 \tag{5.39}$$

as a necessary condition to approach equilibrium, at least within the above scaling ansatz: $G(t) \propto t^{-2}$.

2. We further notice that integrating the continuity equation (5.37) over our domain $(\tilde{\phi}_-, \tilde{\phi}_+)$, as the left hand side is a total derivative, and its argument $w(\tilde{\phi})\tilde{\phi}'$ vanishes at the boundaries (since $\alpha_\pm > -1$). Therefore, the right hand side $\propto \int \tilde{\phi}w(\tilde{\phi})d\tilde{\phi} = \langle\tilde{\phi}\rangle = 0$, which is consistent with our definition of $\tilde{\phi}$ (Eq. 5.31).

We note that the condition $\lambda > 0$ is equivalent to $c > 2$, where we see a power law decay of the standard deviation $\sigma_\phi \propto t^{-1}$ in our numerical simulations (e.g. third row in Table 5.2). Therefore, in spite of the fact that the analysis above is for continuum distributions, it roughly predicts the correct asymptotic behaviour of simple discrete simulations.

5.4.2   Exponential Convergence: $\lambda < 0$

As we saw above, for $\lambda < 0$ (or $\Delta\phi_F > 1$), the power-law ansatz does not lead to a sensible asymptotic steady state distribution. Let us now propose a different anstaz, i.e. that asymptotically $w(\Delta\phi)$ becomes time-independent, *without* additional time rescaling, where $\Delta\phi \equiv \phi - \langle\phi\rangle$. Moreover, we assume $G(t) = \langle\Delta\phi^2\rangle = 0$. Again, since there is no explicit time-dependence left in the evolution equations, the continuity equation (5.36) now reads:

$$\frac{\partial w(\Delta\phi)}{\partial t} + \frac{\partial}{\partial\Delta\phi}\left[w(\Delta\phi) \times \frac{\lambda}{2}\Delta\phi^2\right] = 2w(\Delta\phi)\Delta\phi, \tag{5.40}$$

which can be integrated to give:

$$w(\Delta\phi) \propto |\Delta\phi|^{4/\lambda - 2}. \tag{5.41}$$

Since the integrals over $w(\Delta\phi)$ are divergent for $\lambda < 0$, we have to use a cut-off $\Delta\phi_{\min} \to 0$. After properly normalizing $w(\Delta\phi)$, this yields:

$$\langle\Delta\phi^2\rangle = \left(\frac{\lambda - 4}{-\lambda - 4}\right)\Delta\phi_{\min}^2 \to 0, \text{ for } -1 < \lambda < 0, \tag{5.42}$$

115

consistent with $G(t) = 0$ ansatz above.

Given that this static solution has zero variance, it appears that it cannot have any discrete counterpart. However, one may consider any initial condition $w(\Delta\phi)$ as a perturbation around this static solution, which could be expanded into exponentially decaying modes [3]. While not entirely rigorous, this analytic argument provides an intuitive understanding of why convergence to quantum mechanics is exponential, rather than power-law, for $\lambda < 0$, or $c < 2$, e.g. in the second row in Table 5.2.

5.4.3 Approaching Quantum Mechanics

How does this deviation from quantum mechanics affect physical observable values? Simple manipulations yield:

$$\langle\phi\rangle^{\cdot} = \frac{d}{dt}\sum_i w_i\phi_i = 1 + \langle\Delta\phi^2\rangle + \mathcal{O}(\Delta\phi^4), \tag{5.43}$$

More generally, we can write a hierarchy of equations for all the moments of $\Delta\phi$:

$$\langle\Delta\phi^m\rangle^{\cdot} = (2 + \frac{m\lambda}{2})\langle\Delta\phi^{m+1}\rangle - \frac{m(\lambda+4)}{2}\langle\Delta\phi^2\rangle\langle\Delta\phi^{m-1}\rangle, \tag{5.44}$$

which can provide an alternative approach to numerically study convergence to quantum mechanics.

Instead, here we simply wrap up by making some observations about potential smoking guns of this theory. After reintroducing physical units, Eq. 5.43 reads:

$$\langle\phi\rangle^{\cdot} - \dot{\phi}_{QM} = \langle\Delta\phi^2\rangle \times \dot{\phi}_{QM}, \tag{5.45}$$

which represents a deviation from quantum mechanics proportional to the variance of phases. This correction can be absorbed into the Hamiltonian eigenvalues,

$$\tilde{H}_{ii} = H_{ii}\left(1 + \langle\Delta\phi^2\rangle\right), \tag{5.46}$$

giving an evolving effective Hamiltonian close to the true Hamiltonian. As we saw above (Secs. 5.4.1-5.4.2):

$$\langle\Delta\phi^2\rangle \propto (Et)^{-2n}, n \geq 1. \tag{5.47}$$

Therefore, one expects a time-dependent part of the energy levels of e.g. atoms/nuclei, that decays as $(Et)^{-2}$ or faster asymptotically.

---

[3]Note that there could be no exponentially growing mode, as the total probability is conserved
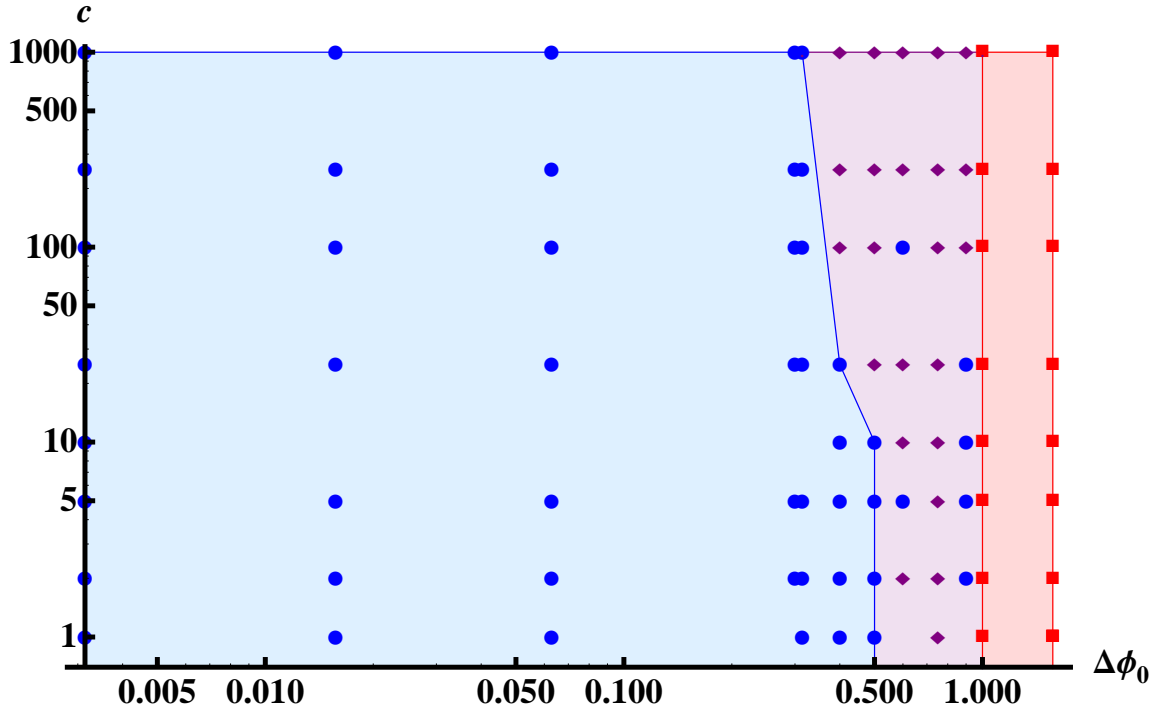
Figure 5.3: Phase space of convergence to quantum mechanics for $H = 2\sigma_z$, $\rho(0) = \{\{0.16, 0.08, 0.06\}, \{0.23, 0.3, 0.17\}\}$, $\phi(0) = \{\{0, \Delta\phi_0, 2\Delta\phi_0\}, \{\frac{\pi}{2} + \Delta\phi_0, \frac{\pi}{2}, \frac{\pi}{2} + \frac{\Delta\phi_0}{2}\}\}$, and F given by Equation 5.17 with varying c (characterizing the compactness of the F-kernel) and $\Delta\phi_0$ (the initial phase difference per value of the observable). Blue circles indicates convergence, red squares indicates lack of convergence, and purple diamonds means spin up converges, but spin down does not.

5.5 Discussions

Many of the issues with the original real ensemble model, presented in Section VI of [194], still remain open. The only exception is the stability of the quantum mechanical equilibrium, which we have demonstrated for a certain class of the non-equilibrium equations. Here, we discuss some of the other conceptual challenges (or features) in Smolin's real ensemble extension of the quantum theory:

5.5.1 Zero Occupancy States

An interesting aspect of this model is the fact that if $\rho_a = 0$, $\dot{\rho}_a = 0$ and this potential observable value is effectively non-existent. This is necessary as Equation 5.1 breaks down when $\rho_a = 0$. In the non-equilibrium extension, this becomes $\rho_i = 0$ meaning $\dot{\rho}_i = 0$. Despite the $\sum_k \rho_k \delta_{a_i a_k}$ term in the denominator of Equation 5.12, it can be seen that this remains true even if all ρ_i terms are zero for a given value of a_i. This will effectively eliminate a set of beables from being possible if at any time in its evolution, that set of beables has a zero probability. This ensures the quantum mechanical case is a fixed point, as if each value of the observable only has one potential phase, no other potential phases will be able to become non-zero, and the condition of one phase per value of the observable is maintained. This also causes a non-quantum mechanical issue at the nodes of a quantum mechanical system in the cases where in quantum mechanics a node ceases to be a node at later times due to the evolution.

This model is also by nature discrete. This implies two things for the property above. First is the finiteness of the number of sets of beables, which will cause issues with the examination of continuous and infinite systems as will be examined in the next section. The second is what happens in a large N system for pairs of beables or times with small enough probability such that N is no longer large enough to prevent the discreteness from effecting the system and its behaviour. This is not just at a node of exactly zero probability, but near one of very small probability. In this case finite behaviours become important, and there is a potential for complete loss of a beable pair by chance, even if the continuous probability dictates that the probability is never exactly zero.

5.5.2 Unitary Equivalence vs Preferred Basis

Technically, our current model chooses a preferred basis of the Hilbert space, defined by the eigenstates of the observable that is realized in the real ensemble theory. However, this would imply that, e.g. only spin in one direction can be measured – it does not account/allow for choice of non-commuting observables, which is part of what contrasts quantum and classical mechanics. Since we would like to account for the existence of non-commuting observables, we need to ask what the model would give if one were to measure a different observable. To do this, the model would either have to define a preferred basis for the theory from which other measurements could be determined or one has to have a definite observable value for many bases. Both proposals have flaws. Since this model is discrete by nature (only continuous by approximation), taking position, or even momentum

Table 5.2: Plots of the standard deviation of the phases for the cases in Figure 5.1. From top to bottom, the functions F within equations 5.11 and 5.12 for the plots are $F = 1$, $F = \cos^2\left(\frac{\Delta\phi}{2}\right)$, and F given by equation 5.17 with $c = 100$. The first two plots have a logarithmic scaling for the y-axis, while the scaling of both axes are logarithmic for the third plot.

119
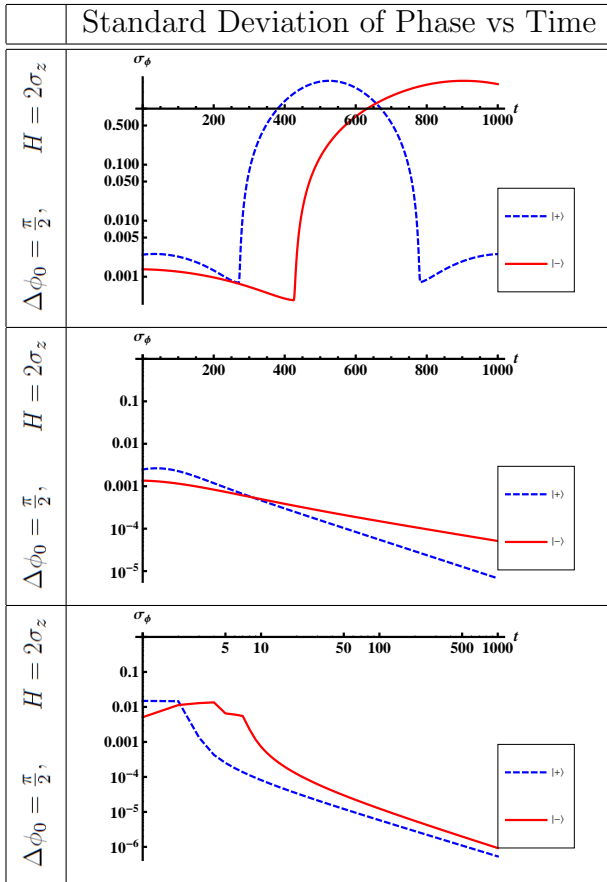
in a continuous space-time would suffer from the "node" problem mentioned above – the probabilities would be spread too thin, exposing the discreteness of the model, causing certain observable values to be unrepresented, and therefore never represented. In order to take one of these as the preferred basis as might be desired, a discrete spacetime is required.

Taking spacetime discrete and position space, momentum space, Hamiltonian, or all three together as the preferred basis/bases, might help if N is large enough. Any discrete eigenspace would work – e.g. that of the Hamiltonian. A discrete but infinite system would not be able to have all eigenstates represented though, for a finite N.

Even for a finite system, however, if we choose to maintain unitarity, the fact that the system is finite is again a problem. There is an infinite number of unitary transformations, unless somehow we discretize this, for instance by having discreteness in angles for the case of the spin-1/2 system. So we must take a finite set of preferred bases, something which in this case, unlike the infinite case, does create a finite number of types of members of the ensemble in the equilibrium model.

In continuing with this, a finite number of represented phases per value of each observable is also required to maintain the fact the system is finite.

The most obvious choice is to take the Hamiltonian eigenspace as preferred, as it exists in all cases and is native to the equations. Of course, this doesn't make it the correct, but rather the simplest possible choice. It is also discrete for finite systems. An issue remains for degeneracies in the eigenstates of this basis, where the Hamiltonian fails to single out a basis, unless the degeneracies are only an idealization/approximation of the system. This choice has both the advantage and disadvantage of simplifying the equations. The advantage being that the simplified system is easy to work with and understand. The disadvantage being that no equilibrium evolution is seen and parts of the equations remain unused – parts that match quantum mechanics in equilibrium and enabled the conclusion that this set of equations matches quantum mechanics.

5.5.3   Real Ensemble Model and Early Universe

Given the experimental success of quantum mechanics in explaining microscopic phenomena, any phenomenologically viable real ensemble theory must be stable to perturbations away from quantum mechanics, at least within the tested regimes. Indeed, as we have demonstrated in this chapter, this is possible for a large space of parameters in our formulation. Therefore, any smoking gun for this theory should be sought beyond the current empirical regime, i.e. very high (or possibly very low) energies, or prior to convergence to

quantum mechanics. Both these conditions are met in the early universe, which implies that one could potentially search for signatures of deviations from quantum equilibrium in cosmological observations.

As we pointed out in the introduction, indeed one of the motivations for studying hidden variable theories away from quantum equilibrium is non-local signalling that could provide a resolution to the cosmological horizon problem [188], as well as observed superhorizon correlations in the CMB. Let us see how this could happen in our framework:

The spectrum curvature fluctuations in the radiation era is given by (e.g., see [195]):

$$P_\zeta(k) = \frac{(1 + 2n_k)}{(4\pi)^2 \sqrt{3}} \left(\frac{k}{M_p} \right)^2, \tag{5.48}$$

where n_k is the mean occupation number of the mode k, and M_p is the Planck mass. In the ground state of quantum mechanics $n_k = 0$. However, as we saw in Eq. (5.46) the phase variance introduces a correction to the effective energy of all the energy eigenstates, including the ground state. Given that energy of a harmonic oscillator scales as $n_k + \frac{1}{2}$, we may interpret this correction as:

$$n_k = \frac{1}{2}\langle \Delta\phi^2 \rangle \simeq \frac{\langle \Delta\phi^2 \rangle_0}{2(E_k t)^2}, \tag{5.49}$$

where we used the results of Sec. 5.4 (e.g., Eq. 5.47) for the asymptotic scaling of the phase variance. Furthermore, for the ground state:

$$E_k = \frac{1}{2}\omega_k = \frac{c_s k}{2} = \frac{k}{2\sqrt{3}}, \tag{5.50}$$

where we used $c_s^2 = 1/3$ for the radiation fluid. Plugging this into Eq. (5.48) yields:

$$P_\zeta(k) = \frac{(k/M_p)^2}{16\pi^2\sqrt{3}} + \frac{\sqrt{3}\langle \Delta\phi^2 \rangle_0}{8\pi^2 (M_p t)^2}. \tag{5.51}$$

We thus see that the correction term to the ζ power spectrum is indeed scale-invariant, and assuming $t \sim 10^4 \sqrt{\langle \Delta\phi^2 \rangle_0} M_p^{-1}$, yields $P_\zeta \sim 10^{-9}$, which is roughly consistent with cosmological observations.

Of course, the interpretation of the result in Eq. (5.51) is far from straightforward. For example, P_ζ should become independent of time on superhorizon scales in standard cosmology. So, at what time, t, should we expect the evolution of ζ to freeze, if at all?

This will be a necessary condition for the scale-invariant term to not be negligible at late times.

A more serious problem with interpreting Eq. (5.51) as the origin of cosmological primordial power spectrum, is that it requires $\langle \Delta \phi^2 \rangle \gg 1$ to match the amplitude of CMB anisotropies, thus invalidating the near-equilibrium approximation. Therefore, we should only consider this result as a suggestive direction for further exploration of the implications of the real ensemble theory for early universe, pending a deeper understanding of its physics.

5.5.4 Real Ensemble Model, Quantum Gravity, and Cosmological Constant Problem

A surprising feature of the real ensemble theory that was discovered here, is that the rate of convergence to quantum mechanics depends on the absolute (and not relative) energy. This suggests a possible connection to gravitational physics, as gravity is the only interaction that is sensitive to the total energy of a system. In other words, total energy of a system sources both its gravity, AND its convergence to quantum mechanics.

As an example, let us consider the expectation for the vacuum energy, or the cosmological constant. In Eq. (5.46), we saw that the effective energies of eigenstates receive corrections as:

$$E = E_{QM} + \frac{\langle \Delta \phi^2 \rangle_0}{E_{QM} t^2}, \tag{5.52}$$

if we interpret $\langle \dot{\phi} \rangle$ as energy, E. Now, this energy has a minimum:

$$E_{\min} \sim \frac{2\sqrt{\langle \Delta \phi^2 \rangle_0}}{t}. \tag{5.53}$$

Now, if we interpret this as vacuum energy within a Hubble patch of the universe:

$$\rho_{\text{vac}} \sim E_{\min} H^3 \sim (14 \text{ meV}^4)\sqrt{\langle \Delta \phi^2 \rangle_0} \; T(\text{TeV})^8, \tag{5.54}$$

which is comparable to the observed dark energy density, if we set t to the time of electroweak phase transition, or temperature $T \sim \text{TeV}$ (and $\langle \Delta \phi^2 \rangle_0 \sim 1$):

This might be a reasonable scale to plug in here, as quantum field theory is not well probed beyond TeV scale.

5.5.5   Alternative Non-Equilibrium Real Ensemble Model

In converting from equations 5.9 and 5.10 to equations 5.11 and 5.12, we note an additional possible extension of the model outside of the quantum mechanical case. This case comes from factoring out a ρ_a term from the square root to remove this term from the denominator of the weight function before taking the equation out of equilibrium. It is equivalent to the case when all instances of $\sum_k \rho_k \delta_{a_i a_k}$ are replaced with $\tilde{\rho}_{a_i}$. The resulting equations governing the model are:

$$\dot{\phi}_i = \sum_j \frac{\rho_j}{\sqrt{\tilde{\rho}_{a_j} \tilde{\rho}_{a_i}}} \times R_{a_i a_j} \cos \left[\phi_i - \phi_j + \beta_{a_i a_j} \right], \tag{5.55}$$

$$\dot{\rho}_i = \sum_j \frac{\rho_i \rho_j}{\sqrt{\tilde{\rho}_{a_j} \tilde{\rho}_{a_i}}} \times 2 R_{a_i a_j} \sin \left[\phi_i - \phi_j + \beta_{a_i a_j} \right]. \tag{5.56}$$

Several aspects make this model appear simpler. The square root denominator is the same for both $\dot{\phi}$ and $\dot{\rho}$. There is only one type of $\tilde{\rho}$ term. In addition, the weighting based on ρ_i is obvious and separate from the square root terms. This change comes from acknowledging this implicit weighting from the equilibrium model, and separating it from the square roots.

Numerically, the new model gives results close to, if not effectively identical to, the original model when analysing for convergence. This means that although the exact evolution may differ, all result obtained for the original non-equilibrium model remain valid. The convergence is invariant to this change in extrapolation.

Both models are identical when $F = 1$.

5.6   Conclusions

Inspired by theoretical and observational motivations for violating relativistic locality, we explored the non-local real ensemble model, in the context proposed by Smolin [194]. In particular, the theory generalizes quantum mechanics by allowing a range of (or uncertainty in) quantum phase per value of an observable.

We first developed the generalized evolution for the real ensemble, which consist of continuous phase evolution, and copy rules. We then provided both numerical and analytic evidence for why quantum mechanics (with one phase per observable value) is a local stable

fixed point for most of the parameter space of the theory. Moreover, the phase variance, as well as deviations from quantum mechanical frequencies decay faster than $(Et)^{-2n}$, with $n \geq 1$, for stable models. The energy scale of this decay is the absolute energy rather than relative energy of the system, which suggests a possible connection to gravitational physics.

Finally, we discussed different conceptual aspects of the real ensemble theory. This includes the need for a preferred basis in the Hilbert space (and/or further interpretation), as well as potential novel applications for the spectrum of primordial cosmological perturbations and the cosmological constant problem.

Chapter 6

Conclusion

In this dissertation, I have introduced four different models for the early universe which are alternative to standard inflationary and bounce models. Each of them has their own strengths, weaknesses, and interesting features. While not all of them can be correct, perhaps each of them has characteristics which help to understand which is possible for the early universe or other areas of theoretical physics.

For three of the four models, we analyzed our model against the Planck CMB anisotropy data, as well as other cosmological observations. Our models in this case were constructed by replacing the primordial power-law power spectrum of the standard ΛCDM cosmology with the appropriate alternative power spectrum.

Holographic cosmology relies on the holographic principle in order to construct an alternative primordial power spectrum by a perturbative computation in a three-dimensional superrenormalizable QFT with a generalized conformal structure. We found that the model becomes non-perturbative at low l values ($l < 30$), but is valid elsewhere. When we analyze the fit with only this data, we found that this theory fits just as well as the power-law expansion. With the full dataset, the model is viable but disfavoured.

For periodic time cosmology (PTC), we developed a cosmological framework with a periodic time dimension. To do this, we match the infinite future and the big bang using a conformal rescaling, as suggested by Penrose [145]. We showed that we can construct a primordial power spectrum constrained by the periodicity and the known cosmic history. When compared to the power-law expansion, we found that such a model can fit observations with a difference 1.8σ from the standard power-law power spectra, favoring the power-law expansion, if we include a non-trivial dark energy equation of state.

Table 6.1:   This table gives the χ^2 and σ difference between each model analyzed with CosmoMC and the standard power-law primordial power spectrum model with the same datasets and astrophysical parameters.

	$\Delta\chi^2$	σ
holographic cosmology	4.8	2.2
holographic cosmology $l > 30$	0.5	0.7
periodic time cosmology ΛCDM	25.8	5.1
periodic time cosmology wCDM	3.4	1.8
holographic big bang	7.8	2.8

The 5D Holographic Big Bang (HBB) framework posits that our universe is a 3-brane with induced gravity, formed from the collapse of 5D star. Previous work had shown that this model can produce a scale invariant primordial power spectrum when the brane travels through a uniform atmosphere. To explain the deviation from scale-invariance observed in the CMB data, we instead studied the case of a thin infalling atmosphere. When compared to cosmological observations, we found that our model is disfavoured compared to a pure power-law by 2.8σ. In addition, the best fit model must break the holographic bound by at least 8 orders of magnitude in order to match the data and for the thin atmosphere approximation to be valid.

The real ensemble model is a hidden-variable model of quantum mechanics where all particles in the universe which would have the same quantum mechanical state are part of a self-interacting ensemble. In this case, the "beables" would be the quantum mechanical phase and the observable values. While the ensembles need not start in a quantum mechanical distribution, they were shown to converge to quantum mechanics. The rate of convergence to quantum mechanics for the distribution of phases of an ensemble of particles in this model was found to be based on the absolute energy of the system rather than the relative energy. The cosmological implications have not yet been examined.

The relative goodness of fit for each model vs. a power-law expansion is given in Table 6.1. The TT anisotropy power spectrum comparison of all four analysed models – power-law, holographic cosmology, periodic time cosmology, holographic big bang – compared to Planck is shown in Figure 6.1.

As we have discussed, there are many open questions in relation to these models which may be studied in the future.
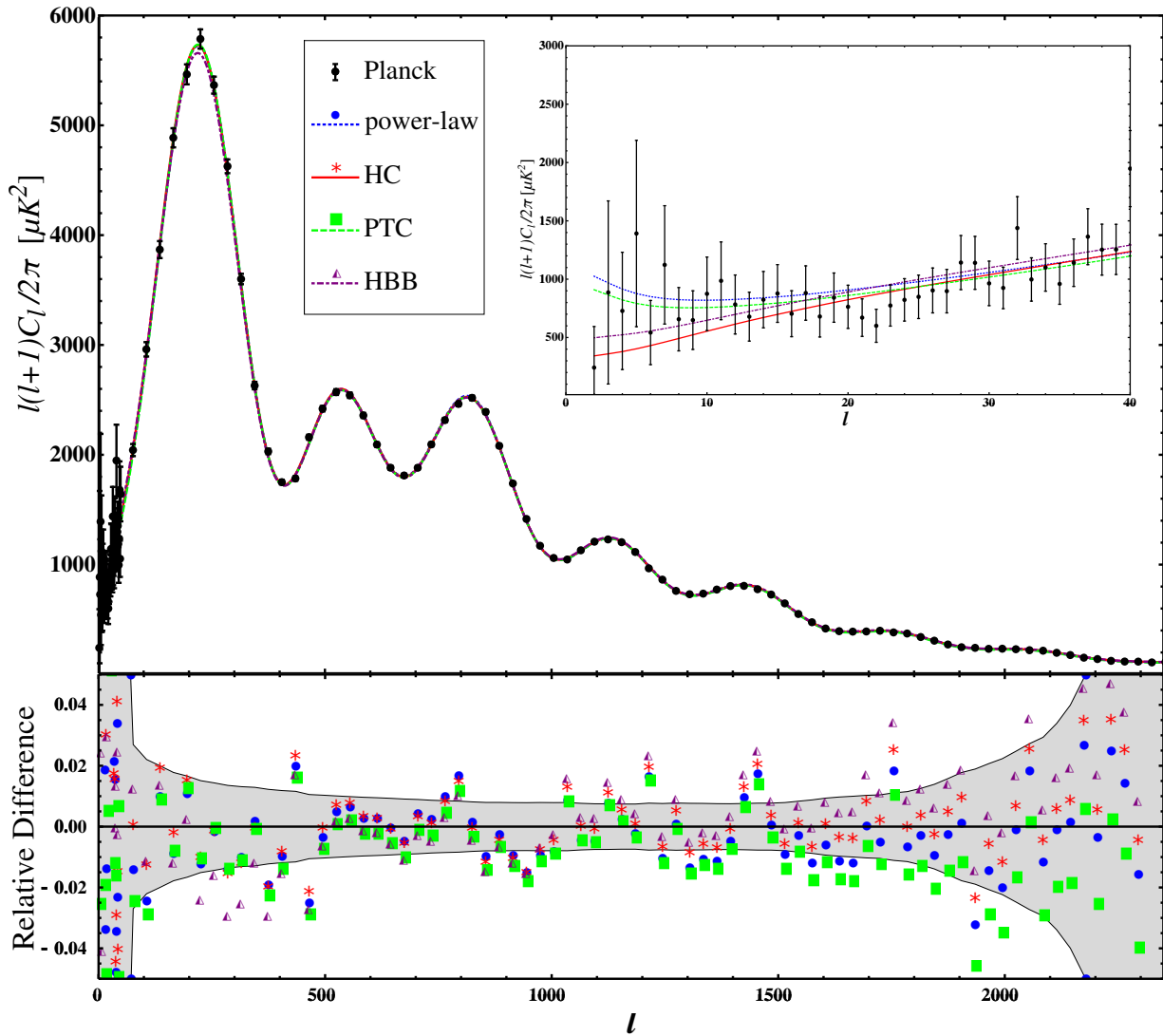
Figure 6.1: A plot of the TT anisotropy power spectrum for all models compared in CosmoMC on top of each other and the Planck observations. The insert focuses on the low l values. The second plot shows the relative difference so the deviations from Planck are more visually obvious.

References

[1] S. Weinberg, *The first three minutes. A modern view of the origin of the universe.* 1977.

[2] N. T. A. Paul J. Steinhardt (Author), *Endless Universe: Beyond the Big Bang.* Doubleday, 2007.

[3] L. Boyle, "PSI Astrophysics Class Notes.".

[4] V. Mukhanov, *Physical Foundations of Cosmology.* Nov., 2005.

[5] S. Dodelson, *Modern cosmology.* 2003.

[6] S. Weinberg, *Cosmology.* Oxford University Press, 2008.

[7] A. Einstein, "Die Feldgleichungen der Gravitation," *Sitzungsberichte der Königlich Preußischen Akademie der Wissenschaften (Berlin), Seite 844-847.* (1915) .

[8] E. Hubble, "A Relation between Distance and Radial Velocity among Extra-Galactic Nebulae," *Proceedings of the National Academy of Science* **15** (Mar., 1929) 168–173.

[9] A. Einstein, "Zur elektrodynamik bewegter körper," *Annalen der Physik* **322** (1905) 891–921.

[10] A. Einstein, "Ist die trgheit eines krpers von seinem energieinhalt abhngig?," *Annalen der Physik* **323** no. 13, (1905) 639–641. http://dx.doi.org/10.1002/andp.19053231314.

[11] A. Friedmann, "Über die krümmung des raumes," *Zeitschrift für Physik* **10** no. 1, (Dec, 1922) 377–386. https://doi.org/10.1007/BF01332580.

[12] G. Lemaître, "Un univers homogène de masse constante et de rayon croissant rendant compte de la vitesse radiale des nébuleuses extra-galactiques," *Annales de la Société Scientifique de Bruxelles* (1927) 49–59.

[13] G. Lemaître, "L'Univers en expansion," *Annales de la Société Scientifique de Bruxelles* **53** (1933) .

[14] H. P. Robertson, "Kinematics and World-Structure," **82** (Nov., 1935) 284.

[15] H. P. Robertson, "Kinematics and World-Structure II.," *Astrophys. J.* **83** (Apr., 1936) 187.

[16] H. P. Robertson, "Kinematics and World-Structure III.," *Astrophys. J.* **83** (May, 1936) 257.

[17] A. G. Walker, "Distance in an expanding universe," *Mon. Not. R. Astron. Soc.* **94** (Dec., 1933) 159.

[18] A. G. Walker, "On the formal comparison of Milne's kinematical system with the systems of general relativity," *Mon. Not. R. Astron. Soc.* **95** (Jan., 1935) 263–269.

[19] **Planck** Collaboration, P. Ade *et al.*, "Planck 2015 results. XIII. Cosmological parameters," arXiv:1502.01589 [astro-ph.CO].

[20] G. Gamow, "Expanding universe and the origin of elements," *Phys. Rev.* **70** (Oct, 1946) 572–573. https://link.aps.org/doi/10.1103/PhysRev.70.572.2.

[21] G. Gamow, "The Evolution of the Universe," *Nature* **162** (Oct., 1948) 680–682.

[22] R. A. Alpher and R. Herman, "Evolution of the Universe," *Nature* **162** (Nov., 1948) 774–775.

[23] A. A. Penzias and R. W. Wilson, "A Measurement of Excess Antenna Temperature at 4080 Mc/s.," *Astrophys. J.* **142** (July, 1965) 419–421.

[24] R. H. Dicke, P. J. E. Peebles, P. G. Roll, and D. T. Wilkinson, "Cosmic Black-Body Radiation.," *Astrophys. J.* **142** (July, 1965) 414–419.

[25] W. F. Hoffmann, *Balloon-Borne Telescopes for Far-Infrared Astronomy*, pp. 155–168. Springer Netherlands, Dordrecht, 1977. https://doi.org/10.1007/978-94-010-1211-9_27.

[26] R. H. Becker, X. Fan, R. L. White, M. A. Strauss, V. K. Narayanan, R. H. Lupton, J. E. Gunn, J. Annis, N. A. Bahcall, J. Brinkmann, A. J. Connolly, I. Csabai, P. C. Czarapata, M. Doi, T. M. Heckman, G. S. Hennessy, Ž. Ivezić, G. R. Knapp, D. Q. Lamb, T. A. McKay, J. A. Munn, T. Nash, R. Nichol, J. R. Pier, G. T. Richards, D. P. Schneider, C. Stoughton, A. S. Szalay, A. R. Thakar, and D. G. York, "Evidence for Reionization at z~6: Detection of a Gunn-Peterson Trough in a z=6.28 Quasar," *The Astronomical Journal* **122** (Dec., 2001) 2850–2857, `astro-ph/0108097`.

[27] S. Perlmutter, M. S. Turner, and M. White, "Constraining dark energy with type ia supernovae and large-scale structure," *Phys. Rev. Lett.* **83** (Jul, 1999) 670–673. `https://link.aps.org/doi/10.1103/PhysRevLett.83.670`.

[28] N. W. Boggess, J. C. Mather, R. Weiss, C. L. Bennett, E. S. Cheng, E. Dwek, S. Gulkis, M. G. Hauser, M. A. Janssen, T. Kelsall, S. S. Meyer, S. H. Moseley, T. L. Murdock, R. A. Shafer, R. F. Silverberg, G. F. Smoot, D. T. Wilkinson, and E. L. Wright, "The COBE mission - Its design and performance two years after launch," *Astrophys. J.* **397** (Oct., 1992) 420–429.

[29] **WMAP** Collaboration, C. Bennett *et al.*, "Nine-Year Wilkinson Microwave Anisotropy Probe (WMAP) Observations: Final Maps and Results," *Astrophys.J.Suppl.* **208** (2013) 20, `arXiv:1212.5225 [astro-ph.CO]`.

[30] Planck Collaboration, R. Adam, P. A. R. Ade, N. Aghanim, Y. Akrami, M. I. R. Alves, F. Argüeso, M. Arnaud, F. Arroja, M. Ashdown, and et al., "Planck 2015 results. I. Overview of products and scientific results," *A&A* **594** (Sept., 2016) A1, `arXiv:1502.01582`.

[31] Y. Zeldovich and M. Khlopov, "On the concentration of relic magnetic monopoles in the universe," *Physics Letters B* **79** no. 3, (1978) 239 – 241. `http://www.sciencedirect.com/science/article/pii/0370269378902320`.

[32] J. P. Preskill, "Cosmological production of superheavy magnetic monopoles," *Phys. Rev. Lett.* **43** (Nov, 1979) 1365–1368. `https://link.aps.org/doi/10.1103/PhysRevLett.43.1365`.

[33] A. D. Linde, "A New Inflationary Universe Scenario: A Possible Solution of the Horizon, Flatness, Homogeneity, Isotropy and Primordial Monopole Problems," *Phys. Lett.* **108B** (1982) 389–393.

[34] A. H. Guth, "The Inflationary Universe: A Possible Solution to the Horizon and Flatness Problems," *Phys. Rev.* **D23** (1981) 347–356.

[35] R. H. Brandenberger, "Inflationary Cosmology: Progress and Problems," arXiv:hep-ph/9910410 [hep-ph].

[36] P. J. Steinhardt, "The inflation debate," *Scientific American* **304** (Apr, 2011) 36–43.

[37] A. Ijjas, P. J. Steinhardt, and A. Loeb, "Inflationary paradigm in trouble after Planck2013," *Physics Letters B* **723** (2013) 261–266, arXiv:1304.2785 [astro-ph.CO].

[38] N. Turok, "A critical review of inflation," *Classical and Quantum Gravity* **19** no. 13, (2002) 3449. http://stacks.iop.org/0264-9381/19/i=13/a=305.

[39] A. D. Sakharov, "The Initial Stage of an Expanding Universe and the Appearance of a Nonuniform Distribution of Matter," *Soviet Journal of Experimental and Theoretical Physics* **22** (Jan., 1966) 241.

[40] C. W. Misner, "Mixmaster Universe," *Physical Review Letters* **22** (May, 1969) 1071–1074.

[41] R. H. Brandenberger, "The Matter Bounce Alternative to Inflationary Cosmology," *ArXiv e-prints* (June, 2012) , arXiv:1206.4196 [astro-ph.CO].

[42] R. A. Sunyaev and Y. B. Zeldovich, "Small-Scale Fluctuations of Relic Radiation," *Astrophysics and Space Science* **7** (Apr., 1970) 3–19.

[43] L. Anderson *et al.*, "The clustering of galaxies in the SDSS-III Baryon Oscillation Spectroscopic Survey: Baryon Acoustic Oscillations in the Data Release 10 and 11 galaxy samples," *Mon. Not. R. Astron. Soc.* **441** (June, 2014) 24–62, arXiv:1312.4877 [astro-ph.CO].

[44] A. J. Ross, L. Samushia, C. Howlett, W. J. Percival, A. Burden, and M. Manera, "The clustering of the SDSS DR7 main Galaxy sample I. A 4 per cent distance measure at $z = 0.15$," *Mon. Not. Roy. Astron. Soc.* **449** no. 1, (2015) 835–847, arXiv:1409.3242 [astro-ph.CO].

[45] L. Anderson, E. Aubourg, S. Bailey, D. Bizyaev, M. Blanton, *et al.*, "The clustering of galaxies in the SDSS-III Baryon Oscillation Spectroscopic Survey: Baryon

Acoustic Oscillations in the Data Release 9 Spectroscopic Galaxy Sample," *Mon. Not. R. Astron. Soc.* **428** (2013) 1036–1054, `arXiv:1203.6594 [astro-ph.CO]`.

[46] N. Padmanabhan, X. Xu, D. J. Eisenstein, R. Scalzo, A. J. Cuesta, *et al.*, "A 2: Methods and Application to the Sloan Digital Sky Survey," *Mon. Not. R. Astron. Soc.* **427** (Dec., 2012) 2132–2145, `arXiv:1202.0090 [astro-ph.CO]`.

[47] F. Beutler, C. Blake, M. Colless, D. H. Jones, L. Staveley-Smith, *et al.*, "The 6dF Galaxy Survey: Baryon Acoustic Oscillations and the Local Hubble Constant," *Mon.Not.Roy.Astron.Soc.* **416** (2011) 3017–3032, `arXiv:1106.3366 [astro-ph.CO]`.

[48] C. Blake, E. Kazin, F. Beutler, T. Davis, D. Parkinson, *et al.*, "The WiggleZ Dark Energy Survey: mapping the distance-redshift relation with baryon acoustic oscillations," *Mon.Not.Roy.Astron.Soc.* **418** (2011) 1707–1724, `arXiv:1108.2635 [astro-ph.CO]`.

[49] A. G. Riess *et al.*, "A 2.4% Determination of the Local Value of the Hubble Constant," `arXiv:1604.01424 [astro-ph.CO]`.

[50] A. G. Riess, L. Macri, S. Casertano, H. Lampeitl, H. C. Ferguson, *et al.*, "A 3Telescope and Wide Field Camera 3," *Astrophys.J.* **730** (2011) 119, `arXiv:1103.2976 [astro-ph.CO]`.

[51] G. Efstathiou, "H0 Revisited," *Mon. Not. R. Astron. Soc.* **440** no. 2, (2014) 1138–1152, `arXiv:1311.3461 [astro-ph.CO]`.

[52] N. Suzuki, D. Rubin, C. Lidman, G. Aldering, R. Amanullah, *et al.*, "The Hubble Space Telescope Cluster Supernova Survey: V. Improving the Dark Energy Constraints Above $z > 1$ and Building an Early-Type-Hosted Supernova Sample," *Astrophys.J.* **746** (2012) 85, `arXiv:1105.3470 [astro-ph.CO]`.

[53] A. B. Mantz, S. W. Allen, R. G. Morris, D. A. Rapetti, D. E. Applegate, *et al.*, "Cosmology and Astrophysics from Relaxed Galaxy Clusters II: Cosmological Constraints," *Mon.Not.Roy.Astron.Soc.* **440** (2014) 2077–2098, `arXiv:1402.6212 [astro-ph.CO]`.

[54] **SDSS Collaboration** Collaboration, M. Betoule *et al.*, "Improved cosmological constraints from a joint analysis of the SDSS-II and SNLS supernova samples," *Astron.Astrophys.* (2014) , `arXiv:1401.4064 [astro-ph.CO]`.

[55] D. Parkinson, S. Riemer-Sorensen, C. Blake, G. B. Poole, T. M. Davis, *et al.*, "The WiggleZ Dark Energy Survey: Final data release and cosmological results," *Phys.Rev.* **D86** (2012) 103518, arXiv:1210.2130 [astro-ph.CO].

[56] **BICEP2, Planck** Collaboration, P. Ade *et al.*, "Joint Analysis of BICEP2/*KeckArray* and *Planck* Data," *Phys.Rev.Lett.* **114** (2015) 101301, arXiv:1502.00612 [astro-ph.CO].

[57] A. Lewis, A. Challinor, and A. Lasenby, "Efficient computation of CMB anisotropies in closed FRW models," *Astrophys. J.* **538** (2000) 473–476, arXiv:astro-ph/9911177 [astro-ph].

[58] C. Howlett, A. Lewis, A. Hall, and A. Challinor, "CMB power spectrum parameter degeneracies in the era of precision cosmology," *JCAP* **1204** (2012) 027, arXiv:1201.3654 [astro-ph.CO].

[59] A. Lewis, "CAMB Notes." http://cosmologist.info/notes/CAMB.pdf.

[60] U. Seljak and M. Zaldarriaga, "A line of sight approach to cosmic microwave background anisotropies," *Astrophys. J.* **469** (1996) 437–444, astro-ph/9603033.

[61] M. Zaldarriaga, U. Seljak, and E. Bertschinger, "Integral solution for the microwave background anisotropies in nonflat universes," *Astrophys.J.* **494** (1998) 491–502, arXiv:astro-ph/9704265 [astro-ph].

[62] C.-P. Ma and E. Bertschinger, "Cosmological perturbation theory in the synchronous and conformal Newtonian gauges," *Astrophys. J.* **455** (1995) 7–25, astro-ph/9506072.

[63] N. Metropolis, A. W. Rosenbluth, M. N. Rosenbluth, A. H. Teller, and E. Teller, "Equation of state calculations by fast computing machines," *Journal of Chemical Physics* **21** (1953) 1087–1092.

[64] W. Hastings, "Monte carlo samping methods using markov chains and their applications," *Biometrika* **57** (1970) 97–109.

[65] A. Lewis, "Efficient sampling of fast and slow cosmological parameters," *Phys. Rev.* **D87** (2013) 103529, arXiv:1304.4473 [astro-ph.CO].

[66] A. Lewis and S. Bridle, "Cosmological parameters from CMB and other data: A Monte Carlo approach," *Phys. Rev.* **D66** (2002) 103511, arXiv:astro-ph/0205436 [astro-ph].

[67] M. Powell, "The BOBYQA algorithm for bound constrained optimization without derivatives." http://www.damtp.cam.ac.uk/user/na/NA_papers/NA2009_06.pdf.

[68] E. Jaynes, "ProbabilityTheory: The Logic of Science," *Cambridge University Press* (2003) .

[69] R. Trotta, "Bayes in the sky: Bayesian inference and model selection in cosmology," *Contemp. Phys.* **49** (2008) 71–104, arXiv:0803.4089 [astro-ph].

[70] M. Hobson, A. Jaffe, A. Liddle, P. Mukherjee and D. Parkinson,, "Bayesian methods in cosmology," *Cambridge University Press* (2010) .

[71] F. Feroz and M. P. Hobson, "Multimodal nested sampling: an efficient and robust alternative to MCMC methods for astronomical data analysis," *Mon. Not. Roy. Astron. Soc.* **384** (2008) 449, arXiv:0704.3704 [astro-ph].

[72] F. Feroz, M. P. Hobson, and M. Bridges, "MultiNest: an efficient and robust Bayesian inference tool for cosmology and particle physics," *Mon. Not. Roy. Astron. Soc.* **398** (2009) 1601–1614, arXiv:0809.3437 [astro-ph].

[73] F. Feroz, M. P. Hobson, E. Cameron, and A. N. Pettitt, "Importance Nested Sampling and the MultiNest Algorithm," arXiv:1306.2144 [astro-ph.IM].

[74] A. A. Michelson and E. W. Morley, "On the Relative Motion of the Earth and of the Luminiferous Ether," *Sidereal Messenger, vol. 6, pp.306-310* **6** (Nov., 1887) 306–310.

[75] H. A. Lorentz, "De relatieve beweging van de aarde en den aether," *Zittingsverlag Akad. V. Wet.* **1** (1892) 74–79.

[76] S. W. Hawking and R. Penrose, "The Singularities of Gravitational Collapse and Cosmology," *Proceedings of the Royal Society of London Series A* **314** (Jan., 1970) 529–548.

[77] R. C. Tolman, *Relativity, Thermodynamics, and Cosmology*. 1934.

[78] J. K. Erickson, D. H. Wesley, P. J. Steinhardt, and N. Turok, "Kasner and mixmaster behavior in universes with equation of state $w \geqslant 1$," *Phys. Rev. D* **69** no. 6, (Mar., 2004) 063514, hep-th/0312009.

[79] G. 't Hooft, "Dimensional reduction in quantum gravity," in *Salamfest 1993:0284-296*, pp. 0284–296. 1993. arXiv:gr-qc/9310026 [gr-qc].

[80] L. Susskind, "The World as a hologram," *J. Math. Phys.* **36** (1995) 6377–6396, `arXiv:hep-th/9409089 [hep-th]`.

[81] J. M. Maldacena, "The Large N limit of superconformal field theories and supergravity," *Int. J. Theor. Phys.* **38** (1999) 1113–1133, `arXiv:hep-th/9711200 [hep-th]`. [Adv. Theor. Math. Phys.2,231(1998)].

[82] C. M. Hull, "Timelike T duality, de Sitter space, large N gauge theories and topological field theory," *JHEP* **07** (1998) 021, `arXiv:hep-th/9806146 [hep-th]`.

[83] E. Witten, "Quantum gravity in de Sitter space," in *Strings 2001: International Conference Mumbai, India, January 5-10, 2001*. 2001. `arXiv:hep-th/0106109 [hep-th]`.

[84] A. Strominger, "The dS / CFT correspondence," *JHEP* **10** (2001) 034, `arXiv:hep-th/0106113 [hep-th]`.

[85] A. Strominger, "Inflation and the dS / CFT correspondence," *JHEP* **11** (2001) 049, `arXiv:hep-th/0110087 [hep-th]`.

[86] J. M. Maldacena, "Non-Gaussian features of primordial fluctuations in single field inflationary models," *JHEP* **05** (2003) 013, `arXiv:astro-ph/0210603 [astro-ph]`.

[87] P. McFadden and K. Skenderis, "Holography for Cosmology," *Phys. Rev.* **D81** (2010) 021301, `arXiv:0907.5542 [hep-th]`.

[88] P. McFadden and K. Skenderis, "The Holographic Universe," *J. Phys. Conf. Ser.* **222** (2010) 012007, `arXiv:1001.2007 [hep-th]`.

[89] P. McFadden and K. Skenderis, "Holographic Non-Gaussianity," *JCAP* **1105** (2011) 013, `arXiv:1011.0452 [hep-th]`.

[90] P. McFadden and K. Skenderis, "Cosmological 3-point correlators from holography," *JCAP* **1106** (2011) 030, `arXiv:1104.3894 [hep-th]`.

[91] A. Bzowski, P. McFadden, and K. Skenderis, "Holographic predictions for cosmological 3-point functions," *JHEP* **03** (2012) 091, `arXiv:1112.1967 [hep-th]`.

[92] K. Skenderis and P. K. Townsend, "Hidden supersymmetry of domain walls and cosmologies," *Phys. Rev. Lett.* **96** (2006) 191301, `arXiv:hep-th/0602260 [hep-th]`.

[93] J. M. Maldacena and G. L. Pimentel, "On graviton non-Gaussianities during inflation," *JHEP* **09** (2011) 045, `arXiv:1104.2846 [hep-th]`.

[94] J. B. Hartle, S. W. Hawking, and T. Hertog, "Accelerated Expansion from Negative Λ," `arXiv:1205.3807 [hep-th]`.

[95] J. B. Hartle, S. W. Hawking, and T. Hertog, "Quantum Probabilities for Inflation from Holography," *JCAP* **1401** no. 01, (2014) 015, `arXiv:1207.6653 [hep-th]`.

[96] K. Schalm, G. Shiu, and T. van der Aalst, "Consistency condition for inflation from (broken) conformal symmetry," *JCAP* **1303** (2013) 005, `arXiv:1211.2157 [hep-th]`.

[97] A. Bzowski, P. McFadden, and K. Skenderis, "Holography for inflation using conformal perturbation theory," *JHEP* **04** (2013) 047, `arXiv:1211.4550 [hep-th]`.

[98] I. Mata, S. Raju, and S. Trivedi, "CMB from CFT," *JHEP* **07** (2013) 015, `arXiv:1211.5482 [hep-th]`.

[99] J. Garriga and Y. Urakawa, "Inflation and deformation of conformal field theory," *JCAP* **1307** (2013) 033, `arXiv:1303.5997 [hep-th]`.

[100] P. McFadden, "On the power spectrum of inflationary cosmologies dual to a deformed CFT," *JHEP* **10** (2013) 071, `arXiv:1308.0331 [hep-th]`.

[101] A. Ghosh, N. Kundu, S. Raju, and S. P. Trivedi, "Conformal Invariance and the Four Point Scalar Correlator in Slow-Roll Inflation," *JHEP* **07** (2014) 011, `arXiv:1401.1426 [hep-th]`.

[102] J. Garriga and Y. Urakawa, "Holographic inflation and the conservation of ζ," *JHEP* **06** (2014) 086, `arXiv:1403.5497 [hep-th]`.

[103] N. Kundu, A. Shukla, and S. P. Trivedi, "Constraints from Conformal Symmetry on the Three Point Scalar Correlator in Inflation," *JHEP* **04** (2015) 061, `arXiv:1410.2606 [hep-th]`.

[104] J. Garriga, K. Skenderis, and Y. Urakawa, "Multi-field inflation from holography," *JCAP* **1501** no. 01, (2015) 028, `arXiv:1410.3290 [hep-th]`.

[105] P. McFadden, "Soft limits in holographic cosmology," *JHEP* **02** (2015) 053, `arXiv:1412.1874 [hep-th]`.

[106] N. Arkani-Hamed and J. Maldacena, "Cosmological Collider Physics,"
arXiv:1503.08043 [hep-th].

[107] N. Kundu, A. Shukla, and S. P. Trivedi, "Ward Identities for Scale and Special
Conformal Transformations in Inflation," *JHEP* **01** (2016) 046, arXiv:1507.06017
[hep-th].

[108] T. Hertog and E. van der Woerd, "Primordial fluctuations from complex AdS
saddle points," *JCAP* **1602** no. 02, (2016) 010, arXiv:1509.03291 [hep-th].

[109] J. Garriga, Y. Urakawa, and F. Vernizzi, "δN formalism from superpotential and
holography," *JCAP* **1602** no. 02, (2016) 036, arXiv:1509.07339 [hep-th].

[110] J. Garriga and Y. Urakawa, "Consistency relations and conservation of ζ in
holographic inflation," arXiv:1606.04767 [hep-th].

[111] N. Itzhaki, J. M. Maldacena, J. Sonnenschein, and S. Yankielowicz, "Supergravity
and the large N limit of theories with sixteen supercharges," *Phys. Rev.* **D58** (1998)
046004, arXiv:hep-th/9802042 [hep-th].

[112] H. J. Boonstra, K. Skenderis, and P. K. Townsend, "The domain wall / QFT
correspondence," *JHEP* **01** (1999) 003, arXiv:hep-th/9807137 [hep-th].

[113] I. Kanitscheider, K. Skenderis, and M. Taylor, "Precision holography for
non-conformal branes," *JHEP* **09** (2008) 094, arXiv:0807.3324 [hep-th].

[114] C. Corianò, L. Delle Rose, and M. Serino, "Three and Four Point Functions of
Stress Energy Tensors in D=3 for the Analysis of Cosmological Non-Gaussianities,"
JHEP **12** (2012) 090, arXiv:1210.0136 [hep-th].

[115] S. Kawai and Y. Nakayama, "Improvement of energy-momentum tensor and
non-Gaussianities in holographic cosmology," *JHEP* **06** (2014) 052,
arXiv:1403.6220 [hep-th].

[116] M. Dias, "Cosmology at the boundary of de Sitter using the dS/QFT
correspondence," *Phys. Rev.* **D84** (2011) 023512, arXiv:1104.0625
[astro-ph.CO].

[117] R. Easther, R. Flauger, P. McFadden, and K. Skenderis, "Constraining holographic
inflation with WMAP," *JCAP* **1109** (2011) 030, arXiv:1104.2040
[astro-ph.CO].

[118] N. Afshordi, C. Coriano, L. Delle Rose, E. Gould, and K. Skenderis, "From Planck data to Planck era: Observational tests of Holographic Cosmology," *Phys. Rev. Lett.* **118** no. 4, (2017) 041301, `arXiv:1607.04878 [astro-ph.CO]`.

[119] D. Anninos, T. Hartman, and A. Strominger, "Higher Spin Realization of the dS/CFT Correspondence," *Class. Quant. Grav.* **34** no. 1, (2017) 015009, `arXiv:1108.5735 [hep-th]`.

[120] A. Jevicki, Y. Kazama, and T. Yoneya, "Generalized conformal symmetry in D-brane matrix models," *Phys. Rev.* **D59** (1999) 066001, `arXiv:hep-th/9810146 [hep-th]`.

[121] C. Corianò, L. Delle Rose, and K. Skenderis, "Quantum Field Theory with generalized conformal structure," `to appear`.

[122] R. Jackiw and S. Templeton, "How Superrenormalizable Interactions Cure their Infrared Divergences," *Phys. Rev.* **D23** (1981) 2291.

[123] T. Appelquist and R. D. Pisarski, "High-Temperature Yang-Mills Theories and Three-Dimensional Quantum Chromodynamics," *Phys. Rev.* **D23** (1981) 2305.

[124] A. Kosowsky and M. S. Turner, "CBR anisotropy and the running of the scalar spectral index," *Phys. Rev.* **D52** (1995) 1739–1743, `arXiv:astro-ph/9504071 [astro-ph]`.

[125] **Planck** Collaboration, P. Ade *et al.*, "Planck 2015 results. XV. Gravitational lensing," `arXiv:1502.01591 [astro-ph.CO]`.

[126] **Planck** Collaboration, N. Aghanim *et al.*, "Planck 2015 results. XI. CMB power spectra, likelihoods, and robustness of parameters," `arXiv:1507.02704 [astro-ph.CO]`.

[127] **Planck** Collaboration, P. Ade *et al.*, "Planck 2015 results. XXIV. Cosmology from Sunyaev-Zeldovich cluster counts," `arXiv:1502.01597 [astro-ph.CO]`.

[128] C. Reichardt, L. Shaw, O. Zahn, K. Aird, B. Benson, *et al.*, "A measurement of secondary cosmic microwave background anisotropies with two years of South Pole Telescope observations," *Astrophys.J.* **755** (2012) 70, `arXiv:1111.0932 [astro-ph.CO]`.

[129] S. Das, T. Louis, M. R. Nolta, G. E. Addison, E. S. Battistelli, *et al.*, "The Atacama Cosmology Telescope: temperature and gravitational lensing power spectrum measurements from three seasons of data," *JCAP* **1404** (2014) 014, `arXiv:1301.1037 [astro-ph.CO]`.

[130] F. Beutler, C. Blake, M. Colless, D. H. Jones, L. Staveley-Smith, *et al.*, "The 6dF Galaxy Survey: $z \approx 0$ measurement of the growth rate and sigma_8," *Mon.Not.Roy.Astron.Soc.* **423** (2012) 3430–3444, `arXiv:1204.4725 [astro-ph.CO]`.

[131] L. Samushia, B. A. Reid, M. White, W. J. Percival, A. J. Cuesta, *et al.*, "The Clustering of Galaxies in the SDSS-III Baryon Oscillation Spectroscopic Survey (BOSS): measuring growth rate and geometry with anisotropic clustering," *Mon.Not.Roy.Astron.Soc.* **439** (2014) 3504–3519, `arXiv:1312.4899 [astro-ph.CO]`.

[132] **Planck** Collaboration, N. Aghanim *et al.*, "Planck 2016 intermediate results. LI. Features in the cosmic microwave background temperature power spectrum and shifts in cosmological parameters," `arXiv:1608.02487 [astro-ph.CO]`.

[133] **Planck** Collaboration, P. A. R. Ade *et al.*, "Planck 2013 results. XXIII. Isotropy and statistics of the CMB," *Astron. Astrophys.* **571** (2014) A23, `arXiv:1303.5083 [astro-ph.CO]`.

[134] **CMB-S4** Collaboration, K. N. Abazajian *et al.*, "CMB-S4 Science Book, First Edition," `arXiv:1610.02743 [astro-ph.CO]`.

[135] O. Dore *et al.*, "Cosmology with the SPHEREX All-Sky Spectral Survey," `arXiv:1412.4872 [astro-ph.CO]`.

[136] K. Gödel, "An Example of a New Type of Cosmological Solutions of Einstein's Field Equations of Gravitation," *Reviews of Modern Physics* **21** (July, 1949) 447–450.

[137] L. Bombelli, J. Lee, D. Meyer, and R. D. Sorkin, "Space-time as a causal set," *Physical Review Letters* **59** (Aug., 1987) 521–524.

[138] E. Anderson, J. Barbour, B. Z. Foster, B. Kelleher, and N. Ó. Murchadha, "The physical gravitational degrees of freedom," *Classical and Quantum Gravity* **22** (May, 2005) 1795–1802, `gr-qc/0407104`.

[139] F. J. Tipler, "Singularities and causality violation.," *Annals of Physics* **108** (1977) 1–36.

[140] N. Ashby, D. F. Bartlett, and W. Wyss, eds., *General Relativity and Gravitation, 1989.* Oct., 1990.

[141] J. Friedman, M. S. Morris, I. D. Novikov, F. Echeverria, G. Klinkhammer, K. S. Thorne, and U. Yurtsever, "Cauchy problem in spacetimes with closed timelike curves," *Physical Review D* **42** (Sep, 1990) 1915–1930. http://link.aps.org/doi/10.1103/PhysRevD.42.1915.

[142] I. D. Novikov, "Time machine and self-consistent evolution in problems with self-interaction," *Physical Review D* **45** (Mar., 1992) 1989–1994.

[143] A. Carlini, V. P. Frolov, M. B. Mensky, I. D. Novikov, and H. H. Soleng, "Time Machines:. the Principle of Self-Consistency as a Consequence of the Principle of Minimal Action," *International Journal of Modern Physics D* **4** (1995) 557–580, arXiv:gr-qc/9506087 [gr-qc].

[144] A. Carlini and I. D. Novikov, "Time Machines and the Principle of Self-Consistency as a Consequence of the Principle of Stationary Action (ii):. the Cauchy Problem for a Self-Interacting Relativistic Particle," *International Journal of Modern Physics D* **5** (1996) 445–479, gr-qc/9607063.

[145] R. Penrose, *Cycles of Time: An Extraordinary New View of the Universe.* Bodley Head, 2010.

[146] J. Silk, "Cosmic Black-Body Radiation and Galaxy Formation," *Astrophys. J.* **151** (Feb., 1968) 459.

[147] D. J. Eisenstein and W. Hu, "Baryonic Features in the Matter Transfer Function," *Astrophys. J.* **496** (Mar., 1998) 605–614, astro-ph/9709112.

[148] V. F. Mukhanov, H. A. Feldman, and R. H. Brandenberger, "Theory of cosmological perturbations. Part 1. Classical perturbations. Part 2. Quantum theory of perturbations. Part 3. Extensions," *Phys. Rept.* **215** (1992) 203–333.

[149] **Planck Collaboration** Collaboration, P. Ade *et al.*, "Planck 2013 results. XVI. Cosmological parameters," *Astron.Astrophys.* (2014) , arXiv:1303.5076 [astro-ph.CO].

[150] **Planck collaboration** Collaboration, "Planck 2013 results. XV. CMB power spectra and likelihood," arXiv:1303.5075 [astro-ph.CO].

[151] **Planck Collaboration** Collaboration, P. Ade *et al.*, "Planck 2013 results. XVII. Gravitational lensing by large-scale structure," arXiv:1303.5077 [astro-ph.CO].

[152] P. G. Ferreira and M. Joyce, "Cosmology with a primordial scaling field," *Phys. Rev.* **D58** (1998) 023503, arXiv:astro-ph/9711102 [astro-ph].

[153] N. Afshordi, D. J. H. Chung, M. Doran, and G. Geshnizjani, "Cuscuton Cosmology: Dark Energy meets Modified Gravity," *Phys. Rev.* **D75** (2007) 123509, arXiv:astro-ph/0702002 [astro-ph].

[154] J. Barbour private communication.

[155] P. J. Steinhardt and N. Turok, "A Cyclic model of the universe," *Science* **296** (2002) 1436–1439, arXiv:hep-th/0111030 [hep-th].

[156] R. Pourhasan, N. Afshordi, and R. B. Mann, "Out of the White Hole: A Holographic Origin for the Big Bang," *JCAP* **1404** (2014) 005, arXiv:1309.1487 [hep-th].

[157] **Planck** Collaboration, P. A. R. Ade *et al.*, "Planck 2015 results. XIII. Cosmological parameters," arXiv:1502.01589 [astro-ph.CO].

[158] G. R. Dvali, G. Gabadadze, and M. Porrati, "4-D gravity on a brane in 5-D Minkowski space," *Phys. Lett.* **B485** (2000) 208–214, arXiv:hep-th/0005016 [hep-th].

[159] R. Gregory, N. Kaloper, R. C. Myers, and A. Padilla, "A New perspective on DGP gravity," *JHEP* **10** (2007) 069, arXiv:0707.2666 [hep-th].

[160] S. D. Mathur, "Tunneling into fuzzball states," *Gen. Rel. Grav.* **42** (2010) 113–118, arXiv:0805.3716 [hep-th].

[161] E. Witten, "Instability of the kaluza-klein vacuum," *Nuclear Physics B* **195** no. 3, (1982) 481 – 492. http://www.sciencedirect.com/science/article/pii/0550321382900074.

[162] O. Lunin and S. D. Mathur, "Statistical interpretation of Bekenstein entropy for systems with a stretched horizon," *Phys. Rev. Lett.* **88** (2002) 211303, arXiv:hep-th/0202072 [hep-th].

[163] M. Pospelov and J. Pradler, "Big Bang Nucleosynthesis as a Probe of New Physics," *Ann. Rev. Nucl. Part. Sci.* **60** (2010) 539–568, `arXiv:1011.1054 [hep-ph]`.

[164] T. Azizi, M. Sadegh Movahed, and K. Nozari, "Observational Constraints on the Normal Branch of a Warped DGP Cosmology," *New Astron.* **17** (2012) 424–432, `arXiv:1111.3195 [astro-ph.CO]`.

[165] **Planck** Collaboration, P. A. R. Ade *et al.*, "Planck 2015 results. XIV. Dark energy and modified gravity," `arXiv:1502.01590 [astro-ph.CO]`.

[166] U. Seljak and M. Zaldarriaga, "A Line-of-Sight Integration Approach to Cosmic Microwave Background Anisotropies," *The Astrophysical Journal* **469** (Oct., 1996) 437, `astro-ph/9603033`.

[167] M. Zaldarriaga, U. Seljak, and E. Bertschinger, "Integral Solution for the Microwave Background Anisotropies in Nonflat Universes," *The Astrophysical Journal* **494** (Feb., 1998) 491–502, `astro-ph/9704265`.

[168] A. Lewis and S. Bridle, "Cosmological parameters from CMB and other data: A Monte Carlo approach," *Phys. Rev. D* **66** no. 10, (Nov., 2002) 103511, `astro-ph/0205436`.

[169] A. Lewis, A. Challinor, and A. Lasenby, "Efficient Computation of Cosmic Microwave Background Anisotropies in Closed Friedmann-Robertson-Walker Models," *The Astrophysical Journal* **538** (Aug., 2000) 473–476, `astro-ph/9911177`.

[170] C. Howlett, A. Lewis, A. Hall, and A. Challinor, "CMB power spectrum parameter degeneracies in the era of precision cosmology," *JCAP* **4** (Apr., 2012) 027, `arXiv:1201.3654 [astro-ph.CO]`.

[171] A. Lewis, "Efficient sampling of fast and slow cosmological parameters," *Phys. Rev. D* **87** no. 10, (May, 2013) 103529, `arXiv:1304.4473 [astro-ph.CO]`.

[172] A. Lewis, "CAMB Notes," *http://cosmologist.info/notes/CAMB.pdf* .

[173] F. Beutler, C. Blake, M. Colless, D. H. Jones, L. Staveley-Smith, L. Campbell, Q. Parker, W. Saunders, and F. Watson, "The 6dF Galaxy Survey: baryon acoustic oscillations and the local Hubble constant," *mnras* **416** (Oct., 2011) 3017–3032, `arXiv:1106.3366`.

[174] C. Blake and others., "The WiggleZ Dark Energy Survey: mapping the distance-redshift relation with baryon acoustic oscillations," *mnras* **418** (Dec., 2011) 1707–1724, `arXiv:1108.2635`.

[175] L. Anderson *et al.*, "The clustering of galaxies in the SDSS-III Baryon Oscillation Spectroscopic Survey: baryon acoustic oscillations in the Data Release 9 spectroscopic galaxy sample," *mnras* **427** (Dec., 2012) 3435–3467, `arXiv:1203.6594`.

[176] F. Beutler, C. Blake, M. Colless, D. H. Jones, L. Staveley-Smith, G. B. Poole, L. Campbell, Q. Parker, W. Saunders, and F. Watson, "The 6dF Galaxy Survey: z 0 measurements of the growth rate and σ_8," *mnras* **423** (July, 2012) 3430–3444, `arXiv:1204.4725`.

[177] N. Padmanabhan, X. Xu, D. J. Eisenstein, R. Scalzo, A. J. Cuesta, K. T. Mehta, and E. Kazin, "A 2 per cent distance to z = 0.35 by reconstructing baryon acoustic oscillations - I. Methods and application to the Sloan Digital Sky Survey," *mnras* **427** (Dec., 2012) 2132–2145, `arXiv:1202.0090`.

[178] L. Anderson and others., "The clustering of galaxies in the SDSS-III Baryon Oscillation Spectroscopic Survey: baryon acoustic oscillations in the Data Releases 10 and 11 Galaxy samples," *mnras* **441** (June, 2014) 24–62, `arXiv:1312.4877`.

[179] L. Samushia and others., "The clustering of galaxies in the SDSS-III Baryon Oscillation Spectroscopic Survey: measuring growth rate and geometry with anisotropic clustering," *mnras* **439** (Apr., 2014) 3504–3519, `arXiv:1312.4899`.

[180] A. J. Ross, L. Samushia, C. Howlett, W. J. Percival, A. Burden, and M. Manera, "The clustering of the SDSS DR7 main Galaxy sample - I. A 4 per cent distance measure at z = 0.15," *mnras* **449** (May, 2015) 835–847, `arXiv:1409.3242`.

[181] **Planck** Collaboration, N. Aghanim *et al.*, "Planck 2015 results. XI. CMB power spectra, likelihoods, and robustness of parameters," *Astron. Astrophys.* (2015) , `arXiv:1507.02704 [astro-ph.CO]`.

[182] C. L. Reichardt *et al.*, "A Measurement of Secondary Cosmic Microwave Background Anisotropies with Two Years of South Pole Telescope Observations," *apj* **755** (Aug., 2012) 70, `arXiv:1111.0932 [astro-ph.CO]`.

[183] S. Das *et al.*, "The Atacama Cosmology Telescope: temperature and gravitational lensing power spectrum measurements from three seasons of data," *jcap* **4** (Apr., 2014) 014, `arXiv:1301.1037`.

[184] **Planck** Collaboration, P. A. R. Ade *et al.*, "Planck 2015 results. XX. Constraints on inflation," `arXiv:1502.02114 [astro-ph.CO]`.

[185] E. W. Kolb and M. S. Turner, *The early universe.* 1990.

[186] J. Bell, "On the Einstein-Podolsky-Rosen paradox," *Physics* **1** (1964) 195.

[187] S. Liberati, "Tests of Lorentz invariance: a 2013 update," `arXiv:1304.5795 [gr-qc]`.

[188] A. Valentini, "Signal-locality in hidden-variables theories," *Physics Letters A* **297** no. 5-6, (2002) 273–278, `arXiv:quant-ph/0112151 [quant-ph]`.

[189] **Planck Collaboration** Collaboration, P. Ade *et al.*, "Planck 2013 results. I. Overview of products and scientific results," `arXiv:1303.5062 [astro-ph.CO]`.

[190] P. Horava, "Quantum Gravity at a Lifshitz Point," *Phys.Rev.* **D79** (2009) 084008, `arXiv:0901.3775 [hep-th]`.

[191] D. Bohm, "A suggested interpretation of the quantum theory in terms of "hidden" variables. i," *Phys. Rev.* **85** (Jan, 1952) 166–179. `http://link.aps.org/doi/10.1103/PhysRev.85.166`.

[192] D. Bohm, "A suggested interpretation of the quantum theory in terms of "hidden" variables. ii," *Phys. Rev.* **85** (Jan, 1952) 180–193. `http://link.aps.org/doi/10.1103/PhysRev.85.180`.

[193] A. Valentini, "Hidden variables, statistical mechanics and the early universe," Tech. Rep. Imperial/TP/0-01/16, Apr., 2001. `http://arxiv.org/abs/quant-ph/0104067`.

[194] L. Smolin, "A Real ensemble interpretation of quantum mechanics," *Found.Phys.* **42** (2012) 1239–1261, `arXiv:1104.2822 [quant-ph]`.

[195] G. Geshnizjani, W. H. Kinney, and A. M. Dizgah, "General conditions for scale-invariant perturbations in an expanding universe," *JCAP* **1111** (2011) 049, `arXiv:1107.1241 [astro-ph.CO]`.

APPENDICES

Appendix A

Supplemental Calculations for the 5D Holographic Big Bang Model

A.1 Inhomogeneous Cosmological perturbations on the bulk

If we consider the metric (4.34) and homogeneous perturbations of the form (4.35) the induced metric on the brane is $\gamma_{\mu\nu} = g_{\alpha\beta}e_\mu^\alpha e_\nu^\beta$ that to first order in ϵ reads:

$$ds_{\text{brane}}^2 = [(f_0'^2 - 1) - 2\epsilon\left(\hat{\Psi}_5^0(f)f_0'^2 + \hat{\Phi}_5^0(f)\right)]dt^2 + [1 - 2\epsilon\hat{\Psi}_5^0(f)][dx^2 + dy^2 + dz^2]\,, \quad \text{(A.1)}$$

where $f' = \frac{\mathrm{d}f}{\mathrm{d}t}$. The induced metric on the brane has to be able to describe a Friedmann universe for which we make the following identifications

$$-d\tau^2 = [(f_0'^2 - 1) - 2\epsilon\left(\hat{\Psi}_5^0 f_0'^2 + \hat{\Phi}_5^0\right)]dt^2\,, \quad a^2 = [1 - 2\epsilon\hat{\Psi}_5^0]\,, \quad \text{(A.2)}$$

where τ is the proper time of the brane and a is the scale factor. On top of the homogeneous perturbations we are now going to consider anisotropies

$$\Phi_5 = \epsilon\Phi_5^0(w) + \epsilon_1\Phi_5^1(x^\alpha)\,, \quad \Psi_5 = \epsilon\Psi_5^0(w) + \epsilon_1\Psi_5^1(x^\alpha)\,, \quad f = f_0(t) + \epsilon_1 f_1(x^\alpha)\,, \quad \text{(A.3)}$$

where $\epsilon_1 \ll 1$ is a parameter that controls the anisotropic perturbations and $\epsilon\epsilon_1 \ll \epsilon, \epsilon_1$. The induced metric can be written as

$$ds_{\text{brane}}^2 = -[1 + \frac{2\epsilon_1}{f_0'^2 - 1}(\hat{\Phi}_5^1 + \hat{\Psi}_5^1 f_0^2 - f_0'f_1')]d\tau^2 + 2a\epsilon_1\frac{f_0'f_{1,i}}{\sqrt{f_0'^2 - 1}}dx^i d\tau + a^2(1 - 2\hat{\Psi}_5^1\epsilon_1)dx^2\,,$$

$$\text{(A.4)}$$

where $\hat{\Psi}_5 = \Psi_5(w = f(x^\mu))$ are the metric functions projected to the brane. The general form of a 4D metric including scalar and vector cosmological perturbation in 4D are that contains all the terms in Eq. (A.4)

$$ds_{\mathrm{brane}}^2 = -(1 + 2\phi_4)d\tau^2 - 2aB_i d\tau dx^i + a^2(1 - 2\psi_4)dx^2 \,, \tag{A.5}$$

and thus we identify

$$\phi_4 = \frac{\epsilon_1}{f_0'^2 - 1}(\hat{\Phi}_5^1 + \hat{\Psi}_5^1 f_0^2 - f_0' f_1'), \quad \psi_4 = \hat{\Psi}_5^1 \epsilon_1 \,, \quad B_i = \epsilon_1 \frac{f_0' f_{1,i}}{\sqrt{f_0'^2 - 1}} \,. \tag{A.6}$$

Note that the Newtonian gauge on the bulk does not translate into a Newtonian gauge on the brane and that some perturbations that are scalars in 5D are projected as a vectorial perturbation component in 4D. The scalar gauge invariant quantities can be constructed from Eq.(A.4) as

$$\Phi_4 = \phi_4 - \partial_\tau(aB) \,, \tag{A.7}$$

$$\Psi_4 = \psi_4 + HaB \,, \tag{A.8}$$

where, H is the Hubble constant and B is the scalar part of the vector metric perturbation B_i. From our construction the Hubble constant is

$$H = \frac{\dot{a}}{a} = -\frac{\epsilon \hat{\Psi}_5^0}{a^2} \,, \tag{A.9}$$

and thus Eq.(A.8) reduces to $\Psi_4 = \psi_4$ to first order in ϵ, ϵ_1.

A.2 Derivation of the power spectrum

With use of the Poisson equation in 4D

$$\nabla^2 \Psi_5(y) = \frac{8\pi G_5}{3} \rho_5(y) \,, \tag{A.10}$$

and the expression for the energy density correlation function

$$\langle \rho_5(y_1)\rho_5(y_2) \rangle \simeq \alpha(T_5)^6 \delta^4(y_1 - y_2) \,, \tag{A.11}$$

we can write the 2-point correlation function of Ψ_5 using the Green's function for the Laplacian operator

$$\langle \Psi_5(x_1)\Psi_5(x_2) \rangle = \alpha \left(\frac{8\pi G_5}{3}\right)^2 \left(\frac{1}{4\pi^2}\right)^2 \int d^4 y \frac{(T_5(y))^6}{|y - x_1|^2 |y - x_2|^2} \,. \tag{A.12}$$

147

The junction condition between the 5D and 4D metrics (4.34) and (A.1) allow us to compute $\langle \Psi_4(\mathbf{x_1}) \Psi_4(\mathbf{x_2}) \rangle$

$$\langle \Psi_4(\mathbf{x_1}) \Psi_4(\mathbf{x_2}) \rangle = \langle \Psi_5(\mathbf{x_1}, x_{1w} = 0) \Psi_4(\mathbf{x_2}, x_{2w} = 0) \rangle$$

$$= \alpha \left(\frac{2G_5}{3\pi} \right)^2 \int d^3\mathbf{y_3} dy_w \frac{(T_5(y_w))^6}{(|\mathbf{x_1} - \mathbf{y_3}|^2 + |y_w|^2)(|\mathbf{x_2} - \mathbf{y_3}|^2 + |y_w|^2)} \quad \text{(A.13)}$$

where we have decomposed the bulk coordinate as $y = (\mathbf{y_3}, y_w)$ and we have set the temperature to be just a function of the w direction of the bulk. Combining expressions (4.45), (4.46), (A.13) and setting $\mathbf{x_1} = 0$ we have

$$P_\zeta(k) = \alpha \left(\frac{2G_5}{3\pi \, \Delta\ln H} \right)^2 \int \frac{d^3\mathbf{y_3} \, dy_w \, (T_5(y_w))^6}{|\mathbf{y_3}|^2 + |y_w|^2} \int d^3x \frac{e^{i\mathbf{k}\cdot\mathbf{x}}}{|\mathbf{x} - \mathbf{y_3}|^2 + |y_w|^2} \, ,$$

$$= \alpha \left(\frac{2G_5}{3\pi \, \Delta\ln H} \right)^2 \int \frac{d^3\mathbf{y_3} \, dy_w \, (T_5(y_w))^6}{|\mathbf{y_3}|^2 + |y_w|^2} \int d^3\mathbf{x'} \frac{e^{i\mathbf{k}\cdot\mathbf{x'}} e^{i\mathbf{k}\cdot\mathbf{y_3}}}{|\mathbf{x'}|^2 + |y_w|^2} \, ,$$

$$= \alpha \left(\frac{2G_5}{3\pi \, \Delta\ln H} \right)^2 \int dy_w \, (T_5(y_w))^6 \left(\int d^3\mathbf{x'} \frac{e^{i\mathbf{k}\cdot\mathbf{x'}}}{|\mathbf{x'}|^2 + |y_w|^2} \right)^2 \, ,$$

$$= \alpha \left(\frac{2G_5}{3\pi \, \Delta\ln H} \right)^2 \frac{1}{(4\pi k)^2} \int dy_w \, e^{-2|y_w|k} \, (T_5(y_w))^6 \, , \quad \text{(A.14)}$$

where we have performed the coordinate transformation $\mathbf{x'} = \mathbf{x} - \mathbf{y_3}$, and use the result $\int \frac{d^3x \, e^{i\mathbf{k}\cdot\mathbf{x}}}{|x|^2 + |m|^2} = \frac{e^{-k|m|}}{4\pi k}$.

With this we are able to write

$$\mathcal{P}(k) = \frac{k^3}{2\pi^2} P_\zeta(k) = \beta \, k \int_0^\infty dw \, e^{-2|w|k} \, (T_5(w))^6 \, , \quad \text{(A.15)}$$

where $\beta = \frac{\alpha}{2} \left(\frac{G_5}{6\Delta\ln H \, \pi^3} \right)^2$. Note that we are in integrating between $[0, \infty)$ because of the $\mathbb{Z}_2$ symmetry. Because the temperature profile is analytic it admits a Taylor expansion of the form

$$(T_5(w))^6 = \sum_{n=0}^\infty \frac{T^{6^{(n)}}(0, \bar{\gamma}, \bar{w})}{n!} w^n \, , \quad \text{(A.16)}$$

and thus the power spectrum Eq.(A.15) admits a series decomposition of the form

$$\mathcal{P}(k) = \beta \sum_{n=0}^\infty \frac{T^{6^{(n)}}(0, \bar{\gamma}, \bar{w})}{k^n} 2^{-1-n} \, . \quad \text{(A.17)}$$

This last expression implies that for large k the correction to a scale invariant power spectrum goes as $1/k$. If the integral in Eq.(A.15) is performed in the rage $(-\infty, \infty)$ the the power spectrum series would be

$$\mathcal{P}(k) = \beta \sum_{n=0}^{\infty} \frac{T^{6^{(2n)}}(0, \bar{\gamma}, \bar{w})}{k^{2n}} 2^{-1-2n} \,, \tag{A.18}$$

giving a correction from scale invariant that goes as $1/k^2$ for large k. This correction renders model disfavourable in comparison with the symmetric case, where we have a $1/k$ decay. This is the reason why we work with the symmetric integral Eq.(A.15).

Appendix B

Various Plots of Numerical Simulations for The Real Ensemble Model

Here are given additional plots of the numerical simulations for those that wish to confirm certain aspects covered in the real ensemble chapter.

Table B.1: Plots of the evolution of spin-$\frac{1}{2}$ systems in the non-equilibrium real ensemble model for the case with a moderate initial separation of phases. Each case has three different phases for each of the two potential values of s_z. The initial conditions are $\rho(0) = \{\{0.16, 0.08, 0.06\}, \{0.23, 0.3, 0.17\}\}$ if marked as uneven or $\rho(0) = \{\{0.2, 0.1, 0.2\}, \{0.2, 0.1, 0.2\}\}$ if marked as even and $\phi(0) = \{\{0, 0.1\pi, 0.2\pi\}, \{\frac{\pi}{2} + 0.1\pi, \frac{\pi}{2}, \frac{\pi}{2} + 0.05\pi\}\}$. The Hamiltonian is $H = \sigma_x + \sigma_z$ for the first two plots and $H = 2\sigma_z$ for the third. The functions F within equations 5.11 and 5.12 for the plots are $F = \cos^2\left(\frac{\Delta\phi}{2}\right)$ for the top plot and F given by equation 5.17 with $c = 100$ for the other two.

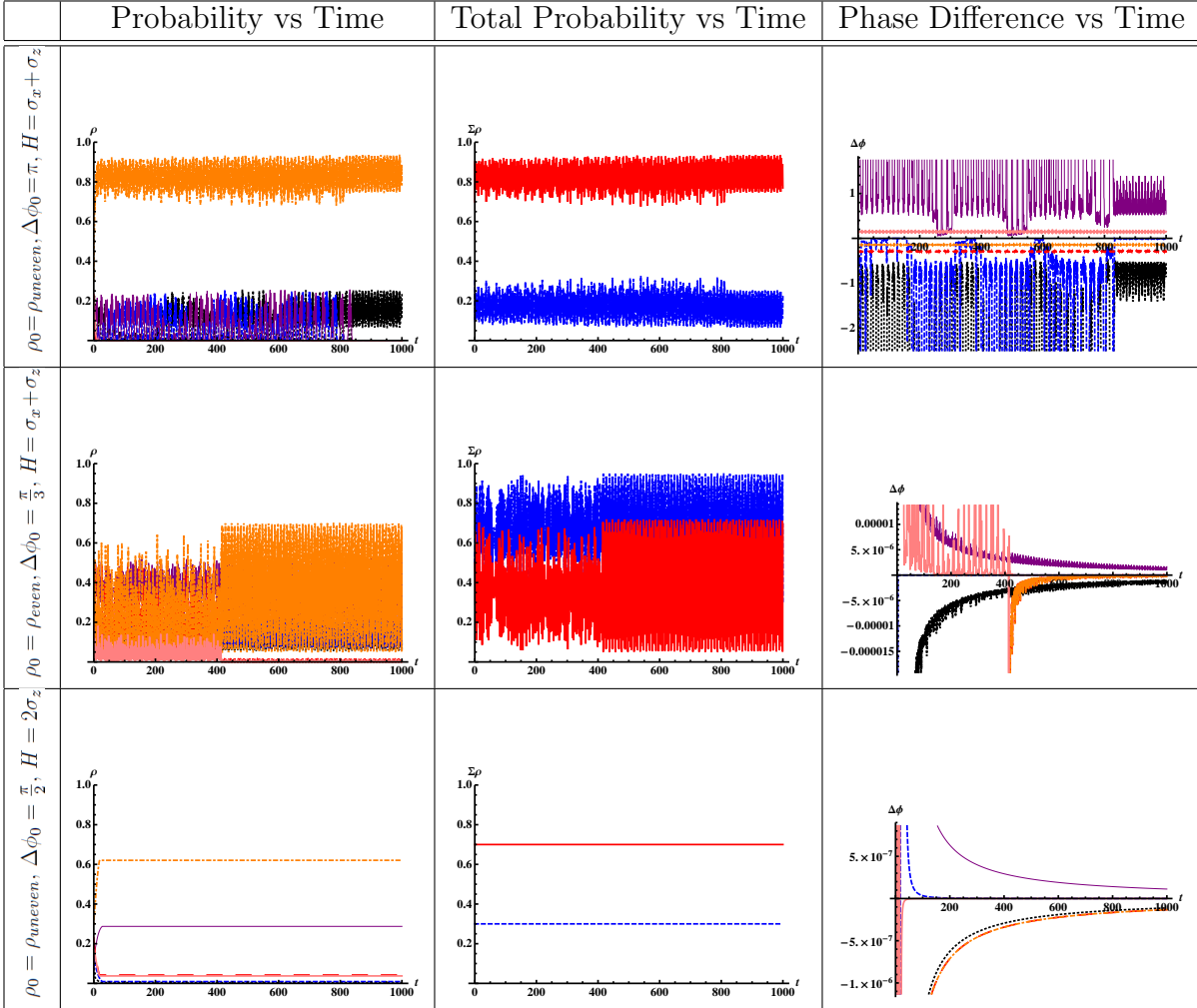|	Probability vs Time	Total Probability vs Time	Phase Difference vs Time
$\rho_0 = \rho_{uneven}, \Delta\phi_0 = \pi, H = \sigma_x + \sigma_z$			
$\rho_0 = \rho_{even}, \Delta\phi_0 = \frac{\pi}{3}, H = \sigma_x + \sigma_z$			
$\rho_0 = \rho_{uneven}, \Delta\phi_0 = \frac{\pi}{2}, H = 2\sigma_z$			

Table B.2: Plots of the evolution of spin-$\frac{1}{2}$ systems in the non-equilibrium real ensemble model for the case of large initial separation of phases. Each case has three different phases for each of the two potential values of s_z. The initial conditions are $\rho(0) = \{\{0.16, 0.08, 0.06\}, \{0.23, 0.3, 0.17\}\}$ and $\phi(0) = \{\{0, 1, 2\}, \{\frac{\pi}{2} + 1, \frac{\pi}{2}, \frac{\pi}{2} + 0.5\}\}$. The Hamiltonian is $H = \sigma_x + \sigma_z$ for the top plot and $H = 2\sigma_z$ for the bottom plot. From top to bottom, the functions F within equations 5.11 and 5.12 for the plots are $F = \cos^2\left(\frac{\Delta\phi}{2}\right)$ and F given by equation 5.17 with $c = 100$.
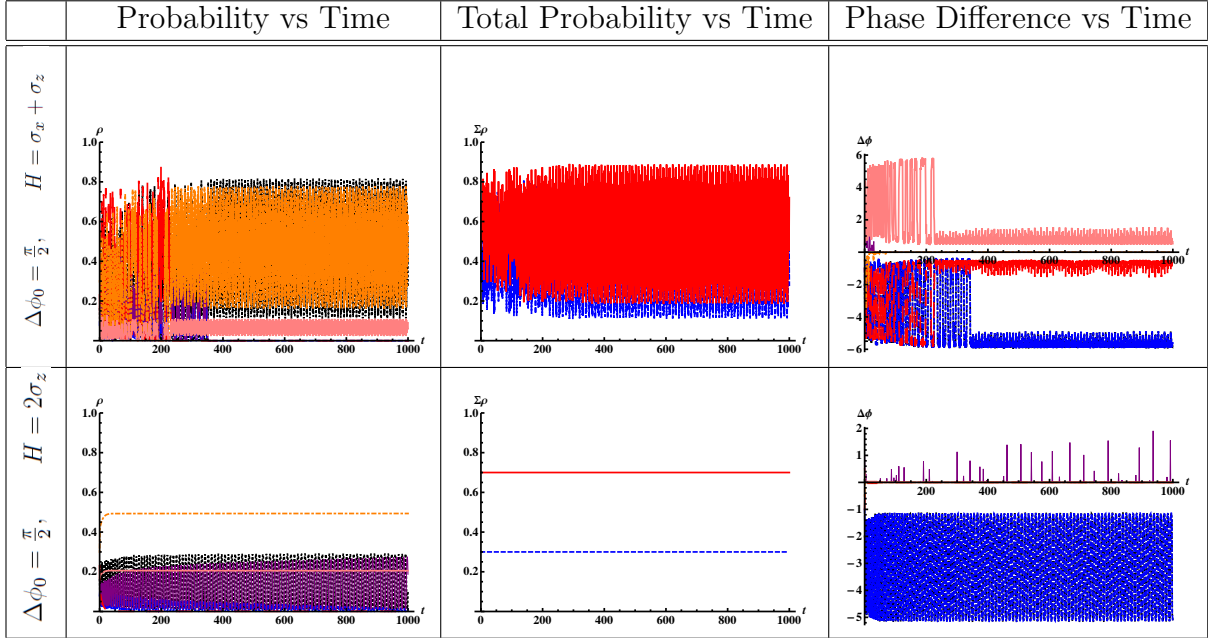

152

Table B.3: Plots of the evolution of spin-$\frac{1}{2}$ systems in the non-equilibrium real ensemble model for the case with a Hamiltonian proportional to the identity. Each case has three different phases for each of the two potential values of s_z. The initial conditions are $\rho(0) = \{\{0.16, 0.08, 0.06\}, \{0.23, 0.3, 0.17\}\}$ and $\phi(0) = \{\{0, 0.001\pi, 0.002\pi\}, \{\frac{\pi}{2} + 0.001\pi, \frac{\pi}{2}, \frac{\pi}{2} + 0.0005\pi\}\}$. The Hamiltonian is $H = 2I$. From top to bottom, the functions F within equations 5.11 and 5.12 for the plots are $F = \cos^2\left(\frac{\Delta\phi}{2}\right)$ and F given by equation 5.17 with $c = 100$. Note that the standard deviation plots are logarithmic in scale on the y-axis, with the second such plot being logarithmic in scale on both axes.

	Probability vs Time	Phase Difference vs Time	Standard Deviation vs Time
$H = 2I$, $\Delta\phi_0 = \frac{\pi}{2}$			
$H = 2I$, $\Delta\phi_0 = \frac{\pi}{2}$			